processes

MDPI

Review

The Potential of CFD in Sustainable Microbial Fermenter Design: A Review

Fatima Imran *, Markus Bösenhofer, Christian Jordan and Michael Harasek

Institute of Chemical, Environmental and Bioscience Engineering, Technische Universität Wien, Getreidemarkt 9/166, 1060 Vienna, Austria; markus.boesenhofer@tuwien.ac.at (M.B.); christian.jordan@tuwien.ac.at (C.J.); michael.harasek@tuwien.ac.at (M.H.)

* Correspondence: fatima.imran@tuwien.ac.at

Abstract

Due to the regulated nature and purity standards of the bioprocess and biotechnology industries, the sector has seen comparatively less sustainable practices than other chemical industries have. The achievement of sustainability in microbial fermenter design requires that quantitative tools with links between process parameters and end-environmental outcomes are employed. This review begins with environmentally friendly metrics such as process mass intensity, water and energy intensity, and related indicators that act as a template for resource usage and waste generation assessment. The objective of this paper is to highlight the primary focus on computational fluid dynamics (CFD) applied to bioprocesses in aerated stirred bioreactors using *Escherichia coli* (*E. coli*). Second, the objective of this paper is to explore state-of-the-art CFD models and methods documented in the existing literature, providing a fundamental foundation for researchers to incorporate CFD modelling into biotechnological process development, while making these concepts accessible to non-specialists and addressing the research gap of linking CFD outputs with sustainability metrics and life cycle assessment techniques. Impeller rotational models such as sliding mesh are an accurate and commonly used method of modelling the rotation of stirring. Multiple different turbulence models are applied for the purpose of stirred bioreactors, with the family of k-ε models being the most used. Multiphase models such as Euler-Euler models in combination with population balance models and gas dispersion models to model bubble size distribution and bubble characteristics are typically used.

Keywords: sustainable biopharmaceutical manufacturing; green metrics; mass transfer; computational fluid dynamics; stirred tank bioreactors; hydrodynamics

Academic Editors: Serena Lima and Francesca Scargiali

Received: 8 August 2025
Revised: 12 September 2025
Accepted: 17 September 2025
Published: 20 September 2025

Citation: Imran, F.; Bösenhofer, M.; Jordan, C.; Harasek, M. The Potential of CFD in Sustainable Microbial Fermenter Design: A Review. *Processes* **2025**, *13*, 3005. https://doi.org/10.3390/pr13093005

1. Introduction

The bioprocess, biotechnological, and biopharmaceutical industries play a large role in the betterment of the quality of life for almost every person on the planet with the production and provision of a wide variety of vital products [1,2]. It is of equal importance to also fulfil their role in sustainable and environmentally friendly practices due to the social responsibility of this sector. The industry faces rigid regulatory structures, legislation, and standards to be able to ensure the quality of such vitally important goods [3,4]. The effort to change existing large-scale processes is both time- and cost-consuming.

The global growth rate of the biotechnological industry between 2015 and 2020 was 1.3%, with an expected steady rise in the following five years, amassing to a global market

share of USD 295 billion [5]. Biopharmaceutical production constitutes a major component of the biotechnology industry, accounting for a substantial proportion of its overall activity and economic value [5]. In 2024, the global biopharmaceutical market is estimated at USD 516.79 billion and is projected to expand, reaching USD 761.80 billion by 2029. Biopharmaceuticals made up 27% of the global pharmaceutical market in 2020 [6].

Biotechnological methods depend on the manipulation and growth of different types of bacteria, yeast, and filamentous fungi [7]. Moreover, microbial fermentations, a very commonly utilized technology within the biotechnology sector, are utilized for a wide variety of products and molecules such as biopharmaceuticals, food ingredients and supplements, monomers, solvents, and biofuels [7]. Among various types of bioreactors used for the purposes detailed above, aerated STBRs are among the most widely employed in microbial fermentation or cell culture unit operations in the biopharmaceutical sector [8]. STBRs play a crucial role in bioprocessing, providing an environment for the growth and production of a diverse range of biologically derived products, including proteins [9,10], enzymes [11], antibodies [12], and vaccines [13]. Microbial fermentations can be energy-demanding for agitation and aeration [14,15], use large volumes of water and solvents [16], and generate extensive amounts of waste [17–19]—all posing sustainability challenges. One vital aspect is the aspect of energy consumption. The energy consumption and distribution between the different components, e.g., stirrer, aeration, and heating, are also included because aerobic fermentation processes consume significant amounts of energy.

Energy demand is one important sustainability concern in microbial fermentations, particularly in STBRs, which require agitation and aeration to provide sufficient mixing and oxygen transfer. Both increase, however with great power requirements; in industrial production, both play an important role in total production costs and environmental impact. As shown by [14], greater stirrer velocity and aeration augment oxygen mass transfer are typically also linked with far greater energy consumption. Similarly, comparative studies show that mixing and aeration in STBRs require extensive amounts of energy relative to other reactors such as oscillatory stirred reactors [15]. These observations thus call for more research on more energy-efficient approaches to bioreactor design and operation.

Solvent usage is extensive during the development phase of a product, where only a few batches are manufactured per step. Early minimization of waste streams, such as used solvents usage for cleaning, is essential to ensuring sustainability as more research is dedicated toward improving the environmental footprint of the biopharmaceutical industry. Proactive efforts to reduce environmental impact at smaller scales during drug and process development can lead to significantly lower waste generation and more sustainable practices at commercial scale. CFD can, therefore, assist in these earlier smaller stages of development in reducing solvent and water usage by identifying dead zones and areas prone to fouling, thereby decreasing the need for extensive cleaning procedures.

Due to vast nature of the different microbial fermentation processes, modes of operation, and configurations utilized within the biotechnology industry, this work constricts the focus on the aerated *E. coli* fermentations occurring in STBRs. The purpose of this work is to fundamentally explore the application of CFD and the different fluid dynamic and numerical models in the design, analysis, and optimization of *E. coli* fermentations in aerated stirred bioreactors.

Mechanistic and empirical models, each serving different objectives, seek to represent aspects such as volume or mass balance, viscosity, temperature, fluid and mixing flow, pH [20], oxygen mass transfer coefficient, dissolved oxygen concentration, oxygen uptake rate, and biomass concentration [21]. Classical optimization has relied predominantly on empirical correlations and minimal 1D or compartment models [22]. These are convenient but unsatisfactory: they imply spatial oxygen, substrate, and shear gradients—factors with

a central influence on microbial performance. Hybrid and structured compartment models are better than these but depend on assumptions that they will break down under complex geometries or multiphase systems.

CFD offers a first-principles framework with the potential to solve in-depth flow, mixing, oxygen transfer, and shear patterns—particularly in multiphase fermentation systems. CFD possesses the potential to integrate hydrodynamics and biological kinetics to make sustainable process design possible [6]. It has seen increasing applications in both upstream and downstream processing in bioprocesses [23–27], offering valuable insights that deepen the understanding of the fermentation process within bioreactors. CFD simulations enable the modelling of local hydrodynamic flow, encompassing fluid flow, gas-liquid mixing, mechanical agitation, and mass transfer [28]. Broadly speaking, there are different aims of applying CFD to model processes within bioreactors. First, CFD is used by simulation experts to achieve a greater understanding of the conditions at a local scale within the bioreactor. Such simulations aid in providing insights into the effects of operational process parameters on the hydrodynamics of the bioreactor, microorganisms, and product yield. All this knowledge collection through CFD simulations potentially optimize the fermentation process. Table 1 indicates the versatility of the application of CFD to STBR processes.

Utilizing CFD, insights into mixing zones, stagnant regions, or areas characterized by intense shear forces can be revealed [29]. This in-depth process knowledge is crucial for aspects such as cell proliferation, nutrient and oxygen availability, and product generation—all vital elements of a stirred bioreactor unit operation within the biopharmaceutical manufacturing process [30]. The integration of CFD simulations into the development and optimization workflows of upstream processes has the potential to promote sustainability improvements in the fermentation step of the overall biotechnological process by identifying issues such as uneven distribution of oxygen bubbles, vortex formation, and high shear stresses [30]. A CFD model allows for the early implementation of potential solutions during the process development stage, contributing to enhanced process optimization, robustness, minimized risks of batch-to-batch variability, and overall improved productivity. Therefore, it offers a means to understand the fermentation process in the bioreactor that may be challenging or costly to achieve through experimental means. CFD modelling enables the prediction of flow phenomena, encompassing bubble distribution and vortex formation.

The use of CFD simulations with suitable validations is conducive in designing a process space for fermentation that ensures consistent and robust product performance [31,32]. CFD results along with subsequent model creation can be integrated in a Design of Experiments (DoE) strategy to define a process space and assess the model robustness. However, the drawback of a multifaceted and complex CFD simulation is its computational expense and time-consuming nature [31,32].

Finally, CFD, as a computational tool, fosters interdisciplinary collaboration as it provides a detailed understanding of fluid flow, heat, and mass transfer within complex systems [33]. By simulating these processes, scientists, engineers, and a broad variety of people from various fields can gain insights into optimizing microbial fermentation [34], leading to enhanced efficiency and sustainability. This foundational understanding of CFD facilitates the integration of diverse expertise, fostering innovations and improvements in bioprocess and biotechnology engineering.

The biopharmaceutical sector demonstrates a lack of agility, flexibility, and robustness because of the prevalent use of batch mode of operation and processing in the biopharmaceutical industry [3]. Continuous manufacturing stands out as a promising innovation with substantial potential to enhance safety [35], selectivity [36], efficiency [37], economic

feasibility [38], and reliability [39] in biopharmaceutical production. By transforming batch processes into more continuous and circular systems, manufacturers can achieve significant reductions in waste generation [40], productivity [41], and resource utilization [42,43]. This is where modelling techniques such as CFD can contribute to the implementation of continuous mode of operation by aiding in the decision of proper sensor placement within the STBR, as the hydrodynamics and thus fouling and accumulation behavior are different in a continuous mode of operation (compared to batch mode).

Recent studies [16,44,45] have underlined that promoting the sustainability of bioprocesses demands not only technological development but also quality metrics to evaluate environmental performance. Tools such as process mass intensity (PMI) and supporting indicators confirm that water, energy, and material inputs are the primary drivers of the footprint of biologics manufacturing. CFD offers a different perspective through the possibility of predicting the effect of design and operation conditions on energy usage, oxygen transfer, and mixing in reactors [14,46]. By combining sustainability indicators with CFD-based data, optimization of the reactor can be aimed at being both environmental and operational optimum.

As such, this review seeks to explore the ways CFD can support sustainable design for microbial fermenters by joining together insights into hydrodynamics and the green metrics and life-cycle thinking. In particular, the paper examines CFD models and techniques reported within the literature, providing a base for researchers seeking to adopt CFD modelling within biotechnological process development. Additionally, this review seeks to present the subject matter for an interdisciplinary field of non-CFD experts, biotechnological engineers, experimentalists, and biochemists. Lastly, this review seeks to highlight the research gap of linking CFD results and sustainability metrics within fermenter design for microbial fermenters. The rest of this review is structured as follows. Section 2 covers biopharmaceutical production sustainability issues and introduces green metrics to measure environmental performance. Section 3 introduces the most significant parameters to describe STBRs, such as power input, mixing time, shear stress, and oxygen transfer. Section 4 presents fluid mechanics principles and discusses state-of-the-art CFD methods, including meshing, impeller modeling, turbulence models, and multiphase methods. Additionally, it describes illustrative case studies in which CFD has been applied in microbial fermentations, with lessons and present limitations drawn. Sections 5 and 6 conclude by summarizing the main conclusions and providing directions for future work on the role of CFD in enabling a more sustainable design of microbial fermenters.

Table 1. CFD modelling applied to biotechnology and biopharmaceutical processes: stirred-tank bioreactors—upstream processing.

Application	Description	Reference
Resolution of contrary process requirements	Bioreactor processes involve multiple functions: • Heat transfer and blending • Gas–liquid dispersion • Mass transfer These functions require conflicting hydrodynamic conditions, necessitating a design compromise. Computational models help in process design through the following: • Allowing specific effects to be toggled on and off • Enabling parametric investigations Using computational models saves time and cost compared to physical experimentation.	[25,47]

Table 1. *Cont.*

Application	Description	Reference
Transition from a batch mode of operation to continuous	Sensor, inlet, outlet, and baffle placement in a continuous stirred bioreactor (CSBR) can be modelled before transitioning from a batch process. This modelling strategy offers the following: • A deeper understanding of the process • Cost and time savings CFD modelling provides insights into the following: • Hydrodynamics • Dead zones • High and low shear stress zones	[47,48]
Scale-down and scale-up analysis	CFD modelling reduces reliance on laboratory experimentation. Flow analysis is crucial when scaling processes up/down. Mean flow and turbulence scale differently with reactor size and speed. Traditional scaling uses empirical rules and experience. CFD simulations help with the following: • Assess hydrodynamics in scaled systems • Identify needed adjustments for consistency	[30,49]
Investigation of new reactor concepts	CFD, combined with kinetic models and data, aids process optimization and scale-up. CFD simulations predict flow, heat transfer, and reactions in reactors. CFD simulations beforehand can be more economical and faster than physical testing. Key contributions include the following: • Optimizes flow and thermal management • Predicts reaction rates and pressure drops • Assists in scale-up and multiphase flow analysis	[50]
Tool for additional process understanding	CFD can help in the design of efficient, safe, and cost-effective reactors. CFD with digital twins reduces time, costs, and resources. Virtual labs help as bioreactors are expensive and require training. Combining CFD and digital twins improves process understanding and efficiency.	[20]
Optimization of operating conditions	CFD optimizes impeller design and operating parameters (speed, temperature, aeration, tank size, liquid height, pH). Enhances mixing efficiency and mass transfer rates. Leads to optimal conditions for cell cultures and improved productivity.	[21,26]
Prediction potential	CFD, combined with kinetic models (e.g., Higbie's penetration model), predicts key process parameters. Helps estimate mass transfer and mixing times.	[31,51,52]

This review, consequently, explores the sustainability challenges associated with microbial fermentations specifically by utilizing CFD as a perspective. We present green metrics not as a separate topic, but rather as a framework that can subsequently be associated with outputs derived from CFD analyses (for instance, mixing time, oxygen transfer rates, and power requirements). Therefore, the focus of this review is the amalgamation of sustainability metrics with CFD techniques to inform the design of microbial fermenters.

2. Green Metrics for Sustainability—Link to CFD-Parametrized Design of Aerated STBRs

This section introduces green metrics solely in the context of variables that CFD can predict for aerated STBRs. Rather than providing a general sustainability primer, CFD outputs—such as power draw, energy dissipation rate, gas hold-up, volumetric mass-

transfer coefficient, bubble size, mixing time, and shear stress—are explicitly linked to specific sustainability metrics including PMI, WARIEN, and E-factor. This linkage enables the quantitative evaluation of design and operating choices on environmental performance, as summarized in Table 2. These CFD sustainability linkages are explored further in Section 4 through case studies and current CFD methodologies.

Table 2. Linking CFD outputs to sustainability metrics in aerated STBRs.

CFD Output	Green Metric(s)	Impact on Process Sustainability
Power draw	WARIEN Energy intensity	Translates directly into electricity consumption; higher power demand increases water-related CO_2 emissions and operational energy footprint.
Volumetric mass transfer coefficient Gas hold-up	PMI WARIEN	Determines oxygen transfer efficiency; influences aeration energy demand and compressor load, affecting both resource use and carbon footprint.
Bubble size distribution	PMI Energy intensity	Controls interfacial area and gas–liquid mass transfer; links sparger and impeller design to oxygen transfer efficiency and energy demand.
Mixing time Residence time distribution	PMI Resource intensity	Affects solvent and buffer consumption for cleaning and process consistency; improved mixing reduces dead zones and associated waste streams.
Shear stress	E-factor Yield-related metrics	High local shear can damage cells, lower yield and increase by-product formation; directly linked to waste generation and overall process efficiency.

2.1. Energy Utilization in Fermenters and Its Quantification

The synthesis of biopharmaceutical products utilizes a number of inputs, produces a variety of outputs and toxic by-products and is associated with a considerable energy and resource consumption [53].

The primary energy demands for aerobic bioreactors that utilize microorganisms like bacteria involve oxygen transfer and cooling, both of which cause significant energy costs [54,55]. The environmental impact includes emissions from energy production, particularly the carbon footprint, and issues related to waste disposal. As a result, multiple design objectives, such as reducing energy consumption, and lessening environmental impact, often conflict with each other, making it challenging to determine the optimal design parameters. These parameters also include oxygen and substrate concentrations in the fermentation broth, air flowrate, impeller power input, and operating temperatures for cooling. CFD simulations enable otherwise energy-intensive elements of these plants to be directly quantified, as variables like impeller power consumption, aeration rates, and heat transfer coefficients can be calculated directly from the hydrodynamic models themselves. This enables, through simulation alone, the comparison of alternative design options—like aeration strategy or impeller shape—not just based on fluid dynamics, but on sustainability metrics like overall energy intensity or water-connected CO_2 emissions. In turn, such goals as reducing energy consumption whilst ensuring adequate oxygen and substrate concentrations can thus be assessed within the framework of CFD simulations.

The relative primary energy demand for an industrial scale STBR can be seen in Figure 1. In lieu of energy data taken from a biopharmaceutical production, a similar process was utilized as a case example for energy data.

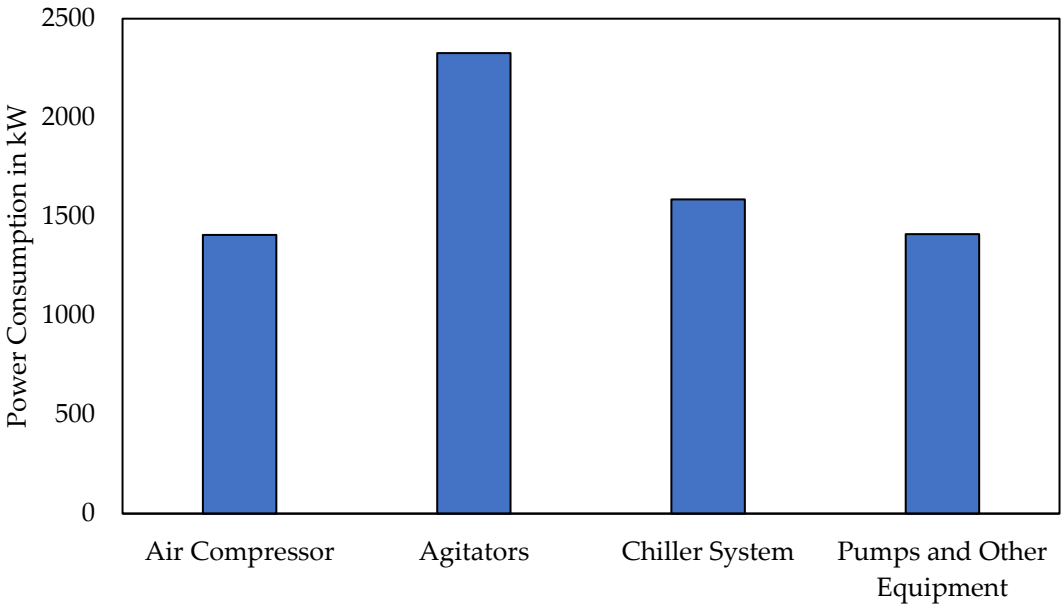

Figure 1. Cellulase production electricity requirements in a fed-batch industrial-scale stirred aerobic fermentation (300 m^3 bioreactor). Adapted from [55].

Power draw is a critical parameter in chemical and bioprocess engineering, referring to the energy needed over time to move fluids within containers (such as bioreactors and mixing tanks) through mechanical or pneumatic agitation [56]. This energy requirement significantly impacts the operational costs of STBRs and fermentation plants. Therefore, efficient mixing with minimal energy expenditure is crucial. The mechanical agitator enhances the oxygen transfer rate by generating smaller bubbles and promoting extensive mixing and turbulence. This process reduces the mass transfer boundary layer resistance and effectively distributes bubbles throughout the vessel. A continuous oxygen supply is essential to prevent it from becoming a rate-limiting factor due to the low solubility of oxygen in water. Numerous studies [54,55,57] have demonstrated the impact of agitation and aeration rates on the oxygen transfer rate, subsequently influencing cell growth and metabolite productivity. Oxygen transfer is heavily influenced by hydrodynamic conditions, which are determined by operational parameters, the physicochemical properties of the fermentation broth, the bioreactor's geometrical characteristics, and the oxygen concentration in the broth. Additionally, aeration rate is a crucial parameter in aerobic systems because it influences air compressor costs and power, both of which can be significant.

Figure 2 indicates the importance of selecting aeration rate carefully to stay within flooding constraints and avoid high total power requirements due to excessive agitator power at low aeration rates. Significant energy savings in the aeration system can be achieved by carefully selecting the aeration rate and the impeller power input throughout the bioprocess, with CFD and mathematical modelling aiding in this selection. The minimum total power that meets all constraints was found at the onset of flooding. Figure 2 underscores the need for careful selection [54].

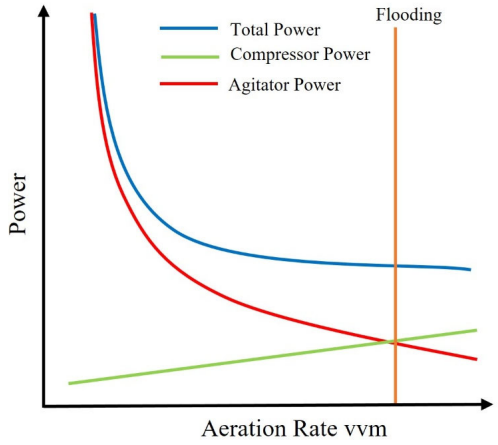

Figure 2. Influence of the aeration rate on compressor, impeller, and total electricity power requirements. Adapted from [58].

Besides the electrical power needed for oxygen transfer, the cooling system's power requirement can also be substantial. Figure 3 displays the average rates of metabolic heat production and agitator heat dissipation, highlighting that metabolic heat is predominant, especially at lower oxygen concentration values. It also compares the power requirements for cooling, the agitator, and the air compressor, illustrating their influence on the oxygen concentration in the broth. According to Fitzpatrick [57], lowering the oxygen concentration in the broth reduces the total electrical power/energy requirement for oxygen transfer due to a higher mass transfer driver. CFD can complement such analyses by resolving heat generation, oxygen transfer, and fluid dynamics simultaneously, making it possible to quantify the relative contributions of cooling, agitation, and aeration to total energy demand; this breakdown is essential for linking hydrodynamic design choices to targeted process optimization.

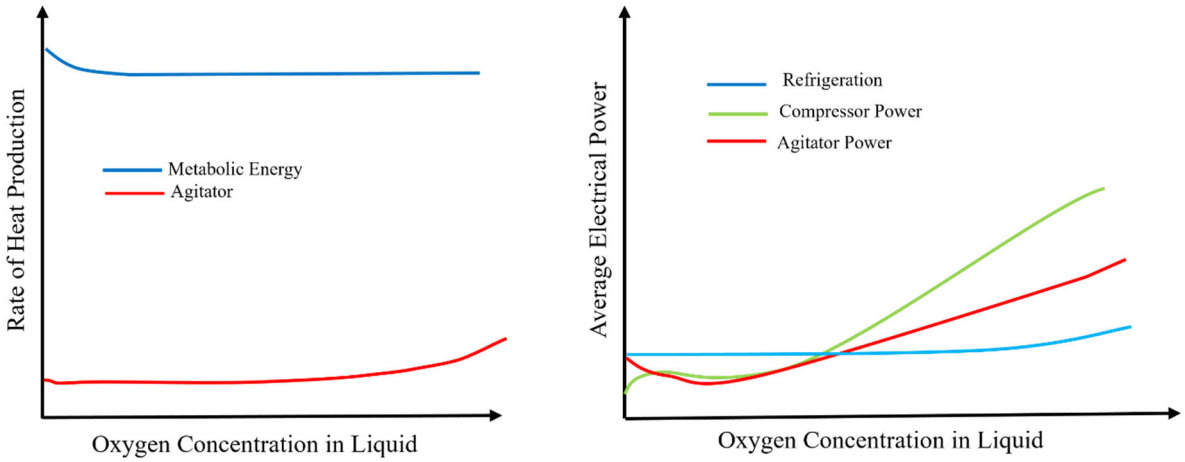

Figure 3. (**Left**): Rate of metabolic heat production and impeller heat dissipation; (**Right**): comparison of average cooling, agitation, and air compression power consumption. Adapted from [57].

In lieu of studies carried out with biopharmaceutical production as the focus point, similar studies [30,59,60] utilizing fermentation in STBRs were focused upon in this work, due to a scarcity of the literature found while researching this concept. Garcia-Ochoa et al. [30] provide insights into the oxygen transfer efficiency related to agitation and aeration but do not detail the electricity consumption aspects comprehensively. Humbird et al. [55] describe a potential biochemical ethanol production process in detail, focusing on process design and optimization, as well as quantifying the specific energy and resource

consumption of the process. A techno-economic analysis (TEA) report [61] investigated the aerobic conversion of lignocellulosic sugars to hydrocarbons via a fatty acid intermediate. Unlike previous ethanol analyses, it found that the aerobic fermentation stage was the main cost driver for integrated cellulosic biofuel production. Fermentation compressors and agitators accounted for the highest power demand in the biorefinery process, making the fermentation step the largest overall contributor to production costs. This analysis is linked to a higher degree of uncertainty in process design and capital cost assumptions as it was the first publicly available TEA for such a process [55].

Recent CFD studies have begun to address these gaps. Gu et al. (2025) [14] demonstrated that novel impeller designs can achieve comparable oxygen transfer with up to 70% lower energy consumption. Jamshidian et al. (2025) [62] validated CFD models for predicting gassed power draw, energy dissipation, and k_La in large-scale STBRs. Xu et al. (2023) [21] showed how CFD combined with Taguchi methods can optimize impeller geometries for energy efficiency and mass transfer. By directly linking such CFD-derived parameters to sustainability metrics like Water Related Impact of Energy (WARIEN) and PMI, it becomes possible to quantify the environmental impact of STBR operation with far greater precision than TEA alone. Therefore, coupling CFD with TEA and life-cycle assessment (LCA) frameworks offers a pathway to reduce uncertainty and provide process-specific predictions of energy requirements in aerated microbial fermenters.

There is a scarcity of the literature and technical reports that comprehensively quantify the electricity requirements of the main components of an aerated stirred bioreactor, which include agitation, aeration (and the gas compression involved with providing aeration), and cooling. This gap in research can be attributed to several factors:

- Quantifying the electricity usage for each component individually requires detailed experimental setups and precise measurement techniques. Many studies do not focus on the quantification of specific energy inputs of each STBR design parameter that is associated with energy consumption.
- The specific design, operational parameters, and biochemical reaction mechanisms and the microorganisms in STBRs can vary widely, affecting the energy consumption of each of the components involved in energy consumption. This variation makes it challenging to create generic models applicable even across different STBR systems.
- Research in bioprocessing often prioritizes parameters like oxygen transfer rates, cell growth, and product yield within the context of the optimization of the hydrodynamic conditions for improved product yields and cell growth and conditions. This focus results in fewer studies dedicated to energy usage quantification and modelling.

As CFD is commonly used as a tool to observe and quantify, among many things, how energy consumption can be optimized, the specification of each energy usage is relevant in determining the validity of the CFD models. Many publications [23,24,63,64] utilize power draw from stirring as validation for their models and hence such information is necessary when working with CFD simulations.

Developing customized stirring systems for specific applications often necessitates prototype fabrication, leading to project delays, increased costs and a higher consumption of energy, resources, water, and solvents. Consequently, employing simulation tools based on CFD emerges as an appealing approach for designing more efficient conceptual projects for these systems. In silico models like CFD enable engineers to rapidly and effectively assess the performance of various stirrer concepts and optimize them to achieve the desired outcomes. Only after the model is optimized should a prototype be constructed to validate the simulated performance [65]. Not only are the conceptual design and prototype creation stages of a process faster, but also a better understanding of the phenomena in the prototype is achieved and the overall sustainability (as measurable by the multitude of green metrics

outlined below and in literature) of the process—from concept to industrial scale-up is also highly improved as well and is also highlighted below.

2.2. Green Metrics and CFD

Numerous metrics have been developed to assess the "greenness" of a process. These metrics evaluate various aspects such as water, solvent, and reagent usage, energy consumption, and greenhouse gas emissions, as shown in Figure 4. It is suggested that other sustainable metrics should also be considered in the stages of CFD modelling.

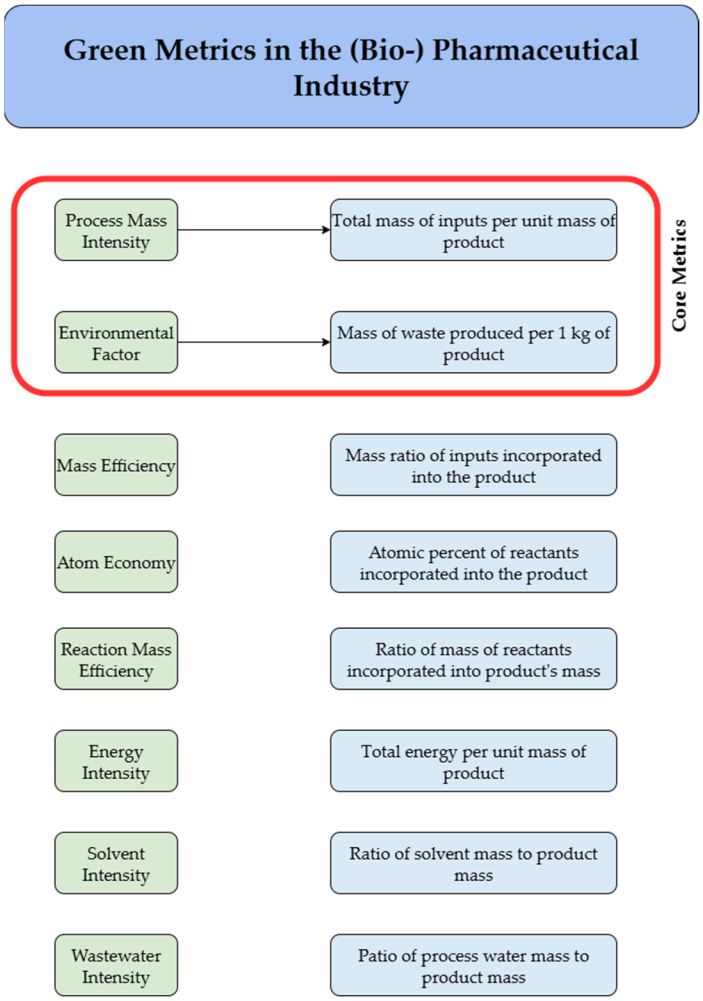

Figure 4. Green metrics that are useful in benchmarking the different aspects in which an aerated fermentation in an STBR can be run in a sustainable way. Adapted from [18,19,66,67]. PMI and environmental factor are the most commonly utilized core metrics identified within this review.

Green metrics should facilitate strategic analysis and continuous improvement. Metrics must be regularly assessed and used for decision making. Organizations must identify and implement context-specific metrics, leveraging existing frameworks and multidisciplinary expertise. More research has been performed in developing new metrics that tackle different aspects of waste and resource minimization such as the Mass Manufacturing Intensity (MMI) [18] and WARIEN [45].

The WARIEN metric developed by Cataldo et al. [45] enables further application of the PMI metric and connects resources used by the bioprocesses with the production train of water. This metric was developed to assess the water related CO_2 emission of

biopharmaceutical manufacturing processes and analyzed the impact and correlation between water related process costs and its carbon footprint.

The PMI metric was expanded by Benison and Payne [18] to include previously excluded categories such as cleaning, equipment conditioning, output management, abatement, etc. Assessing these areas during process design offers opportunities for resource optimization and process improvement. CFD-resolved hydrodynamics in aerated STBRs area able to predict power input and kLa as functions of agitation and gas rates, which enables direct estimation of mixing and aeration energy for PMI accounting. Recent studies [23] validate such CFD predictions and even use them to reduce operational power. Additionally, waste streams such as CO_2, solvents, and by-products must be considered in sustainability assessments. CFD-based mass transfer models can predict dissolved gas dynamics [62,68] and by-product accumulation [69], providing quantitative inputs to E-factor calculations.

Conventional manufacturing facilities use large-scale bioreactors (up to 20,000 L), which must operate in cleanroom environments. These stainless-steel vessels require extensive cleaning and sterilization between batches, typically involving chemicals, steam, and high-grade water like purified water or water for injection. In contrast, single-use systems (SUS), made from mixed plastics and sterilized using gamma irradiation, are becoming more common—particularly for smaller-scale operations (2000–6000 L).

While SUS eliminate the environmental burden of cleaning and sanitization, they generate significantly more plastic waste, which poses disposal challenges due to inconsistent regional waste regulations and limited recycling options for complex plastic materials [44,70–72]. CFD has been increasingly applied to evaluate mixing and oxygen transfer in SUS, providing insights into whether these benefits offset potential hydrodynamic limitations compared to traditional stainless-steel fermenters [73]. While SUS reduce PMI by lowering solvent and cleaning agent demand, they increase solid waste generation due to disposable plastics [70]. A key trade-off is that SUS generates additional solid plastic waste, which increases the E-factor. CFD can provide valuable input here by testing whether optimized mixing and gas dispersion in SUS can achieve equivalent performance at lower energy input, partially offsetting waste concerns.

CFD modeling can act both as a predictive tool for hydrodynamics and a tool to mitigate the experimental requirements of microbial fermenter design. By providing initial evaluations of power input, mixing efficiency, and gas transfer rates, CFD can inform sustainability metrics like WARIEN and PMI before starting resource-intensive experiments. Scully et al. (2020) [74] demonstrated such a scenario at the industrial level, demonstrating that a CFD-based multiparameter scale-up design for microbial fermenters of 2 kL to 10 kL led to a decrease in the time to market and hence further highlighted CFD's potential to replace certain features of costly pilot-scale experiments. In a similar fashion, Jamshidzadeh et al. (2023) [75] applied Euler–Euler CFD models to *Pseudomonas putida* fermentations and generated simulated aeration and agitation conditions that condense operating parameter selection without extensive physical probing. In the single-use system paradigm, Mishra et al. (2021) [28] overlaid CFD with population balance modeling to predict oxygen transfer with below 10% deviation from experimental values, hence giving confidence to design decisions while lowering prototyping requirements. Taken together, these studies further show CFD's contribution to facilitating evaluations of sustainability and in reducing the resource footprint of experimental design procedures in the domain of microbial fermenters.

Important parameters such as power consumption, mixing time, and oxygen mass transfer can be quantified using CFD and directly linked with these sustainability metrics, enabling systematic evaluation of microbial fermenter performance. Thus, metrics such as

PMI, MMI, WARIEN, and E-factor provide a sustainability framework, while CFD delivers the hydrodynamic and mass transfer parameters needed for these metrics.

3. Important Parameters for STBR Characterization

Utilizing CFD proves valuable in the characterization of STBRs by enabling the simulation of various operating conditions that subsequently influence key parameters. These parameters include power input, dimensionless numbers like Reynolds, Newton and Power numbers, mass transfer, and shear stress. Before delving into CFD models for bioreactor design and optimization, it is imperative to thoroughly comprehend the fermentation process, the hydrodynamic conditions within the STBR, and their effects on the cells (Table 3).

Modern biopharmaceutical production typically uses either glass (typically in lab-scale environments) or stainless-steel (typical in industry) bioreactors, where cells are cultured in a growth medium to produce the desired product—often a protein, or in the case of some vaccines and gene therapies, a virus [58]. The product is then isolated from the cell culture fluid through multiple purification steps, including centrifugation, depth and tangential flow filtration, homogenization, and chromatography, to ensure high purity and accuracy [25]. These filtration steps to remove harmful microbes and viruses, and the use of water for injection for both product formulation and cleaning processes. Cell culture fermentation is typically carried out using either fed-batch or perfusion methods. In fed-batch processes, the culture is progressively scaled up through bioreactors of increasing size until it reaches peak cell density in a large production bioreactor, sometimes over 40,000 L [58]. The culture is then harvested before entering the cell death phase. In contrast, perfusion culture maintains a pseudo-steady state, where cells are grown to an optimal density and then transferred to the production bioreactor. Fresh medium is continuously supplied while culture fluid is simultaneously removed. Cell retention systems help sustain cell density, and controlled cell bleeds may be used to avoid overgrowth [76].

Irrespective of the fermentation process's scale, it is crucial for the dimensions of STBRs to adhere to well-established relationships documented in literature [30,76]. The effectiveness of these bioreactors heavily depends on complex interactions involving fluid dynamics [77], geometric parameters [78], and operational conditions [79]. The rates of various reactions that take place within the process, such as mass transfer, biomass growth, production rates and product formation, are dependent on these factors. Therefore, strategies that enhance both mixing and oxygen mass transfer, particularly through impeller systems, hold significant importance.

Baffles and stirrers are commonly used to enhance the oxygen mass transfer in STBRs. These elements improve gas–liquid mass transfer by disrupting the liquid flow and reducing bubble size, thereby increasing the contact area between the gas and liquid phases [80]. The achievement of effective gas distribution and the provision of an extended residence time for air bubbles within the culture are pivotal for improved mixing. This is closely linked to the careful selection of appropriate impeller designs [54]. The impeller choice significantly influences shear rates or power dissipation in the system.

Radial impellers, characterized by high shear rates, concentrate power dissipation at the blade tips, leading to non-uniform distribution throughout the STBR [81]. This imbalance increases the likelihood of stagnant and dead zone development in the outer reactor region while promoting higher mass transfer in the impeller stream. In contrast, axial impellers have limitations in gas breakup, allowing a large number of bubbles to pass through the impeller zone without being split into smaller bubbles [81]. Various impeller configurations are employed in both laboratory-scale and industrial processes and can increase the volumetric mass transfer if designed appropriately. Stirring speeds also affect gas–liquid mass transfer [77].

Power input and dissipation stand as two pivotal parameters for the characterization of STBRs [23,62]. As power dissipation in the STBR increases, the bubble diameter decreases. This reduction in bubble diameter leads to an increase in interfacial surface area as bubbles break apart due to the induced shear force exceeding the surface tension (force) [82]. Furthermore, coalescence is suppressed, as the bubbles lack sufficient contact time for film drainage between neighboring bubbles [83]. While the agitation-induced breakup of bubbles is essential for enhancing oxygen mass transfer by increasing the contact area, the cell disruption caused by high shear rates needs to be mitigated. Striking a balance between the power input and the shear stress experienced between the cells is crucial to ensure that mixing and aeration are adequate for achieving optimal growth rates without causing cell damage [30].

Ensuring effective mixing within STBRs is important for successful cultivations. The quality of mixing is influenced by various factors, such as the rheology of the broth, the type and number of impellers, vessel geometry and size, and the power input. However, it is important to note that while achieving homogeneity within the vessel is relatively straightforward at the laboratory scale, scale-up often imposes limitations on mixing time. On an industrial scale, inadequate mixing can significantly impact bioprocess efficiency because of the development of undesirable nutrient concentration gradients and limitations in oxygen transfer rates [84]. Therefore, evaluating mixing time is a crucial parameter. Power input and tank geometry have substantial effects on mixing time, where, for a conventional STBR with a fixed T/D_i (tank diameter/stirrer diameter) ratio, the mixing time increases only when the energy dissipation rate decreases [30].

Controlling heat transfer in stirred vessels is crucial for successful biochemical processes. Fermentation typically requires a tightly regulated temperature range [85]. Usually, STBRs often include heat exchange systems, such as jackets or internal coils, to manage heating or cooling. The efficiency of heat transfer depends on the agitator type, vessel design, and operating conditions. In STBR design, the impeller, vessel shape, and baffles should meet the process's mixing needs, but it is not feasible to design an impeller to achieve a specific heat transfer coefficient [85]. The key factor in agitator selection is fluid type [86]. Large, slow-moving impellers work well for high-viscosity fluids, offering good mixing and heat transfer [87]. In contrast, small, fast-spinning impellers—like turbine types—are better for low-viscosity fluids. Turbine impellers typically have 4–6 flat blades on a central disc, with a diameter-to-vessel ratio between 1/3 and 2/3. Baffles are critical in batch vessels to ensure effective mixing by reducing swirling and enhancing vertical flow. Since baffling increases turbulence, it also influences heat transfer [85].

Finally, two of the foremost characterizing parameters for the STBR are the k_La value and the resulting oxygen mass transfer rate. Many fermentations in the STBR are aerobic. Oxygen exhibits low solubility in water-like media. Consequently, continuous aeration is essential for successful cell growth and product formation. As a general rule, the OTR should equal or surpass the OUR in the broth to avoid a shortage of oxygen for the cells in the STBR. The OUR is contingent on the specific needs of the cell culture (q_{O_2}) and the cell concentration (X), while the OTR is directly proportional to k_La and the concentration difference between the gas–liquid interface and the bulk fluid $(dO_2{}^* - dO_2)$. This concentration difference signifies the driving force of mass transfer [88]. With increasing agitation speed and aeration rate, the OTR also rises, making it one of the most crucial parameters for the scaleup, design, and performance optimization of aerated STBRs [30]. Multiple methods, both experimental and empirical, exist for measuring and calculating the k_La value in an STBR [30,88–91].

Table 3. Some important parameters for STBR characterization.

Parameter	Definition	Equation	References
Power number P_0 (also known as the Newton number)	Directly related to the stirrer torque Often utilized to compare different impellers If critical level of turbulence is exceeded P_0 becomes constant for many impellers	$P_0 = \frac{P}{\rho \cdot N^3 \cdot {D_i}^5}$	[81,92]
Reynolds number Re	Dimensionless number used to characterize flow regime based on the ratio of inertial to viscous forces	$Re_i = \frac{\rho N {D_i}^2}{\mu}$	[93,94]
Mixing time t_m	Ability of a bioreactor to efficiently mix the contents are defined by the mixing time A measure of how much time is required to achieve a desired degree of homogeneity (usually 95%) Convection and turbulence are driving forces for mixing and mass transfer	$t_m \propto P\sqrt[3]{V}$ $t_m = 57.4\sqrt[3]{\left(\frac{T}{D_i}\right)}\frac{\sqrt[3]{T^2}}{\sqrt[3]{\varepsilon}}$	[30,88,95,96]
O_2 mass transfer coefficient	As O_2 as a low solubility in water-like media, continuous aeration of the system is required O_2 can become the limiting factor in high cell density cultivations	$q_{O_2}X \leq k_L a(dO_2{}^* - dO_2)$	[88]
Shear stress τ	Velocity gradients act on the cells as shear and normal stresses Depends on the effective viscosity of the broth and the shear rate, which depends on the impeller geometry and stirring speed	$\tau = \mu\sqrt{2\left(\frac{\delta u_x}{\delta x}\right)^2}$ $\tau_{ave} = \mu_{eff}\gamma_{ave}$	[93]
Volumetric mass transfer coefficient $k_L a$	Used to describe the mass transfer capacity in a bioreactor Different approaches towards calculating $k_L a$ Values of k_L and a depend on the eddy dissipation rate (ε_1) Describes how efficiently the gas is distributed in the medium by the impeller	$k_L = C_1\sqrt{D_L}\sqrt[4]{\left(\frac{\varepsilon}{\nu_L}\right)}$ $a = \frac{A_G}{V} = \frac{6\alpha_G}{(1-\alpha_G)d_B}$ $C_1 = \frac{2}{\sqrt{\pi}}$	[88,97]

Dimensionless Numbers

Based on the application and the case, different dimensionless numbers can be used to characterize different aspects of a fluid flow. Additionally, they aid in the comparison of different cases with differing characteristics (e.g., fluid viscosity). Dimensionless numbers can also be used to select the correct models for CFD simulations. One example is the utilization of the Re number to determine the flow regime; hence, the turbulence model used. Dimensionless numbers are usually ratios of different types of forces acting within a flow. There are a number of different dimensionless numbers that are commonly used in fluid dynamics for different purposes [93]. Subsequently, the important dimensionless numbers are briefly described and examined.

The component of Newton's second law that involves the rate of momentum change can be viewed as inertial forces indicating the difficulty of accelerating the fluid due to its mass. These forces are determined by the product of the fluid's density, velocity, and a chosen characteristic length. The selection of the characteristic length depends on the geometry of the object through which the flow occurs. Viscous forces arise from frictional

interactions between fluid layers and are influenced by the fluid's viscosity. To assess the relative magnitudes of inertial and viscous forces in fluid flow, their ratio is calculated, known as the Reynolds Number (Re), as shown in Equation (1) [94].

$$\text{Re} = \text{inertial forces}/\text{viscous forces} = (\rho u L_{char})/\mu, \quad (1)$$

However, Re for stirrers in STBRs is defined by [80]:

$$\text{Re}_i = (\rho N \pi D_i^2)/\mu, \quad (2)$$

The stirrer Reynolds number Re_i can be utilised to determine if the flow regime within the STBR is laminar, in the transition zone, or turbulent. Re_i takes the impeller diameter as the characteristic length and the rotational speed as the velocity component. Thus, the type and size of the impeller affect the type of flow regime within an STBR, as well as how fast the stirrer is being rotated. As geometry of the STBR plays a role in the Re_i, it is evident that the value for the transition Re_i depends on the geometry of the impeller, tank, and baffles as well. For commonly used systems, however, it is generally accepted that at $\text{Re}_i < 10$, the flow regime can be characterized as laminar and as turbulent at $\text{Re}_i > 10^4$, with any Re_i values in between being characterized as a transitional flow regime [98].

The Knudsen number Kn characterizes the boundary conditions of a fluid flow. The no-slip boundary condition is usually assumed between the wall and the fluid layer in direct contact with the wall and this boundary condition holds true for Kn less than 0.001. This means that the characteristic length chosen is significantly larger than the mean free path of the fluid molecules, and that the fluid can, at least numerically, be considered to follow the continuum hypothesis. For Kn greater than 0.001, the slip boundary condition is assumed. For Kn greater than 0.1, the continuum hypothesis cannot be met, and the fluid flow must be observed using other methods [99]. The Kn number aids in the definition of the lower limit of the length scale, in which the Navier–Stokes equations are valid and relevant as well as the transitions to other transport forms in micro- to nanometer- scale flow channels [100]. As CFD finds its basis with the Navier–Stokes equation, therefore the Kn number was chosen for its relevance to CFD applications.

$$\text{Kn} = (\text{mean free path length})/(\text{characteristic length}) = \lambda/L_{char}, \quad (3)$$

Heat transfer is an essential parameter during aerobic fermentation processes, as a tightly regulated temperature is crucial for the growth and health of the microorganisms, as well as for a successful biochemical process. Due to the complexity of heat transfer in these systems, empirical models using dimensionless analysis are often applied to estimate average heat transfer at the jacketed walls of the STBR [85]. Thus, dimensionless numbers relating to heat transfer are of particular interest here.

The Prandtl number Pr correlates the fluid viscosity with its thermal conductivity. It can be defined as shown in Equation (4). Liquids having low Prandtl numbers exhibit high thermal conductivity, making them favorable options for conducting heat [93].

$$\text{Pr} = (\text{momentum transport})/(\text{heat transport}) = (\mu c_p)/\lambda_h, \quad (4)$$

The mass transfer within the fermentation process in an STBR (oxygen, nutrients, etc.) is also of utmost importance for a successful biopharmaceutical production. However, it can also be formulated in a dimensionless number [101]. This results in a combination of the Schmidt number, a volume number ($\frac{\text{reactor liquid volume}}{(\text{reactor diameter})^3}$), the Froude number, and the Galilei number. Thus, these numbers are given a closer look below.

The Schmidt number Sc is a dimensionless quantity that establishes a correlation between the fluid viscosity and its diffusion coefficient [93]:

$$\text{Sc} = (\text{momentum transport})/(\text{mass transport}) = \mu/\rho D, \quad (5)$$

The Froude number $\text{Fr} = \frac{V}{c}$, is a dimensionless parameter originally used in open channel hydraulics. It represents the ratio of the average flow velocity across the channel's cross-section (V) to the speed at which shallow water waves travel, known as the wave celerity (c) [102].

The Fr number represents the ratio between inertial and gravitational forces [103]. Dimensionless geometric parameters encompass all relevant dimensions—the impeller, the vessel, or their combined configuration, scaled typically by a single reference dimension, usually the vessel diameter [103]. This methodology was further advanced by Hixson and Luedeke [104] and culminated in the influential work of Rushton [92]. In their work, the Froude number was defined as follows:

$$\text{Fr} = (\text{inertial forces})/(\text{gravitational forces}) = (N^2 D)/g, \quad (6)$$

The Froude number proved especially relevant for describing swirling flow created by a centrally located impeller in a cylindrical tank. However, when baffles were added to the vessel to eliminate swirling, the Froude number became less significant [103].

The Galileo (or sometimes Galilei) number is defined by the ratio of the gravity to viscous forces [105]:

$$\text{Ga} = (\text{gravitational forces})/(\text{viscous forces}) = ({L_{char}}^3 g)/\nu^2, \quad (7)$$

The Péclet number Pe correlates convective and diffusive transport phenomena. It is associated with both the Pr and the Re numbers. Similar to Re, the Péclet number is not a material constant; its value relies on both the velocity of the flow field and the characteristic length of the system [93]. The Péclet number can be defined for mass transport:

$$\text{Pe} = (\text{convection transport})/(\text{diffusion transport}) = (uL_{char})/D, \quad (8)$$

Pe can also be defined as follows [100]:

$$\text{Pe} = (\text{convection transport})/(\text{heat transport}) = (uL_{char})/\lambda_h, \quad (9)$$

The Weber Number We can be defined as the ratio of inertia to surface tension forces. It is usually a parameter that aids in the analysis of multiphase flows that deal with two different fluids at curved interfaces such as bubble or droplets [106]. Since aeration is of the utmost importance in aerated fermentations in STBRs, and the amount of gas present in the broth gives a measure of cell activity, the bubble characteristics is an important parameter. Therefore, the Weber number is deemed to be crucial for the observation of bubble formation in this special case of aerated STBRs [93]:

$$\text{We} = (\text{inertial forces})/(\text{surface tension}) = (\rho u^2 L_{char})/\gamma, \quad (10)$$

Other dimensionless numbers, such as the Grashof, Nusselt, Mach, and Eckert numbers, are all applied in fluid dynamics to evaluate different forces and characteristics of a fluid and/or heat flow.

The last dimensionless number is different than the ones listed above and is related to the numerical solutions. The Courant number corresponds to the Courant–Friedrichs–Lewy

condition, where the distance any information travels within a computational cell during a time step is defined. The Courant number can be defined as follows [107]:

$$C = u\ \Delta t/\Delta x, \tag{11}$$

The Courant number represents the distance travelled by the fluid compared to the cell size [107,108]. When the Courant number is greater than 1, the information passes through the cell in one time step. When the Courant number is less than 1, the particle might not be able to skip the neighboring cells completely. It is advised to always aim for the largest Co number possible (but usually < 1) to achieve stable and accurate solutions (Table 4).

Table 4. Summary of the relevant dimensionless numbers in this work.

Dimensionless Number	Definition	Equation
Power number P_0 (also known as the Newton number)	Directly related to the stirrer torque Often utilized to compare different impellers If critical level of turbulence is exceeded, P_0 becomes constant for many impellers	$P_0 = \frac{P}{\rho \cdot N^3 \cdot D_i^5}$
Reynolds number Re	Used to characterize flow regime based on the ratio of inertial to viscous forces	$Re_i = \frac{\rho N \pi D_i^2}{\mu}$ $Re = \frac{\rho v L_{char}}{\mu}$
Knudsen number Kn	Characterizes the boundary conditions of a fluid flow	$Kn = \frac{\lambda}{L_{char}}$
Prandtl number Pr	Correlates the fluid viscosity with its thermal conductivity	$Pr = \frac{\mu c_p}{\lambda_h}$
Schmidt number Sc	Establishes a correlation between the fluid viscosity and its diffusion coefficient	$Sc = \frac{\mu}{\rho D}$
Froude number Fr	Represents the ratio between inertial and gravitational forces	$Fr = \frac{V}{c}$ $Fr = \frac{N^2 D}{g}$
Galilei number Ga	Defined by the ratio of the gravity to viscous forces	$Ga = \frac{L_{char}^3 g}{\nu^2}$
Peclet number Pe	Correlates convective and diffusive transport phenomena	$Pe = \frac{u L_{char}}{D}$ $Pe = \frac{u L_{char}}{\lambda_h}$
Weber number We	Defined as the ratio of inertia to surface tension forces	$We = \frac{\rho u^2 L_{char}}{\gamma}$
Courant number C	Represents the distance travelled by the fluid compared to the cell size	$C = u \frac{\Delta t}{\Delta x}$

4. Basics of Fluid Mechanics and CFD

4.1. Fermentation and Fluid Mechanics

The performance of microbial fermentations is tightly linked to the underlying fluid mechanics, which are in turn governed by key thermophysical properties of the broth and dispersed phases. Accurate representation of viscosity, density, surface tension, and diffusivity are essential in CFD models, as each property directly shapes hydrodynamics, mass transfer, and energy demand within STBRs.

In *E. coli* Fab'-producing fermentations, broth viscosity changes significantly over time, with distinct phases correlating to biological events. As shown by Newton et al. (2016) [109], viscosity of the broth during the course of the fermentation increases during exponential cell growth, stabilizes in stationary phase, and subsequently increases during cell lysis. This correlates with DNA release, product leakage, and cell viability loss. Viscosity monitoring can serve as a rapid and important indicator of fermentation progress.

Therefore, applying thermophysical properties like viscosity into CFD models is crucial for the prediction of mixing behavior and mass transfer rates, as changes in viscosity strongly influence the oxygen mass transfer [110]. According to Buckland et al. (1988) [111], k_La decreases in proportion with the square root of the broth viscosity. An increase in broth viscosity prevents adequate oxygen transfer, leading to lower levels of dissolved oxygen for microorganisms. This leads to a shift toward fermentative metabolism, production of undesirable by-products and lower energy generation, which ultimately results in a substantial decrease in yield [110]. High broth viscosity has a great influence on gas-liquid hydrodynamics and the rheology of in the STBR. Higher broth viscosity slows down the bubble rise velocity, which increases the gas hold-up and the residence time of the bubbles, and thus can improve the oxygen transfer. However, due to lower effective working volume and increased foam stability, it may have negative effects as well. Many of the broth constituents cause these increases in viscosity, such as filamentous microbial growth (entangled hyphae), polysaccharides and nucleic acids, and high-concentration sugars. Polymer-producing fermentation is mainly strongly pseudoplastic due to chain entanglement, where the viscosity of the broth diminishes at high shear as the chains disentangle. In addition, filamentous fungi develop highly viscous pseudoplastic broths with the flow behavior index down to 0.2–0.4, whereas pelleted growth produces lower-viscosity broths due to minimized interacting surface area-to-volume [110].

Another thing to consider is the broth rheology. Many fermentation broths have non-Newtonian behavior and in specific fermentations like bacterial alginate batch production [112], the broth becomes more pseudoplastic as the alginate concentration increases, which negatively affects the mixing performance. In this study [112], the influence of the interaction of the changing broth rheology and impeller mixing was investigated using CFD modeling. It was found that the model validation showed a good agreement with the experiments; thus, the evolution of the mixing mechanisms could be studied. Although overall liquid velocities were found to decrease during fermentation, the relative volume of the stagnant regions remained nearly unchanged. The flow regime evolved from unstable to more stable, parallel streamlines over time. Characteristic large-scale vortical structures, including trailing and processional vortices, were observed. The impeller-centered vortex geometry was identified as a key driver of flow instability. It was further proposed that aeration modifies these vortical structures, thereby increasing mixing times. The mixing time and mass transfer in STBR and how they are affected by the broth rheology (water, a Newtonian fluid versus xanthan gum solutions, a shear thinning fluid) was also investigated [31]. Experimental NaCl tracer conductivity experiments were conducted, and the mixing performance was simulated with CFD. Additionally, the mas transfer was predicted from the Higbie's penetration model from multiphase CFD simulations, which utilized a correlation of bubble size and power input. The mixing time was not significantly affected by the different rheologies and was observed in both experiments and the CFD model. The CFD model successfully reproduced mixing behavior in both water and non-Newtonian xanthan solutions, accurately predicting tracer profiles and mixing times across a range of power inputs. Bubble size, determined indirectly from process data, was shown to depend on gas flow rate and power input. The approach reliably predicted k_La values with accuracy comparable to empirical correlations, and sensitivity analysis indicated reduced uncertainty in bubble size effects. Overall, both studies [31,112] demonstrate how CFD models informed by process data and experiments can provide a robust basis for biologically relevant predictions, such as substrate dispersion and uptake.

In addition to explaining why viscosity and rheology matter, recent studies have begun to predict these properties dynamically. For example, *Penicillium chrysogenum* fermentation broths were shown to follow a power-law behavior with viscosity—and the

flow-behavior and consistency indices—directly correlated to biomass concentration via empirical models [113]. Similarly, fermentation broths exhibiting shear-thinning behavior under varying stir speeds were modeled with power law fits, capturing changes in mixing efficiency and mixing time [114].

Building on this, a comprehensive study on alginate fermentations used evolving broth rheology in CFD simulations to predict changes in impeller torque, flow regimes, and mixing structures. This validated a workflow that accounts for pseudoplastic behavior during batch operations [112].

More recently, data assimilation techniques have enabled simultaneous reconstruction of flow fields and rheological parameters—specifically Carreau model coefficients—by integrating velocimetry data in a Bayesian inverse Navier–Stokes (N-S) framework [115].

In practice, these rheological predictions are often implemented via user-defined functions (UDFs) or dynamic constitutive routines within CFD platforms (e.g., ANSYS Fluent 2025 R2 or OpenFOAM.org 13/OpenFOAM ESI-v2506), where viscosity is updated in space and time as a function of local biomass or shear rate [116,117]. Information on the viscosity and rheology of the broth can improve CFD modeling as it can aid in providing even better predictions on fluid parameters. However, modeling non-Newtonian behavior in CFD still remains rather complex, due to time-dependent changes occurring during fermentation and computational expense [112].

For the successful application of CFD in bioengineering purposes, input parameters such as density of the phases, surface tension, diffusivity, viscosity, and rheology must be specified, as the models utilized within CFD require such thermophysical properties to calculate the flow. Moreover, the models may use dimensionless numbers, and this also aids the CFD models to calculate the hydrodynamics and the fluid flow. From the calculations, parameters such as shear stress distribution, power consumption, k_La, and other specific parameters can be predicted and subsequently be utilized for STBR design and linked to sustainability metrics and tools, like life cycle assessments, as shown in Tables 5 and 6, and detailed in the following sections as well. Accurate multiphase CFD simulations depend on the correct specification of surface tension, density, and diffusivity. For instance, broth composition (e.g., presence of surfactants or metabolites) directly impacts bubble size, gas hold-up, and flow regime transitions, all of which are driven by surface tension and density variations [118]. In many CFD studies [119,120], parameters like density and surface tension are sometimes assumed to be equal to those of pure water, simplifying computation. However, this introduces uncertainty in predicting dispersion and mass transfer.

The spatial distribution of other fluid mechanic properties such as shear stress and rate distribution within an STBR is equally important, as this has a defining impact on cell growth and death [29,121]. Ebrahimi et al. (2019) [79] compared different double-impeller configurations at agitation rates of 50–150 rpm, showing that the segment-segment impeller yielded lower average strain rates by nearly 40% and turbulence dissipation over 25% with more uniform stress fields, making it more suitable for shear-sensitive cultures. Impeller diameter and type and their effect on shear rates and oxygen transfer were evaluated by Ramírez et al. (2020) [27]. This study found that smaller diameter propellers reduced peak shear rates by approximately 35% while maintaining adequate oxygen transfer of 120–140 h^{-1}, thereby lowering energy consumption without compromising performance. In highly viscous systems, Sharifi et al. (2023) [122] investigated a dual coaxial mixing bioreactor with Herschel–Bulkley rheology and mapped local shear rate distributions under multiple pumping and rotation modes. The study concluded that an up-pumping and co-rotating operation minimized stagnant zones and produced the most homogeneous shear environment. These case studies show that CFD-derived shear and strain-rate fields can be utilized for the optimization and design of impeller geometry, rotation strategy,

and geometric configurations (e.g., baffles and the tank geometry) to create an appropriate shear stress distribution that the microorganisms can withstand in an STBR.

4.2. The Governing Equations and Conservation Laws

CFD as a modelling technology aims to analyze and calculate fluid movements in both space and time through computational means. The behavior of a fluid can be predicted based on specified constraints, forces, and prior behaviors by CFD simulations. This process relies on three fundamental principles: mass conservation, Newton's second law of motion (from which momentum conservation, the N-S equations can be derived), and energy conservation [123] (p. 3).

The principle of mass conservation asserts that the mass of a fluid remains constant; it cannot be generated or eliminated. Mass transfer across system boundaries can alter the mass in a system [124,125]. Any fluid entering a specified region must undergo a corresponding change. In certain scenarios, this incoming fluid may either (1) prompt an equivalent mass of fluid to exit the domain, or (2) result in an increase in fluid density and pressure as it enters the domain. In this case, as the focus of this paper is on STBRs, the domain is defined as the inside of the reactor. Therefore, all the parts of the reactor, such as the impeller, sparger, and baffles, and their geometry affect the simulation of the fluid(s) within the domain [123,126].

According to Newton's second law, the rate of change of momentum of an object with constant mass is equal to the sum of forces acting on it. In fluid dynamics, the consideration extends beyond tracking individual fluid molecules, which would be computationally impractical. Instead, the focus is on examining how different forces exert their influence on a small region of the fluid, which is commonly referred to as a control volume [119].

The last governing equation to be considered is the energy conservation equation. The terms in the equation below can be considered as variations in temperature over time, the transport of heat by convection, factors contributing to the heat source, and thermal diffusion [123,126].

4.3. The CFD Simulation Process

The initial step in setting up a CFD simulation for applications in chemical and biochemical engineering involves constructing the geometry using a suitable CAD (computer-aided design) software like CATIA [127], FreeCAD [128], SolidWorks [129], etc. [23,27]. This geometry is then exported to the chosen CFD software (OpenFOAM [130], ANSYS Fluent [131], etc.), which includes the discretization of the simulation domain via a mesh. Additionally, the definition of fluid properties, boundary conditions, and initial conditions are required. Discretization schemes and solvers must be specified before initiating the simulation. Subsequently, the various momentum, mass, and energy balances are solved using the chosen schemes and algorithms. Finally, post-processing is conducted to analyze and interpret the acquired data, among others vector plots [29], contour plots [8], and calculations of essential variables such as power [132], mixing performance [89], shear rate [27], mass transfer coefficient [133], velocity and flow patterns [134], and RTD (residence time distribution) [135,136], are used for this purpose [137].

4.4. CFD Simulation Methodologies

4.4.1. Mesh Influence on the Simulation

The first step toward CFD simulations is the meshing. During the meshing process, the geometric object on question undergoes discretization into multiple cells, each containing a distinct number of nodes. These cells exhibit predictable shapes that effectively capture the physical form of the object. CFD solvers are capable of employing structured, unstructured,

or hybrid meshing techniques, utilizing 2D shapes (such as triangles or quadrilaterals) or 3D shapes (including tetrahedra, hexahedra, etc.) with varying densities [138].

Beyond the most common finite volume and finite element discretization methods, other numerical strategies can be encountered in CFD. CFD in bioprocess engineering can also be classified according to the underlying numerical method employed. Mesh-free strategies, such as the smoothed particle hydrodynamics (SPH), do not use structured meshes and are highly suited to highly deformable interfaces [139]. Spectral strategies, which model solution variables as expansions in orthogonal basis functions, hold the potential for very high accuracy for smooth flow but are not highly suited to complicated geometries [140]. Lattice Boltzmann methods (LBM) also emerged as an alternative to N-S solvers, with advantages in handling multiphase flows and complicated boundaries [141,142]. While these are not as widely used industrially in bioreactor CFD as finite volume methods (FVM) or finite element methods (FEM), they are avenues that need to be explored when it comes to modelling microbial fermentations, particularly in the treatment of multiphase hydrodynamics [24,141–143]. For example, Nikolić and Frawley (2016) [144] applied SPH to stirred tank systems, demonstrating that mesh-free methods can efficiently predict global mean flow and be coupled with population balance models, highlighting their potential in bioprocess contexts. Table 5 provides an overview of the most common numerical approaches and their typical application areas in microbial fermenter design.

Table 5. Classification of CFD numerical methods for bioprocess applications.

Numerical Method	Bioprocess CFD Applications	Advantages/Notes	References
FVM (with Reynolds Averaged Navier–Stokes RANS, Large Eddy Simulations LES, Direct Numerical Simulation DNS)	Hydrodynamics, mixing, impeller effects, turbulence models, mixing time in stirred bioreactors	Common in industrial and research settings; supports turbulence modeling (RANS, LES, DNS)	[47,62,69,79,89,145–149]
Euler–Lagrange/Compartment (Parcel-Based)	Modeling environmental gradients, Lagrangian microbial phase, zone-wise behavior for scale-down applications	Enables tracking microbial exposure to gradients; high computational intensity	[6]
LBM with LES hybrid	Substrate gradients, hydrodynamics in large-scale stirred reactors, microbial perspective	Offers dynamic accuracy with reduced computational costs vs. FVM; promising method	[24,141–143,150]
Multiphase Modeling with Population Balances (Euler–Euler + Multiple Size Groups MUSIG)	Gas-liquid mixing, bubble size distribution, $k_L a$ and oxygen transfer in industrial-scale fermenters	Captures multiphase interactions and mass transfer; computationally intensive	[151–157]
FEM	Multi-physics modeling, enzymatic/kinetic network integration, broader bioprocess simulations	Accurate for complex coupled systems; less common in fluid flow-specific bioreactor studies	[158]
Compartmental/Hybrid Models (CFD-based)	Integration of kinetics and fluid dynamics without full CFD; mixing time prediction in fermenters	Balances accuracy and efficiency; useful for real-time or scale-up models	[84,159–163]

It is usually highly recommended to create a high-quality mesh, as irregularities in the cell shape can affect the solution of the partial differential equations (PDEs); thus, the end solution can differ from what was expected. A mesh is usually deemed to be of high quality if it improves convergence, stability, or/and accuracy without negatively influencing other simulation parameters [164].

4.4.2. Impeller Rotation Modelling Approaches

Since the STBR is at the core of this work, the stirring performed by the impeller must be modelled as well. There are different approaches to model the rotation of the impeller

depending on the tip speed, turbulence, shear stresses on the cells, and the geometry of the impeller. Some of the most common approaches to model impeller rotation are discussed in this section. The most used approaches are the multiple reference frames (MRF), or the sliding mesh (SM) or arbitrary mesh interface (AMI) approaches [142,165–168]. While other impeller modelling methods exist, like the inner-outer iteration [169], and the circumferential averaging method [170], this work focuses on the MRF and SM techniques.

MRF model is a steady-state approximation, where the distance between the impeller and baffles is large enough. The flow can be assumed to be time-independent with respect to the impeller as the distance between the impeller and the baffles is assumed to be large enough [146]. Two distinct reference frames are employed to address the rotating domain and the stationary frame [8]. Within the MRF method, the "inner" and "outer" steady-state solutions are implicitly matched along a single boundary surface. The selection of this surface is not arbitrary, as it must be assumed in advance as a surface where flow variables exhibit minimum changes either with angular location or over time [171]. The MRF approach is computationally less demanding than the SM method due to the absence of overlap between the inner and outer regions [168]. On the other hand, the SM approach assumes a transient state of fluid flow. In employing this approach, the computational domain is partitioned into two submeshes, including one rotating with the impeller and the other fixed. The SM method permits the mobile mesh to undergo shearing and sliding relative to the rest of the mesh along the interface which enhances numerical stability [168]. Unfortunately, achieving a full-time solution for the low in a stirred tank significantly increases computational costs by an order of magnitude compared to those required for steady-state simulations [172,173].

Many studies have indicated that the validity of the MRF method is highly sensitive to the configuration of the rotating zone. Reid et al. (2025) [64] discovered that predicted mixing time is highly dependent on the chosen width of the rotating region, and De La Concha et al. (2019) [174] noted that both velocity distributions and power number predictions are strongly affected by the size of this region. Despite these sensitivities, the MRF method has been shown to be able to mimic experimental observation to an acceptable level of accuracy in simulations of multiphase and gas–liquid systems, provided that the model is implemented carefully [8,168]. In comparison, the sliding mesh method provides a time-dependent description of baffle–impeller interaction and thus is more accurate in resolving unsteady flow characteristics [146,175]. The increased fidelity comes at the expense of computational demand, which typically is one order of magnitude higher than that of the multiple reference frame approach. Thus, the MRF method is used in large-scale design studies, while the SM method is used in more detailed studies of local hydrodynamics. For instance, Foukrach et al. (2020) [171] showed that steady-state simulations can be used for comparing impeller geometries and screening out designs that reduce power consumption by up to 50 percent over traditional designs. These comparative studies illustrate that the choice of the method of simulating impeller motion directly affects the accuracy and utility of CFD predictions in STBRs.

4.4.3. Turbulence Modelling

Turbulence can be defined as the random variations in fluid properties, encompassing a broad spectrum of length and time scales [176]. While laminar flows exhibit stability, turbulent flows are chaotic, with turbulent diffusion leading to swift mixing, time-dependence, and encompass three-dimensional vorticity fluctuations with diverse time and length scales [176]. The range of the length and time scales depends on the Re number [177,178]. The prevailing theory on turbulence is grounded in the "energy cascade" concept developed by Kolmogorov [179]. According to this theory, turbulence consists of eddies of

varying sizes, each possessing a specific amount of energy determined by its dimensions. The larger eddies undergo disintegration, transferring their energy to smaller eddies in a cascading process. The newly formed smaller eddies, in turn, go through a similar break-up process, transmitting their energy to even smaller eddies. This sequence of break-up and energy transfer continues until the smallest possible eddy size is reached.

The N-S equations are not simple to solve, especially in complex cases. Therefore, it is necessary to utilize numerical methods to calculate approximate solutions. The calculation of these solutions, without incorporating any additional approximations is referred to as DNS [180]. However, this method is typically hard to employ due to the presence of turbulence. In practical terms, achieving DNS simulations is infrequent, except in scenarios involving very low flow rates, simple geometries or when substantial computational resources are accessible [168,178]. DNS is deemed to be not so useful for engineering interest due to the magnitude of the Re number [181]. This is because at equilibrium, the viscous dissipation rate at the smallest scale must equal the rate of the energy supply from the largest scales. However, potential advancements in computer technology could alter this scenario in favor of DNS in the future [106].

Two other very commonly used turbulence models in the field of turbulence modelling in STBRs are RANS and LES [182]. The prevalent method for addressing turbulent flow issues in industrial STBRs involves solving the RANS equations. In this approach, statistical averaging is performed based on a suitable time scale. The fundamental technique involves breaking down the flow variables into a time-mean value component and a fluctuating component [168]. These components are then substituted into the original equations, and the resulting equations are subjected to time averaging.

Many different turbulence models that are based on the RANS approach are based on the concept of eddy viscosity. Eddy viscosity is analogous to the fluid kinematic viscosity and characterizes the turbulent mixing or diffusion of momentum [88,123]. The two most common two-equation models used in the description of turbulence flow in STBRs are the k-ε family [183] and the shear stress transport (SST) k-ω models [106], and these are applied because they provide stable results for global quantities like circulation, mixing time, and power number at modest computational cost [47,88,146]. A third approach that has been observed in the literature is the Reynolds stress model [184]. These models encompass equations for each of the individual Reynolds stress components. Reynolds stress closures improve fidelity by resolving the stress tensor and are able to better reproduce anisotropic features such as secondary flows [184].

The biggest disadvantage with RANS approaches is the inability to capture flow details and its dependence on empirical correlations. Additionally, the k-ε models are insensitive to streamline curvature and system rotation [47,146,183] and are known to not be appropriate for anisotropic flows like the impeller discharge and baffle zones, which can lead to incorrect predictions turbulent dissipation and mixing predictions [185].

Another technique is LES, where the simulation directly captures large-scale turbulent structures, and smaller turbulent scales are represented using subgrid scale models. The central idea in LES involves filtering the N-S equation to decide which scales to retain and which to discard. This is accomplished by applying a spatial statistical filter represented by a specific function. LES is still quite computationally expensive [186]; however, with recent advancements in computer technology [147,187], the utilization of LES for solving industrial problems is gaining popularity.

LES and hybrid approaches [147,182,186,187] have demonstrated substantially greater accuracy in resolving transient eddies, blade-pass effects, and mixing-time distributions. An important feature that distinguishes transient approaches from Reynolds-averaged models is their ability to resolve the blade-pass effect, the periodic vortical structures generated as

impeller blades sweep past baffles and tank walls. These unsteady eddies play a critical role in driving macro-mixing, turbulence intensity, and gas dispersion, but are smoothed out in steady RANS models. LES and hybrid formulations have been shown to reproduce blade-pass fluctuations with good agreement to experimental data [147,182,186,187].

Lastly, a hybrid of the LES and RANS models can be utilized. One such example is the Detached Eddy Simulation (DES). The turbulence model equations act as RANS equations near the wall but progress to LES away from the walls. The DES approach seeks to combine the advantages of both RANS and LES; however, this approach cannot capture flow details near the wall regions due to the size of the scales near the walls [147,178].

The selection of turbulence model greatly affects the validity of CFD predictions in stirred-tank bioreactors, with comparison studies showing much variability in accuracy and applicability. LES provides improved resolution of unsteady vortices and blade-pass behavior, which leads to more realistic mixing-time predictions than Reynolds-averaged closures [145,165]. Within the k–ε family of models, Re-normalization Group (RNG) and realizable formulations perform superior to the standard version for the prediction of velocity distributions and power numbers, especially in regions of high anisotropy such as impeller discharge streams [174]. More recent evaluations demonstrate that even among widely used RANS models, the choice of closure—i.e., between k-ε, realizable k-ε, and SST k-ω—can alter mixing-time predictions significantly, underscoring the sensitivity of design outcomes to turbulence modeling assumptions [64]. At an industrial scale, CFD simulations have been compared with experimental measurements, showing the ability of state-of-the-art turbulence models to predict power consumption and mixing performance in production-scale bioreactors [23]. Rushton impeller research further demonstrates that turbulence modeling influences circulation and dispersion: LES and sliding-mesh simulations more realistically represent double-Rushton tank transient flow fields than steady approximations (simulations run on a single core—CPU) [188], and stress-blended eddy simulation enhances velocity and turbulence intensity prediction over RANS [187]. Additional comparative LES subgrid-scale model studies confirm their ability to resolve fine-scale structures governing mixing and mass transfer [189], and simulations of flow regimes spanning early to fully turbulent operating conditions illustrate how model choice affects predicted transition behavior for baffled and unbaffled tanks [190]. These case-specific studies are in line with more comprehensive reviews, which emphasize that turbulence closure selection remains one of the most important modeling decisions in pharmaceutical and biopharmaceutical CFD applications, as it dictates accuracy in mixing, oxygen transfer, and power-consumption predictions [191].

As highlighted by [168], the predictive accuracy of CFD depends strongly on turbulence modeling choices, which directly influence estimates of power input, mixing time, and oxygen transfer. Since these parameters are used to guide impeller design, baffle configuration, and aeration strategies, turbulence model selection plays a central role in bioreactor engineering decisions rather than being a purely numerical consideration.

4.4.4. Multiphase Modelling

Lastly, models describing two (or more) phase flows and the behavior of each fluid within the domain are to be discussed. These models fall under the category of multiphase modelling and typically find their purpose in the description of gas–liquid [23,63,134,192], solid–liquid [193], or even solid–liquid–gas [8,194,195] flows in CFD. As aerated fermentation in STBRs are the crux of this work, it is necessary to predict and model the gas and liquid phases in the domain.

Multiple different approaches with different use cases have been developed over the years, with the most used ones being Volume of Fluid (VOF) and Eulerian multiphase

models. Using such models, in addition to population balance models (PBM), bubble break-up, and coalescence models (for Eulerian models), enables the prediction of parameters such as the gas hold-up within a STBR, specific surface area, and oxygen mass transfer rates.

The VOF method demonstrates a high level of precision in accurately delineating the location and shape of the free surface [196]. It offers a straightforward technique for computing the movement of the free surface throughout each time step in a simulation. Moreover, the VOF method facilitates the uncomplicated enforcement of dynamic surface conditions in the cells surrounding the interface [197]. This model operates on the assumption that there is no interpenetration between distinct phases. By assuming that the phases share identical velocity and pressure fields, a single momentum equation is employed. The model introduces continuity equations for the volume fraction of each phase to track their respective interfaces. The model is particularly recommended for scenarios involving slug bubbles or larger bubbles, as commonly encountered in orbitally shaken systems [88].

In contrast, Eulerian multiphase methods are more widely used for STBR characterization and prediction of key parameters, as is evident by the number studies [8,63,152,192,198] that have applied a variety of Eulerian methods in combination with Lagrangian approaches and population balance distributions. Within this method, both fluids or phases act as interpenetrating continua and are represented by their volume fractions [199,200]. The Euler–Euler method involves the separate consideration of mass and momentum for each phase, allowing for the examination of interactions between phases [134,198]. This approach is particularly recommended when dealing with volume fractions of the dispersed phase exceeding 10% [88]. The Euler–Euler is more computationally efficient in terms of memory storage requirements and computer power. Consequently, the Euler–Euler approach is applicable across scenarios with both low and high superficial gas velocities. However, a drawback of this method is its limited ability to straightforwardly account for bubble-bubble and bubble-liquid interactions, necessitating the application of specific models to address these interactions [90].

Additionally, the Euler–Lagrange approach offers an alternative for multiphase modelling [73,198,201]. In this method, the continuous (liquid) phase is described in combination with a separate dispersed (solid/gas) phase that is tracked through Lagrangian equations. The trajectory of Lagrangian phase particles inherently requires a time-resolved treatment based on the flow pattern of the Eulerian phase [88]. The advantage of this approach is that each individual bubble is modelled, and therefore a better understanding of bubble–bubble and bubble–liquid interactions can be achieved. Mass transfer, redispersion and bubble coalescence can be easily modelled due to this advantage. However, not all the particles or bubbles can be tracked due to computational limitations [202]. Additionally, this model works better when superficial velocities are low [90].

In cases where the dispersed phase (in this case, the gaseous phase) exhibits a broad distribution of one or more physical properties, such as size, density, or shape, models based on the population balances equation (PBE) can be employed. The majority of Euler-Euler models typically adopt the assumption of an average bubble size [198]. This assumption is rationalized when modelling systems with a low bubble number density, such as bubbly flow regime in bubble columns, where weak bubble–bubble interactions and a narrow distribution of bubble sizes are prevalent [90]. However, in many industrially significant flows, there exists a considerably high bubble number density, leading to substantial bubble–bubble interactions. In such cases, a wide distribution of bubble sizes is observed, deviating significantly from the average bubble size assumption, most commonly seen in STBRs [152,203]. In the context of bioreactor CFD models, PBEs are commonly introduced to depict the size distribution of bubbles generated during aeration, where the characteristic parameter is the bubbles' number density. The number density within a control volume

can undergo changes due to processes such as convection, bubble coalescence and breakup, gas expansion, and mass transfer. Given that both bubble coalescence and break-up result in simultaneous increases and decreases in bubble sizes (i.e., two small bubbles merging into one larger bubble or one large bubble breaking into multiple smaller ones), the PBE incorporates four source terms that account for the "birth" and "death" of bubbles. The computation of these values necessitates specialized models, often derived from turbulence theory [88,202]. Additionally, population balance MUSIG models are also utilized often to model bubble break-up and coalescence within the STBRs. The bubble size distribution with this model is assumed to be divided into an appropriate number of size classes. For each of these size classes, the continuity equation as well as the source and sink terms due to coalescence and break-up are solved, with a single set of momentum conservation equation for all size classes [204,205]. The MUSIG model assumes a polydispersed gas and has been successfully implemented to predict key aspects of the STBR such as gas hold-up, mixing time, and aerated power input [152,204].

A major distinction is made between the homogeneous and inhomogeneous MUSIG formulations. In the homogeneous MUSIG model, it is assumed that all the bubble classes travel with the same mean velocity, which is less computationally demanding but restricts applicability to flows where slip velocities are minor. On the other hand, the inhomogeneous MUSIG model considers separate momentum balances for each bubble class, thereby improving bubble size distribution and gas–liquid slip velocity prediction in polydisperse flows [155,157,206]. Applications to bioreactor system problems have shown that these advanced formulations provide more realistic bubble dynamics and interphase mass transfer representations compared to simpler models [152,204]. Although computationally more demanding, they are more accurate and increasingly employed in CFD studies of stirred tank bioreactors.

Building upon these theoretical contributions, recent work has compared the predictive accuracy of alternative multiphase formulations. Euler–Euler models remain the most widely applied framework in both laboratory and industrial contexts because they efficiently predict gas holdup, circulation patterns, and overall hydrodynamics at relatively modest computational cost [8,192,203]. Their limitation lies in averaging bubble-scale dynamics, which restricts accuracy in interfacial area and local oxygen transfer predictions. Euler–Lagrange approaches overcome this by explicitly tracking individual or parcels of bubbles, allowing detailed analysis of turbulence–bubble interactions [202] and direct representation of coalescence and breakup [201]. However, both studies emphasize the high computational load of Euler–Lagrange formulations, which constrains their applicability to large-scale bioreactors.

PBMs are frequently coupled with Euler–Euler or Euler–Lagrange frameworks to capture bubble size distribution dynamics. Seidel and Eibl (2021) [198] showed that PBM coupling substantially improved predictions of the k_La in stirred tanks. Wang et al. (2021) [152] reported similar gains for bubble size and gas holdup predictions in dual impeller systems, while Maluta et al. (2022) [203] demonstrated that PBM integration is essential under high gas-holdup conditions to achieve reliable oxygen transfer predictions.

Geometric configuration further modifies multiphase performance, reinforcing the need for turbulence–closure–PBM combinations. Zhang and Yang (2023) [134] showed that semi-circular baffles enhanced circulation and gas dispersion but introduced flow structures that required advanced turbulence closures for accurate CFD results. Zhang et al. (2017) [194] quantified how different triple impeller arrangements altered power numbers and volumetric oxygen transfer coefficients, demonstrating the sensitivity of mass transfer performance to impeller configuration. Zheng et al. (2019) [195] validated

CFD predictions in three-phase reactors, confirming that impeller design and turbulence model choice directly influence phase dispersion and mixing uniformity.

Extensions to three-phase systems have confirmed the growing maturity of multiphase CFD frameworks. Gu et al. (2023) [193] combined experiments with CFD to validate solid–liquid mixing predictions in self-similar impeller tanks, while Chernyshev et al. (2023) [205] showed that discrete resolution of bubble size distribution functions strongly affects predicted flow structures in bubble columns. Together, these studies illustrate that accurate representation of solids and gas–liquid interactions require both validated multiphase closures and careful treatment of interfacial population balances.

Contemporary bioprocess-focused applications stress that theoretical robustness alone is insufficient; practical utility requires selective closure choice and systematic validation. Panunzi et al. (2022) [23] demonstrated that multiphase CFD models can reproduce industrial-scale mixing times and power draw when tested against experiments. Werner et al. (2014) [88] demonstrated the effect of shear stress distributions on cell viability, the influence of oxygen and nutrient gradients on cell growth and how CFD modelling can support STBR optimization to balance the hydrodynamic parameters such as mixing performance and quality with biological parameters. Kreitmayer et al. (2022) [73] validated CFD-based hydrodynamic predictions in SUS. Montante et al. (2008) [204] systematically analyzed bubble size distributions in aerated stirred tanks, where the role of breakup and coalescence models in shaping predicted bubble size, interfacial area, and gas holdup were investigated, all of which govern oxygen transfer performance. Collectively, these studies reaffirm that the multiphase modeling approach selection—either Euler–Euler, Euler–Lagrange, or hybrid PBM—has a direct impact on the calculated gas holdup, dispersion for the bubble, and mass transfer for the oxygen variables, all which are key parameters for scaling up aerobic bioprocesses for optimization.

4.5. CFD Models in Bioreactor Modelling

Characterizing and improving fluid flows in bioreactors is of utmost importance due to the high sensitivity of biological microorganisms to environmental changes [207]. Critical engineering parameters such as power input, mixing time, and oxygen mass transfer coefficient can be established to optimize cell growth and productivity while ensuring product quality during the active pharmaceutical ingredient (API) production process. Simulation of hydrodynamic conditions within the STBR can significantly reduce the necessity for time-consuming and expensive trial-and-error experiments, especially when working with limited biological materials like primary tissues or stem cells. Considering the uneven distribution of shear stress and turbulence within most bioreactors, the significance of obtaining spatially detailed flow data becomes even more evident. Such data can be acquired through either experimental technique (that are costly and resource-intensive) or computational simulations [88].

Table 6 depicts the literature that was utilized within this work to examine state-of-the-art CFD modelling techniques to model different aspects of the fluid flow. It is evident from examining the literature that almost all articles carried out a mesh independence studies with two to three differently sized meshes to analyze the effects of the mesh on parameters such as the velocity magnitude [79], k_La [208], and the power number [152]. Table 6 gathers select CFD case studies of stirred tank bioreactors that reflect the extent of approaches utilized in biotechnology. Making early seminal contributions to fundamental issues of turbulence modeling, Aubin et al. [146] comprehensively assessed how turbulence models and schemes affect stirred-tank prediction, and Lapin et al. [209] proposed a structured-segregated methodology to elucidate microbial population dynamics in turbulent flow environments. Following efforts expanded to cover gas–liquid systems and multiphase mix-

ing situations, with Ahmed et al. [210] simulating gas dispersion in multi-impeller reactors, Delafosse et al. [211] deploying Euler–Lagrange schemes to appraise heterogeneities, and Sarkar et al. [212] incorporating PBM to enhance multiphase mixing descriptions. Large eddy simulations have furthermore been used, for example by Zadghaffari et al. [145], to explicitly resolve turbulent structures in the vicinity of Rushton turbines. More recent work focuses on process intensification and optimization. Shu et al. [213] coupled CFD with Taguchi methodology for process optimization, while Wright et al. [214] assessed uncertainty in microbial growth kinetics propagation to CFD-based scale-up prediction. Other recent works reflect applied applications, with Mittal and Kikugawa [215] modeling stirred tank reactors in industrial applications, and Amer et al. [208] expressing CFD-derived oxygen transfer coefficients in operating parameters. A number of studies furthermore explore digital and data-driven architectures, such as Bach et al. [31] in pilot-scale assessment of mass transfer, Ebrahimi et al. [79] in double impeller hydrodynamics, and Oblak et al. [29] in digital twinning of stirred tanks. Complementary advances in multiphase modeling consist of Hu et al. [8] with OpenFOAM-based simulations of multiphase systems and Wang et al. [152] with CFD-PBM coupled model for dual-impeller setups. Generalizing, these papers demonstrate that CFD has evolved from validation of turbulence closure and hydrodynamics to integral schemes combining PBM, process optimization, and digital twins. But they also mirror persistent issues like needing robust experimental verification, coping with biological heterogeneity, and computational expense of new turbulence or population balance schemes.

Building upon the overview presented in Table 6, the application of CFD and its contribution to different aspects of bioreactor design and optimization, with particular attention to microbial systems such as *E. coli*, was investigated. Recent applications [6,216–218] of CFD in *E. coli* bioreactors highlight its growing role as a predictive tool for STBR design and parameter optimization. Nadal-Rey et al. (2023) [216] coupled CFD with lifeline analysis to show that such modeling can capture oxygen and substrate heterogeneities experienced by *E. coli* in large-scale stirred tanks. Their approach provided actionable insights for optimizing impeller and baffle geometry to minimize metabolic stress. Similarly, Mayer et al. (2023) [217] used CFD to guide the development of a plug-flow scale-down reactor. Of course, this paper does not model an STBR, but this approach can be applied to an STBR configuration. They validated the model with E. coli BL21(DE3) cultivations. This CFD-informed flow field design significantly improved experimental fidelity. Singh et al. (2024) [6] discusses the potential of integrating CFD-predicted hydrodynamics with kinetic models, thereby linking mixing conditions directly to cellular metabolism. In their review, they provided detailed information on how hydrodynamic parameters such as agitation and aeration as well as biological parameters such as feeding strategies can be combined to optimize product yields. Ganguly et al. (2021) [218] applied CFD to assess impeller-sparger configurations in oxygen-water systems, showing that geometric choices directly influenced bubble distribution and oxygen transfer. Collectively, these studies establish CFD as a versatile tool that can be integrated with biological and kinetic models. Such integration makes it possible that informed decisions on impeller selection, sparger placement, mixing strategy, and scale-down design in microbial STBRs, can be made with both hydrodynamic and biokinetic parameters combined. Such strategies are promising as they ensure both process efficiency and experimental relevance.

At an industrial scale, CFD is commonly applied to validate power consumption and mixing predictions under realistic operating conditions. Panunzi et al. (2022) [23] presented a case study of aerated stirred-tank bioreactors. The study combines CFD simulations with plant-scale measurements of mixing time and power draw. A strong agreement between the CFD model and experimental data was achieved, thus, confirming that CFD can reliably

reproduce industrial hydrodynamics and serve as a tool for operational optimization. Prado and Dyrness (2020) [219] outlined a generalized framework in their work. Multiphase CFD simulations are linked to key performance indicators, such as mixing efficiency and k_La. Their study emphasized that integrating CFD multiphase models provides a quantitative basis for evaluating bioreactor performance. Nadal-Rey et al. (2022) [89] validated their CFD model of an industrial fermenter using Newtonian broths. CFD predictions of mixing behavior and oxygen transfer were validated against experimental data. The findings show that CFD can not only capture global mass transfer characteristics but also resolve localized gradients that impact microbial performance. These case studies depict CFD as an important modelling tool for STBR design, as it aids engineers in the prediction of power consumption, optimization of agitation and aeration strategies, and anticipation of oxygen and mass transfer limitations before costly and rigorous pilot studies or plant trials.

Lastly, many recent works [26,132,193,220,221] have drawn their focus on the improvement of impeller design and optimization of geometric configurations to enhance hydrodynamics and mass transfer in STBRs. Hoseini et al. (2021) [26] coupled CFD with fluid–structure interaction for the purpose of impeller shape optimization. They demonstrated that structural deformations under load can influence flow fields and that CFD-FSI coupling gave crucial information on impeller shape. This proved to improve mixing while reducing mechanical stress. Similarly, Jia et al. (2022) [132] employed CFD to evaluate novel disc turbine configurations. The work achieved in showing that modified blade geometries enhanced circulation patterns and mixing efficiency. Maluta et al. (2023) [220] systematically analyzed hydrodynamics, power consumption, and bubble size distributions in gas-liquid stirred tanks. They showed that there is a strong interaction between impeller design and aeration efficiency. Additionally, Gu et al. (2023) [193] combined CFD simulations with experimental validation to study solid–liquid mixing using a self-similarity impeller. They confirmed that optimized impeller geometries improve suspension quality and reduce dead zones. Ali et al. (2022) [221] investigated the effect of geometric parameters such as blade angle and clearance on k_La in non-Newtonian fluids and succeeded in providing a direct link between design choices and oxygen transfer performance. These studies show how CFD-driven analysis of impeller and geometry design can aid in the identification of important parameters and their interactions and connections with each other. This can aid engineers to make informed performance-based decisions on STBRs design in an efficient and cost-effective way.

The most used impeller rotational model was the MRF approach. The popularity of this approach is caused by the simplicity of application and the lower computational expense as compared to the SM. However, MRF can only be utilized with proper accuracy when the fluid flow (with reference to the impeller) remains the same between the impeller and the baffles. Wang et al. [152] has utilized the SM approach, using MRF and single phase as a starting point (to simulate steady state flow) and then switching to SM (transient state) with two-phase flow after the single phase MRF simulation had converged.

Recent studies have shown that Lattice Boltzmann large eddy simulations (LB-LES) offer an efficient and accurate approach for resolving hydrodynamics in stirred bioreactors used for microbial fermentation. For instance, Haringa (2022) [142] used LB-LES with Euler–Lagrange particle tracking to simulate substrate gradients and microbial "lifelines" in a pilot-scale stirred tank, demonstrating reliable predictions of flow velocity, turbulence, and mixing relevant to fermentation scale-down. Meanwhile, Kersebaum et al. (2024) [24] validated LB-LES models of Rushton and pitched-blade turbines, matching impeller discharge hydrodynamic metrics and mixing times across viscosity regimes typical of fermentation media. Despite its promising attributes—such as mesh-free simulation and efficient runtime—Lattice Boltzmann CFD (particularly LB-LES) has not yet been broadly adopted

in industrial stirred bioreactor applications for microbial fermentation [24,150]. While validation studies (e.g., [142]) showcase its accuracy for hydrodynamics modeling, developers note a lack of extensive industrial validation and deployment. Reviewing broader industrial CFD trends, Sharma et al. (2019) [150] highlight limitations in handling high Reynolds number turbulence and the relative immaturity of turbulence models within LBM compared to mature N-S-based methods.

In addition to momentum, mass, and energy balances, another fundamental balance required by bioprocess modelling is the species balance. It describes the transport and consumption or production of substrates, gases, and metabolites in the STBR. Equation (12) describes a general format of the species balance [222].

$$\frac{\partial \omega_\alpha}{\partial t} + \vec{v}.\vec{\nabla}\omega_\alpha = D_{\alpha s}\nabla^2\omega_\alpha + r_\alpha \quad (12)$$

where $\vec{v}.\vec{\nabla}\omega_\alpha$ is the convective mass transfer, $D_{\alpha s}\nabla^2\omega_\alpha$ is the molecular diffusion, and r_α is the net rate of production.

4.6. CFD Models and Artificial Intelligence (AI) Methods

The integration of CFD with AI tools such as machine learning (ML) and artificial neural networks (ANNs) has emerged, over the last few years, as a promising strategy to overcome the limitation of high computational demand characterized by CFD application in STBRs modelling. Cantarero-Rivera et al. (2024) [223] demonstrated that ANNs can correct coarse-mesh-induced errors in CFD simulations of cell culture bioreactors, effectively reducing the computational cost of mesh refinement without sacrificing accuracy. Similarly, Chen et al. (2025) [224] applied ML to predict mass transfer in gas-liquid STBRs, achieving reliable k_La predictions without full-scale CFD runs. Chen and Xia (2024) [225] highlighted the potential of optimization frameworks incorporating ML to improve fermentation scale-up parameters, while Helleckes et al. (2023) [226] emphasized the transition of ML in bioprocess development from conceptual promise to practical deployment.

Hybrid frameworks are also gaining traction. Jiang et al. (2025) [227] developed a CFD-ANN-NSGA-II model for stirred reactor design by combining CFD simulations with evolutionary optimization, with the aim of accelerating reactor configuration screening. Zhao et al. (2024) [228] demonstrated multi-objective optimization of radially stirred tanks by integrating CFD with ML algorithms, showing the utility of such approaches for design space exploration. Rahimzadeh et al. (2024) [229] applied ML to coaxial bioreactors, predicting torque and flow classification directly from CFD-generated data, illustrating how data-driven surrogates can capture key hydrodynamic responses. Karimi Alavijeh et al. (2024) [230] provided a perspective on ML in bioreactor scale-up. They outlined opportunities for surrogate models and hybrid CFD-AI approaches to manage the complexity of industrial-scale simulations. Savage et al. (2024) [231] further illustrated that CFD remains essential for hydrodynamic accuracy. However, they also show that integrating CFD modeling with ML can significantly reduce computational expense in large-scale multiphase flows.

Such studies demonstrate that AI-enabled CFD not only reduces computational demand but also broadens CFD applicability in the bioprocessing field by enabling faster predictions, sensitivity analyses, and parameter optimization. The incorporation of ML into CFD frameworks therefore represents a critical step toward making high-fidelity simulations practical for bioreactor scale-up and industrial deployment.

Recent reviews and methods papers consistently report that bioreactor ML suffers from heterogeneous, non-standardized datasets, limiting model training and out-of-domain generalization across geometries, impellers, and operating regimes [226,230]. Unlike other

CFD areas that now publish public benchmarks (e.g., CFDBench; curated turbulence datasets), the stirred-bioreactor domain lacks comparable, shared datasets and verification protocols, slowing reproducible progress [232–234]. Consequently, while AI is a powerful complement to CFD, fully integrated, biologically informed, industry-scale frameworks are still being actively developed [235].

Table 6. Different case studies of CFD applied to STBRs in biotechnology.

Aim	Operational Set-Up	Operating Conditions	Validation	CFD Model	Results	Reference
Experimental validation comparison with simulation	Two cylindrical bioreactors STBR 1: baffled, Rushton turbine, air injected with a ring sparger at the bottom of the tank into water STBR 2: baffled, three impellers with the bottom impeller being a Rushton, and the middle and top are pitched-blade downflow turbines	Superficial velocity: 0.01 m/s Uniform bubble diameter 0.5 cm for STBR 2 For tri-phase the particle diameter is constant at 150 μm and density of 1190 kg/m^3 Impeller speeds of 3.78 and 5.08 RPS for two-phase simulations	X-ray Computed Tomography (CT) Experiments for gas hold-up measurements	Solvers: Reacting two phase Euler foam for STBR 1, Reacting multiphase Euler foam with tri-phase for STBR 2: air, water and polymethyl methacrylate particles No-slip boundary condition at the tank wall and baffles Constant gas inlet velocity and atmospheric pressure at gas inlet and outlet respectively	Good agreement of gas hold-up in STBR 1 between simulations and experimental data Similarly also for STBR 2 with the exception of the calculated gassed power consumption smaller than experimental value Bottom Rushton turbine flooded with particles in tri-phase simulation, with a radial pumping flow at the upper turbines	[8]
MRF evaluation	Reactor: Height = Diameter = 30 cm Four baffles of 3 cm width arranged at 90° intervals along the tank Impeller: 45° pitched turbine blade “Pumping down” impeller with four blades Axial location 10 cm from reactor bottom and diameter of 10 cm	-	Laser-Doppler Anemometry (LDA)	MRF RANS k-ε turbulence model Solver: SIMPLE algorithm	Simulation results somewhat match the experimental velocity profiles Velocity vector plots and turbulence intensity contour plots Axial velocity depicted as a function of dimensionless radial coordinate Biggest discrepancy in the axial velocity profile near the impeller Size of MRF domain near the impeller can influence the solution Zone interfaces should not be close to the impeller or baffles	[215]
Mixing time and k_La with prediction potential	Torispherical-bottomed cylindrical and baffled STBR with one impeller in an up-pumping configuration Liquid level H = 0.7–1.65 T Loading volume range of 150–350 L	Agitation speeds of 150, 320 and 400 RPM	Tracer experiments with sodium chloride Power number	Standard RANS k-ε turbulence model Average Navier–Stokes Euler–Euler approach for steady state runs Transient rotor–stator interface approach for unsteady state runs	Mixing time θ_{95} for power inputs for water and xanthan gum ranging from 0.5 to 9.2 kWm^{-3} using the CFD model CFD model to predict k_La validated with independent data and as accurate as empirical correlations for k_La estimation Bubble size dependent on gas flowrate and power input for the investigated conditions	[31]
Validation of a Euler–Lagrange modelling approach coupling a CFD-based compartment model (Eulerian approach) and a stochastic model based on a Continuous-Time Markov Chain (Lagrangian approach)	Hemispheric bottom vessel H = T = 0.305 m Working volume of 20 L Axial impeller D_i = 0.125 m Clearance from bottom C_i = T/3 Two baffles positioned 180° from each other	Water as single phase Rotational speed 100 RPM	PIV optical trajectography Tracer experiments with 4 mL NaCl solution	Standard RANS k-ε turbulence model SM	Good reproducibility of the concentration evolution after pulse injection by the CFD simulation Good representation of the turbulent flow by the CFD/compartment model However, no consideration of gas phase and thus only suitable for cultures with low oxygen demand	[211]
Evaluation of mixing in baffled and unbaffled vessels	Different reactor types	Distilled water at 25° Mixing speeds of 30, 90, 120 and 200 RPM	Tracer experimental tests with 1M NaCl solution and conductivity measurements Dissolution of sucrose	MRF RANS k-ε turbulence model Python script utilized to discretize the normal distribution of the sucrose crystals into 100 size classes	Good agreement between experimental and simulated tracer and sucrose dissolution tests 3D geometry of the stirred vessel and the impeller strongly affect the fluid flow, and it should be good practice to use CFD to examine this effect as assumptions (such as the improvement of axial flow with baffles) is not always to be observed	[29]

Table 6. *Cont.*

Aim	Operational Set-Up	Operating Conditions	Validation	CFD Model	Results	Reference
Prediction of bubble size distribution (BSD) and a more efficient approach towards optimized mixing	Cylindrical STBR with spherical bottom Three impellers: Rushton impeller, two three-blade propeller type impellers with each blade bent at a 24° angle Four baffles in STBR Pipe sparger	Impeller speed 200 RPM	k_La prediction	MRF k-ε turbulence model Euler–Euler multiphase Population balance model	Optimized mixing achieved by increasing shear in the system through an increase of impeller speed to create smaller bubbles Good agreement of CFD with experimental results	[212]
Modelling: Aerobic fermentation	STBR with impeller types of bent blade disc turbine, concaved blade disc turbine, and Rushton turbine of 4 baffles T = 175 mm Height of the tank = 240 mm H = 125 mm B_w = 12 mm; height of baffles = 220 mm; clearance of baffles and tank wall = 2 mm D_i = 12 mm Height of impeller above tank bottom C = 47.5 mm Height of air sparger above tank bottom G = 10 mm Thirteen holes are evenly distributed along sparger	Impeller speeds: 400–700 RPM	Experimental fermentation	CFD-Taguchi approach Iteration: 1000 steps Two-phase RNG k-ε turbulence model Eulerian multiphase conditions: average bubble diameter 4 mm	Three key viscosity values and their corresponding consistency phases as control parameters were identified by examining the viscosity growth curve throughout the reaction Control parameters were subjected to quantitative assessment to gauge their impact on the fermentations	[213]
CFD-based kinetic in an industrial bioreactor	Stirred tank reactor with Rushton turbines Sparger in the rotating domain Baffles and coils in the stationary field	Glucose was inserted through the top at feed rates: 0.5 kg/s, 1.0 kg/s, 1.5 kg/s, and 2.0 kg/s Impeller speed 69 RPM	-	Single liquid phase Standard RANS k-ε turbulence model Steady state	Cells were found to flourish in aerobic conditions, but some sections also experienced anaerobic digestion As the mass flow rate increased, the area undergoing anaerobic digestion expanded Glucose content varied by 2–5% at all flow rates due to uncertainties in the kinetic factors that govern aerobic metabolism As the fed-batch process advanced, the glucose gradient level increased due to the larger capacity and longer mixing time At the beginning of the study, the model showed the most significant response to the basic model	[214]
Investigation of gas-liquid two-phase flow characteristics in stirred tank with two combined dual impellers	Cylindrical tank (T = 420 mm) with standard ellipsoidal at the bottom of the tank Four equally spaced baffles Clearance between baffle and tank wall 2 mm Heigh of liquid in tank 500 mm Ring sparger (diameter 210 mm) below the lower impeller with 20 downward-facing holes Three impellers used with diameter T/2 (2 impellers used in combination in each set-up): Six-bent-bladed turbine (6BT) as the lower impeller Six-inclined-blade down-pumping turbine (6ITD) Six-inclined-blade up-pumping turbine (6ITU) as the upper impeller	Tap water and air used Gas flowrate 0.76 m^3/h For CFD simulations: Impeller speed 60–120 RPM For PIV measurements: Impeller speed 60 RPM	PIV CFD-PBM coupled model validated based on power consumption experiments and BSD	MRF Standard RANS k-ε turbulent model Euler-Euler multiphase model PBM to solve BSD with Luo break-up and Luo and Svendsen coalescence—MUSIG model	Effects of impeller speed and gas flowrate on flow fields, gas hold-up, BSD, gas-liquid interfacial area examined Presence of gas changes the flow field structure and can improve fluid mixing with 6BT + 6ITU 6BT + 6ITU can achieve more uniform bubble sizes with improved bubble dispersion performance compared to the other impeller configuration (6BT + 6ITD) Gas hold-up distribution and gas-liquid interfacial area with this configuration more well-distributed Gas hold-up vastly improved with increasing impeller speeds compared with increasing gas flowrates High impeller speeds more beneficial to the increase of gas hold-up in comparison to gas flowrates CFD simulations of power consumption close to experimental data with a maximum deviation of 6.3%	[152]

Table 6. *Cont.*

Aim	Operational Set-Up	Operating Conditions	Validation	CFD Model	Results	Reference
Investigation of utilization of LES approach to simulate and predict different aspects of mixing in a stirred tank	Baffled tank with diameter T = 270 mm Liquid height in tank H = T = 270 mm Rushton turbine with diameter 90 mm with a distance of 90 mm from the vessel bottom	Water at 25 °C used Impeller speed 250 RPM	Experimental data available in literature	MRF as a starting point and then switched to unsteady state (SM) Standard RANS k-ε turbulent model used as a starting point until steady state flow field; these results used as initial approximations for LES turbulent model Smagorinsky–Lilly model as a subgrid model	Flow field, power consumption, mixing time, turbulent kinetic energy and turbulent dissipation rate were predicted Good agreement between CFD simulations and experimental data—mean tangential and axial velocities, radial average velocities, power consumption and mixing time Mixing time depends on feed points due to a couple of reasons: 1. Inner rotating mesh was main promoter of tracer distribution 2. Lack of tangential exchange of tracer between flow loops which were in between the baffles Increasing the Re value creates a stronger radial out-flow which pushes the tracer into the recirculation loops and reduces mixing times Comparison of LES and RANS predictions of the tracer concentration profile with experimental data demonstrates improved predictions with LES that can result in more reliable design of the mixing process CFD model deviate from experimental data closer to the impeller tip as the simulated flow field shows this to be mostly symmetrical but experimental data are slightly skewed toward the upper side of the impeller	[145]
Investigation of the effect of modelling approach, discretization scheme and turbulence model on turbulent flow in stirred tanks	Dish-bottomed cylindrical tank T = H = 0.19 m Four equally spaced baffles with width T/10 Six-blade 45° pitched blade turbine with diameter D_i = T/2 Hub diameter 0.2D Positioned at T/3 on a shaft that extended from the vessel base to the liquid surface	Water at 273 K Impeller rotational speed 300 RPM (Re = 45,000) Up- and down-pumping configuration	LDV	SM, frozen-rotor model and circumferential averaging model Standard RANS k-ε turbulent model and RNG k-ε turbulent model	Choice of impeller model only slightly affect the mean radial and axial flow patterns in the impeller discharge region and only slightly underpredict the dimensionless turbulent kinetic energy Discretization scheme had no effect on mean radial and axial velocities in the vessel and underpredicted the dimensionless turbulent kinetic energy, with first order schemes underpredicting it the most First order UW underpredicted a swirling region underneath the impeller Both turbulence models had no significant effect on the mean radial and axial velocities Dimensionless turbulent kinetic energy values also underpredicted by both turbulence models, especially in the discharge region of the impeller CFD simulations somewhat underpredicted dimensionless turbulent kinetic energy and power numbers and overpredicted the circulation numbers in both up- and down-pumping configurations LES predicted better the kinetic energy levels that match better with the experimental data Discrepancies in the prediction of turbulent parameters maybe come from Reynolds averaging	[146]
Identification of various flow regimes in dual Rushton turbines stirred bioreactor for various gas flowrates and impeller speeds	Baffled cylindrical acrylic vessel with T = 160 mm and height 250 mm Dual impellers mounted on the shaft First impeller 90 mm and the second 110 mm from the vessel bottom Rushton turbine with diameter 64 mm Liquid height of 240 mm Ring sparger	Different flowrates and impeller speeds used for various different tests Gas flowrates 0.3, 0.5 and 1.0 vvm Impeller rotation speeds range 200–600 RPM Tracer experiments: hydrochloric acid	Tracer experimental tests with 1 M hydrochloric acid solution and pH measurements Measurements of gas hold-up distribution	MRF Standard k-ε turbulence model Euler–Euler multiphase model MUSIG model with break-up and coalescence modelled using isotropic turbulence theory	Gas hold-up increases with an increase in impeller rotational speed Mixing time varied depending on the operating flow regimes Good agreement between experimental data and CFD simulations	[210]

Table 6. *Cont.*

Aim	Operational Set-Up	Operating Conditions	Validation	CFD Model	Results	Reference
Model development of gas-liquid mixing and bubble size distribution to predict the effect of using ring or pipe spargers and impeller diameter on k_La	50 L two-chamber single-use bioreactor vessel T = 38 cm and height = 67 cm H = 42 cm Three-blade impeller pitched at 30° D_i = 22.8 cm Air sparger was a pipe with length 3.1 cm and pore sizes of 10 µm	For CFD, different D_i, pipe spargers with different lengths and ring sparger with different diameters examined. Impeller tip speeds of 0.6, 1.2 and 1.8 m/s Air sparging rate set at 0.02, 0.05 and 0.1 vvm	k_La measurements PIV	MRF k-ε dispersed turbulence model Euler–Euler model Population balance model with different sizes of bins	Population balance model accounted for bubble coalescence and break-up absolutely necessary for accurate prediction of multiphase flow Ring sparger showed better performance over the pipe sparger when comparing k_La and ga hold-up Optimum diameter shown to be 80% of the impeller diameter k_La prediction with constant bubble size simulation proved to be very different from experimental results Population balance with different bin sizes predicted more realistic k_La values k_La directly proportional to the impeller-to-vessel diameter ratio raised to the power of 2.8	[208]
Analysis of the influence of impeller configuration and rotational speed on hydrodynamic behavior and mixing performance of the STBR with double impeller	0.02 m^3 fermenter; T = 0.263 m Two different impeller configurations utilized Clearance from tank bottom C_i = 0.088 m Four baffles Baffle width 0.025 m Total liquid volume 0.015 m^3; H = 1.14T	Water at room temperature Three different impeller speeds: 50, 100 and 150 RPM	Power number comparison	Simulations performed with the High-Performance Computing Virtual Laboratory Canada MRF k-ε turbulence model	Good agreement of power values between simulations and experimentally measured values Higher interaction between impellers with an increase in rotational speed Increase in rotational speed leads to a rise in power values, average strain rate magnitude and average shear stress values, with a simultaneous decrease in mixing time Different impeller configurations exhibit different Flow numbers, power numbers and average shear stress values	[79]
Characterization of heterogenous cell population in an STBR with unideal mixing	*E. coli* 0.9 m^3 stirred tank reactor		Only indirectly experimentally validated	Euler–Lagrange simulations with Lagrangian reaction coupling Structured cellular model applied for sugar uptake	CFD simulations and kinetic model validation with experimental data from literature Glucose concentration field data is qualitatively verified from experimental observations from the literature	[209]

4.7. Limitations of CFD

Despite the different ways in which CFD can be utilized for the prediction of optimum operating conditions in an STBR, for greater comprehension of the fluid flow and fluid characteristics and their effects on the cell nutrition and growth, there are some limitations of this modelling technique that need to be kept in mind. The preceding results shed light on how CFD can enhance the efficiency of process development and optimization in the production of biotechnology products. However, it is crucial to be mindful of certain limitations when utilizing CFD modelling.

The most significant limitation arises from the fact that CFD solutions primarily rely on physical models of real processes, and as such, the accuracy of these solutions is inherently constrained by the precision of the models incorporated into the software [168,236]. Given that CFD is often employed to simulate highly complex problems, these models are susceptible to inaccuracies. For instance, turbulence modelling, essential for various flow processes, can frequently deviate from experimental data [47]. Because simulations inherently cannot replicate reality perfectly, CFD simulations are usually meant to be accurate enough to serve as a cost-effective complement to physical experiments [88]. Errors in CFD simulations can be classified into model errors, discretization errors, iteration-convergence errors, rounding errors, and programming/user errors, with the latter being the only avoidable type [188]. Model errors, often the largest and hardest to estimate, play a significant role, especially in two-phase bioreactor simulations where choosing the right model is critical [237]. CFD faces limitations due to the lack of suitable models for complex physical aspects, particularly within the realm of RANS-based two-fluid (or Eulerian–Eulerian) models [238]. These

models are essential for simulating industrial bioreactors. For example, the aerated power consumption of aerated fermenters is significantly influenced by factors such as gas cavity patterns, aeration rates, impeller speed [239], and bubble size distribution [240]. These are challenging to predict, especially when a high-volume fraction of the gas phase alters the turbulent flow field of the liquid phase compared to a single-phase system with the same geometry and impeller speed.

Specific challenges arise in the realm of biopharmaceutical CFD. Reaction modelling, especially capturing complex chemical reactions involved in biopharmaceutical synthesis, poses a significant challenge [6,159]. Modelling the behavior of biomass, particularly cells producing the desired product within their cell membranes, adds another layer of complexity [241]. Additionally, the inherent time scale of fermentation processes can be incompatible with the simulation time, making it challenging to accurately model and predict real-time fermentation dynamics [6,159,216]. As can be seen by the research conducted within the scope of this work, studies utilizing CFD as the only method of bioprocess investigation have made an indicative impact on process improvement through the identification of non-ideal hydrodynamics and how that can cause yield losses. Additionally, it has helped with bioreactor design [242,243]. However, process improvement is still dependent on comprehensive experimentation, as the complete application of data generated through CFD simulations cannot be achieved if it is unable to fully capture cellular responses to spatiotemporal flow information [6,244]. Modeling large-scale processes using CFD is complex due to the wide range of time and spatial scales involved. While the overall mixing efficiency depends on the global flow patterns within the reactor, localized interactions between the liquid flow and gas bubbles affect bubble formation and merging, which in turn impacts oxygen transfer between phases [201]. Additionally, because fermentation is often carried out in fed-batch mode, the model must account for the process's dynamic behavior over time. This is especially the case when biological activity alters the broth's rheological properties through substrate depletion, production of metabolic by-products, or temperature changes [245].

While CFD offers very detailed information about flow, mixing, and mass transfer, application of CFD to microbial bioreactors also reveals draconian limitations. First, CFD models attempt to classify microorganisms as a homogeneous phase, hence overlooking heterogeneity at the single-cell level; this heterogeneity has been shown to significantly affect microbial population robustness and process performance [246]. Second, combining CFD with detailed metabolic or genome-scale models has the potential to provide valuable mechanistic insight, although such combination is computationally intensive and remains at case-study levels [6,247]. Third, validation of CFD predictions is hindered by the challenge in quantifying precise local oxygen, substrate, and by-product gradients at industrial scale; additionally, such simulations become computationally demanding, which confines their wider application to routine bioprocess design [248]. Finally, despite all these troubles, recent applications reveal CFD potential in sustainable design. Yu et al. (2025) [46] successfully employed CFD for bioreactor optimization in *Bacillus subtilis* and achieved substantial cost reduction in enzyme manufacturing. As such, these examples outline the dual reality of CFD in bioprocess engineering: current constraints in biological modeling, computational requirement, and experimental verification, but more so, a growing body of proof for its revolutionizing role in sustainable microbial fermenter design.

Another notable challenge with CFD involves truncation errors resulting from approximations in the governing equations. These errors diminish as the mesh becomes finer. However, this refinement also leads to increased computational time and memory usage [237]. Factors affecting mesh quality, such as skewness, smoothness, and aspect ratio, play a pivotal role in ensuring accuracy and convergence of the solution [25,167]. Con-

sequently, mesh independence studies are conducted during the model creation process. These studies ensure that the mesh strikes a balance, avoiding excessive coarseness that might yield an inaccurate or suboptimal solution while preventing excessive fineness that would result in unnecessarily prolonged processing times [27,88,168]. Conducting mesh independence studies is a mandatory practice in CFD, involving systematic variations in mesh parameters to ensure that the results are insensitive to changes in mesh density [249]. This rigorous approach is vital to guarantee that the obtained solutions are robust and free from numerical artifacts arising due to inadequacies in the mesh. Additionally, discretization errors can be reduced through the utilization of techniques like Richardson extrapolation, grid systematic refinement, or the grid convergence index, with higher quality meshes improving accuracy [237]. However, refining the grid increases computational time exponentially and only gradually improves the solution's accuracy [237].

CFD predictions and simulations are validated by comparing them with experimental data to precisely quantify any model-related errors and make informed use of the results [237]. To manage complexity and computational time effectively, assumptions are frequently introduced while preserving the essential characteristics of the problem. Experimental data serves as a crucial benchmark for assessing the accuracy of computational models that have been described within this work, ensuring that they faithfully capture the underlying physical phenomena. This alignment is particularly critical in applications like fluid flow in STBRs, where precise knowledge of the fluid characteristics and their connection with biotechnological parameters is of crucial importance [25]. Estimating total error requires validating CFD results with physical experiments, using methods such as PIV, LDA, or laser-induced fluorescence for flow field validation. For custom-developed CFD codes, verification is also essential [237].

Validation studies provide an essential feedback loop, allowing researchers to refine and improve their models based on empirical evidence, enhancing the fidelity of CFD predictions. When applied to process design, validation typically proceeds after a thorough and precise simulation [88]. A comprehensive understanding of the process, including its hydrodynamics and flow patterns, is essential for the accurate interpretation of data derived from the simulation. Validation and simulation often operate synergistically, each informing the other in a quasi-iterative process. However, simulations can be conducted before experimental validation to formulate hypotheses and propositions regarding the most optimized mode of operation. Different validation methods have been found in literature (Figure 5), ranging from tracer experiments with dye, NaCl, or HCl/mixing time/RTD [23,49,79,250], power consumption and power number [27,79,193], k_La measurements/oxygen mass transfer [208], and gas hold-up [134]. Additionally, contactless measurement methods such as particle image velocimetry (PIV) [77,152,165,204,251,252], planar laser-induced fluorescence (PLIF) [253,254] and laser-doppler velocimetry (LDV) [255,256] are all common experimental methods to validate CFD simulations.

In the PLIF, fluorescent dyes are introduced into the fluid, which are then excited by a laser sheet. The resulting fluorescence is captured by cameras, and the intensity variations are analyzed to visualize and quantify concentration fields, gas distribution or mixing patterns within the bioreactor [254]. In PIV, the liquid is seeded with tracer particles, and the flow is illuminated with a laser sheet. High-speed cameras capture the particle movements, and software analyses the displacement between consecutive images to calculate the velocity field within the bioreactor [257]. In the shadowgraphy technique, diffuse light is shone on one side of the bioreactor, while the shadows cast by gas bubbles are captured on the opposite side by a charge-coupled device (CCD) camera and analyzed using image processing software [258]. A laser, paired with a diffuser, can serve as the light source. In the LDA method, the laser beam is divided by a beam splitter,

and the beams intersect within the bioreactor through a lens [257]. The measurement occurs in the region where the beams cross. The Doppler-shifted frequency is detected by a photomultiplier tube and then analyzed. In the ultrasonic method, a transparent bioreactor is not required. A ring of transmitters and receivers can monitor the horizontal plane of the bioreactor, allowing for simultaneous measurement of multiple gas bubbles. The bubble size is calculated by assessing the time of flight [259].

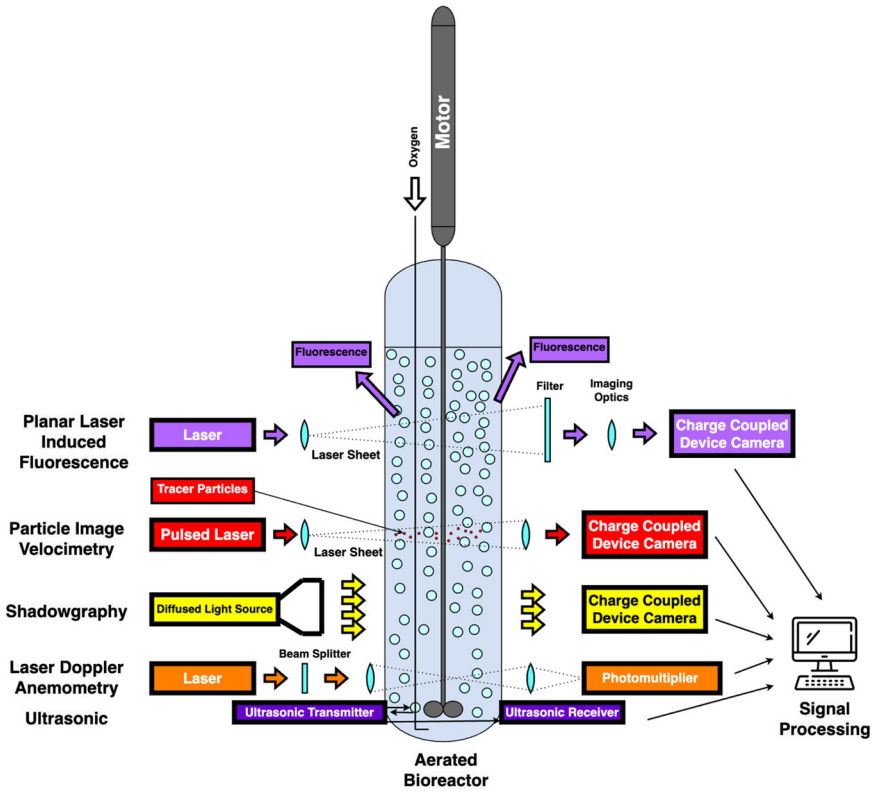

Figure 5. Schematic representation of five optical methods for validation; dimensions not to scale.

Additionally, there are still some limitations to multiphase modelling for bubbly flows in CFD. The Euler–Euler approach, commonly used for two- or multi-fluid modelling, treats the phases as interpenetrating and accounts for their local and transient phase fraction distributions [260]. However, in this approach, important information about the interface structure is lost and must be accounted for through closure models [260]. These models are necessary to complete the balance equations for mass, momentum, and energy, and they attempt to capture unresolved local phenomena. Unfortunately, these phenomena are often poorly understood, partly due to the challenges in obtaining measurements in dense gas–liquid flows. As a result, the literature contains numerous and often conflicting proposals for closure models addressing the same phenomenon [261]. Most CFD simulations of two-phase flows presented in the literature are post-test simulations of experiments, where closure models and free parameters are adjusted to achieve reasonable agreement with experimental data. However, this does not necessarily indicate that the CFD models have reliable predictive capabilities [260]. Moreover, when applying PBM, the inclusion of high-dimension functions combined with kinetic models is computationally expensive. In addition, the history of the trajectory of the cells within the fluid cannot be accounted for [6].

Therefore, the accuracy of CFD simulations is significantly constrained by the proper selection of closure models for interphase mass, momentum, and heat exchange between the dispersed and continuous phases [260]. Among these, the closure models for interfacial

forces play a crucial role in determining the precision of CFD predictions. Modelling turbulent bubbly flow is particularly challenging due to the complex interactions of hydrodynamic forces, bubble coalescence, and breakup [262]. Since no perfect closure models exist for interfacial forces, careful selection of simulation parameters is essential. Despite extensive research, accurately modelling these forces remains an unresolved issue in bubbly flow simulations. The key interfacial forces include drag, lift, wall lubrication, virtual mass, and turbulent dispersion forces [262].

Currently, a variety of interfacial force models have been proposed, derived from experimental, analytical, and computational approaches. While researchers generally agree on the basic formulation of interfacial forces for CFD, there is significant divergence in the choice of closure models for the force coefficients, even for simple bubbly flow regimes [60]. This variation arises because the shape of individual bubbles changes based on the continuous phase flow field, physical properties, and bubble diameter. These factors influence the dimensionless numbers—Eötvös, Morton, and bubble Reynolds numbers—making the modelling of these coefficients complex. Therefore, a detailed discussion of the available expressions for these coefficients is necessary [262].

The broad range of bubble sizes in bubbly flow significantly influences the outcomes of multiphase CFD simulations. Interfacial force models rely on bubble diameter or size, while the bubble's diameter and shape depend on factors such as liquid flow conditions, local pressure, fluid properties, and inlet conditions [262]. As a result, bubble diameter is a critical parameter, and accurate characterization of local bubble size is essential for precise modelling of interfacial momentum exchange between the phases [152,198,262]. For surface-aerated systems, the VOF model is suitable, while the Euler–Euler model works well for benchtop forced-aerated bioreactors typical in cell culture, where bubble coalescence and breakup have minimal impact on k_La values. However, in microbial systems or larger bioreactors, coupling CFD with PBM is necessary, incorporating models for drag, lift, and other forces, as well as bubble coalescence and breakup [198].

For transient simulations, time discretization must also be considered, and stability is typically managed using the Courant-Friedrichs-Lewy number, which must be less than one for explicit methods [107,108]. Implicit methods can handle CFL numbers greater than one, but accuracy diminishes as CFL increases [107,108]. The computational expense associated with CFD simulations is a critical factor that influences the feasibility and practicality of applying numerical methods to solve fluid dynamics problems. Achieving highly accurate and detailed simulations with intricate geometries, turbulent flows, and complex physics often demands significant computational resources [32]. Balancing the need for accuracy with available computational power is a constant challenge. Researchers must optimize simulation parameters, adopt parallel computing strategies, and explore advancements in hardware to manage computational expenses effectively [106,168]. Striking a pragmatic balance ensures that CFD simulations remain both scientifically meaningful and practically achievable within realistic timeframes.

The lack of systematic reporting of computational resources and runtimes was discovered over the course of this research. While almost all studies specify mesh size, discretization schemes, turbulence models, and multiphase models, the hardware details and CPU time are rarely disclosed in interdisciplinary CFD and biotechnology works. This unfortunately limits reproducibility and hinders realistic assessments of scalability. For example, Hu et al. (2021) [8] and Wang et al. (2021) [152] describe gas--liquid simulations with Euler–Euler and PBM models, yet do not specify hardware specifications utilized in their work. Similarly, Jamshidian et al. (2023) [192] and Maluta et al. (2022) [63,203] provide detailed validation of their respective multiphase models, but no information on computational demands.

Where comparisons are available, studies highlight that model choice directly determines computational cost. Aubin et al. (2004) [146] showed that while LES can more accurately capture transient turbulence structures, it requires much finer grids and smaller timesteps than RANS models. This makes LES simulations far more computationally demanding. Similarly, Zadghaffari et al. (2010) [145] demonstrated that LES of Rushton turbine flows required over one million cells and tens of thousands of time steps. These examples show that steady-state RANS approaches can generally be run on workstation hardware, whereas LES or Euler–Lagrange multiphase simulations can require high-performance computing resources. More transparency in the hardware type, number of cores, and wall clock runtimes should be established in the future in this interdisciplinary field.

Encouraging interdisciplinary collaboration and action is another significant challenge faced by the implementation of CFD in the biopharmaceutical industry. Successful modelling in biopharmaceutical processes often requires expertise from diverse fields such as chemistry, biotechnology, and fluid dynamics. Facilitating effective communication and collaboration among interdisciplinary teams becomes crucial to harnessing the full potential of CFD. This challenge involves effective collaboration between different scientific domains and fostering an environment where experts from various fields can work seamlessly toward optimizing biopharmaceutical processes.

5. Outlook and Future Applications

It has been observed that the application of CFD in bioprocess engineering, biotechnology, and the biopharmaceutical field is more and more being complemented by novel computational approaches, kinetic compartment modeling and data-driven techniques. These new directions are shaping the design, scale-up, and operation of the STBRs, with wide impact seen from optimization of the fermentation process to environmental effectiveness. The above trends highlighted by Table 6 reflect the methods that become the subject of study in this day and age. Yet, careful analysis shows that all of them have not attained the same level of maturity nor face the same barriers to implementation (Table 7).

Table 7. Emerging trends in CFD for stirred-tank bioreactors: implications, research tasks, sustainability/credibility impacts, and representative references.

Trend	Topic	Research Tasks	Sustainability/Credibility Impact	References
Hybrid CFD + AI/ML surrogates	Efficient investigation of process space design Reduced computational burden	Develop benchmark datasets Validate surrogate accuracy	Lower energy use for simulation Faster optimization, leading to reduced experimental trials	[6,159,223]
Digital twins and real-time control	Online monitoring and prediction Soft-sensors for gradients and k_La	Integrate CFD-reduced models with process analytical technology sensors Demonstrate predictive control in pilot STBRs	Enables continuous/circular manufacturing Improved resource efficiency and robustness	[235,263–265]
Verification, validation, and uncertainty quantification	Higher credibility and reproducibility	Standardize reporting (mesh, turbulence models, CPU, runtimes)	Accurate predictions Improved regulatory acceptance Reproducible science	[64,266]
Advanced multiphase modeling (PBM-CFD, LBM)	Better bubble/droplet size prediction Interfacial dynamics	Benchmark breakup/coalescence kernels Compare Euler–Euler vs. Euler–Lagrange vs. mesh-free	More accurate O_2 transfer and k_La leads to optimized aeration and lower power demand	[24,141–143,150–157]

Table 7. *Cont.*

Trend	Topic	Research Tasks	Sustainability/Credibility Impact	References
Dynamic thermophysical property modeling	Capture time-dependent viscosity	Couple biomass/ rheology correlations with CFD	Better representation of real broth leads to improved scale-up reliability	[112,115]
CFD + biokinetic modeling via compartmental or integrated approaches	Link hydrodynamics to metabolic kinetics Simulate gradients of substrates, oxygen, and products Accelerate fermentation modeling	Develop hybrid CFD-kinetic models Validate compartment approaches	Enables realistic prediction of product yield, quality, and waste streams and supports efficient scale-up and process sustainability	[6,69,159,161,211,222,248]
CFD × Sustainability metrics	Link reactor physics to environmental footprint	Combine CFD outputs (power consumption, k_La, mixing) with lifecycle and technoeconomic assessment frameworks Case studies for *E. coli* STBRs	Enables energy- and carbon-aware design Supports sustainable bioprocessing	[23,267]

Strategies that leverage established CFD frameworks, such as solvers accelerated by graphics processing units (GPUs), hybrid compartment models, and the integration of CFD with biokinetics, demonstrate the most immediate potential for impact. The application of GPU acceleration has been validated in commonly utilized software such as OpenFOAM, facilitating LES or Euler–Lagrange simulations that were formerly confined to academic supercomputing facilities [268]. Likewise, compartment models grounded in CFD [211] and their automated generation [159] offer a practical approach to minimizing computational expenses while maintaining the relationship between hydrodynamic and kinetic phenomena. These methodologies are currently being employed in industrial settings to forecast mixing, dissolved oxygen levels, and substrate gradients [161], and they can plausibly be incorporated into bioprocess development workflows within the forthcoming years.

Digital twins, hybrid CFD-AI surrogates, and dynamic rheology or property modeling demonstrates much development. Their cross-industry application during fermentation, however, remains to be validated further. Digital twins are being developed for bioprocesses [263], and validated CFD has guided manufacturing-scale operating decisions [264]. Their extension to the large-scale STBRs will be subject to the development of standardized data exchange between CFD, control systems, and process analytical technology sensors. Artificial intelligence and ML-based surrogate modeling lowers simulation times by orders-of-magnitude [223,269], carries out careful error quantification, and shows clear-cut benchmarking protocols. Dynamic thermophysical property models also demonstrate promise in efficiently simulating the fermentation process' evolving viscosity during fermentation [112], and data-driven learning of shear-thinning parameters from velocimetry [115]. However, their reliability is hindered by the availability of sufficient in-situ measurements and the complexity of the broth rheology.

More ambitious avenues—like the full integration of CFD outputs within sustainability indicators (PMI, E-factor, and LCA)—are mostly theoretical. Although the quantities of interest can be easily obtained by CFD (e.g., by the power input, the mixing time, the oxygen transfer, the by-products accumulation) [23,69], no study has connected them directly to PMI nor to E-factor on STBR bioprocesses. Likewise, the integration of CFD with advanced genome-scale metabolic models is theoretical. These constitute promising research avenues: the connection of the hydrodynamics to the productivity as well as

to the by-products formation and the environmental impact would put the modeling by CFD on the sustainability target of the biopharmaceutical and the industrial biotech industries [267,270].

CFD articles in the biotechnology field often do not report mesh independence, runtime, or model-form uncertainty, and it is difficult to compare between sets of results. To have lasting impact, biotechnology CFD needs also to adopt best-practice protocols like aerospace or nuclear engineering, where this is a fundamental condition of model credibility [64,271]. Analogously, the community requires openly available benchmark datasets—of geometries, of conditions of operation, and of experimental validation data—so that rapid development of models can be made easier and novel methods can be properly compared. Linking CFD and compartmental kinetic modeling already sit on the threshold of application to design and optimization efforts. Digital twins and AI surrogates become operational decision tools and real-time monitoring tools. Dynamic property modeling and coupling of the CFD-LCA follow and hold the promise of directly linking reactor design and operation to green manufacturability metrics. These trajectories collectively point the path that can take today's high-fidelity simulation to the sustainable, data-driven biomanufacturing ecosystems of the future.

6. Conclusions

Published research on CFD simulations in the biopharmaceutical industry, that follow the course of a fermentation within a STBR with appropriate resolution, is notably scarce due to the interdisciplinary nature of this topic. Despite the growing adoption of CFD software in production and Research and Development (R&D) sectors, there seems to be a reluctance to share findings and technologies. However, the few available publications on this topic primarily concentrate on evaluating shear rates in bioreactors [27,29], forecasting bubble size distribution through population balance modelling [152], assessing mixing efficiency and homogenization times [23,79,210], identifying inadequately mixed regions [132], and performing scale-up/down calculations [31,49,272,273] involving turbulent kinetic energy [132], average fluid velocity [192], power number and power per volume [166,274], among other parameters.

In the context of turbulent mixing simulations, the RANS equations are favored for their lower computational cost and demonstrated accuracy, as opposed to more resource-intensive methods such as DNS, LES, DES, among others. For mixing simulations, the MRF is frequently employed for simpler implementation and lower computational cost. Such models allow for lower computational cost and accuracy, compared to more complex simulations that involve the physical rotation of mixers using moving (sliding) mesh methods. These models require significantly longer computational times. Euler–Euler multiphase models coupled with gas dispersion models were the most commonly used to model bubble size distribution, as well as the break-up and coalescence behaviors. Briefly catalogued in Table 6, CFD application progress for stirred tank bioreactors ranges from initial turbulence modeling and hydrodynamic validation to recent studies that combine population balance modeling, optimization schemes, and digital twinning methodology. This work demonstrates that CFD has become a multifaceted tool that can assist with fundamental bioprocess knowledge as well as with process intensification at Industrial scale. Even so, variety of methodology serves to underline that future work remains necessary in experimental validation, biological heterogeneity handling, and management of computational cost of sophisticated multiphase and turbulence models.

Understanding the influence of agitation and OTR on the generation and selectivity of particular biochemical pathways for product formation is essential for optimizing the performance of bioprocesses). While there is extensive guidance on designing, improving, and

operating aerobic bioprocesses in STBRs, predicting fermentation performance has become more intricate, necessitating an increased reliance on both experimental and computational approaches [136].

In order to implement more sustainable practices in biopharmaceutical fermentation processes, it is crucial to clearly define the criteria for sustainable production of selected biopharmaceuticals. This involves identifying specific metrics and techniques for analyzing and comparing the manufacturing process with others. The goal of minimizing the environmental footprint of the API and the overall API development process is essential for the future sustainability of the biopharmaceutical industry. By explicitly linking CFD modeling and output parameters such as power consumption, mixing performance and quality and oxygen mass transfer with sustainability indicators, this review demonstrates that CFD is not only a predictive tool for hydrodynamics but also a quantitative framework for evaluating the environmental impact of microbial fermenter operation.

To implement more sustainable practices in biopharmaceutical fermentation processes, it is crucial to clearly define the criteria for sustainable production of selected biopharmaceuticals. This involves identifying specific metrics and techniques for analyzing and comparing the manufacturing process with others. Among these considerations, efficient mixing within STBRs plays a vital role, as it directly influences mass transfer, oxygen delivery, and energy consumption. Poor mixing can lead to the formation of dead zones and gradients in pH, temperature, or nutrients, which compromise product quality and increase waste. CFD can be effectively applied to analyze and optimize mixing performance in STBRs, ensuring uniform conditions throughout the reactor while reducing energy use and minimizing solvent and water consumption during cleaning operations. By incorporating CFD-driven design and process improvements, manufacturers can align mixing strategies with broader sustainability goals, ultimately reducing the environmental footprint of both the active pharmaceutical ingredient and the overall production process—an essential step toward a more responsible and future-proof biopharmaceutical industry.

Author Contributions: F.I. was responsible for the conceptualization and investigation of the topic and wrote the original draft of the manuscript. M.B. and C.J. contributed to the review and editing of the manuscript, supervised the work, and provided essential resources. M.H. was responsible for acquiring funding for the project, provided supervision, and participated in the review and editing process. All authors have read and agreed to the published version of the manuscript.

Funding: This research was performed with the financial support of the EU Horizon project ENVIROMED under grant agreement ID: 101057844.

Acknowledgments: The authors would like to thank Rüdiger Lück for aiding in providing insight into the fermentation process as well as Alexandra Bauer, Amal El Gohary Ahmed, and Mirmehrshad Emamshoushtari for feedback with preparing the manuscript.

Conflicts of Interest: The authors declare no conflicts of interest.

Abbreviations

The following abbreviations are used in this manuscript:

Symbol	Definition
a	Specific Surface
A_G	Gas Bubble Surface
c_p	Specific Heat Capacity
C_1	Constant for Oxygen Diffusivity
d_B	Gas Bubble Diameter
D_L	Oxygen Diffusivity
D, Γ	Diffusion Coefficient

dO_2	Solved Oxygen Concentration
dO_2*	Maximum Solved Oxygen Concentration
$F^{\rightarrow}$	Force Vector
Δx	Differentially Small Change in Distance
Δt	Differentially Small Time Step
k	Turbulent Kinetic Energy
k_L	Oxygen Transfer Coefficient
L_{char}	Characteristic Length
M	Torque
N	Rotational Speed
P	Power
P_o	Power Number
q_{O2}	Specific Oxygen Requirement
S_φ	Source Term of Variable φ
T	Temperature
t_m	Mixing Time
$u^{\rightarrow}$	Velocity Vector
u_x	Velocity Component in x-Direction
u, v, w	Velocity Components in 3 Directions
V	Volume
x	3D Cartesian Coordinate
X	Biomass Concentration
α_G	Phase Fraction of Gaseous Bubbles
α_k	Phase Fraction of Phase k
γ_{ave}	Average Shear Rate
γ	Surface Tension Force
δ	Partial Derivative
ε	Turbulent Energy Dissipation Rate in Liquid Phase per Unit Mass
ϵ	Average Viscous Dissipation Rate of Turbulent Energy per Unit Mass
η	Molecular Viscosity (Spatial Scale)
λ	Mean Free Path Length
λ_h	Heat Conductivity
μ	Dynamic Viscosity
μ_{eff}	Effective Viscosity
μ	Liquid Viscosity
ν_L, ν	Kinematic Viscosity
π	Pi
ρ	Density of Liquid Phase
θ_{95}	Mixing Time at 95% Homogeneity
τ	Shear Stress
τ_{ave}	Average Shear Stress
τ_η	Time Scale
φ	Any Generic Variable
ω	Specific Dissipation Rate
Δ	Nabla Operator
$\vec{v}.\vec{\nabla}\omega_\alpha$	Convective Mass Transfer
$D_{\alpha s}\nabla^2\omega_\alpha$	Molecular Diffusion
r_α	Net Rate of Production
Sub- and Superscripts	
ave	Average
char	Characteristic

eff	Effective
i	Impeller
G	Gaseous Phase
h, k	For Two Different Phases
L	Liquid Phase
m	Mixing
0	Referred to Actual Value
95	95% Homogeneity
Acronyms and Abbreviations	
AI	Artificial Intelligence
AMI	Arbitrary Mesh Interface
ANN	Artificial Neural Network
API	Active biopharmaceutical Ingredient
B_w	Wall Baffles
BSD	Bubble Size Distribution
C	Courant Number
CAD	Computer-Aided Design
CAGR	Compound Annual Growth Rate
CCD	Charge Coupled Device
CFD	Computational Fluid Dynamics
CFD-ANN-NSGA	Computational Fluid Dynamics–ArtificialNeural Network–Non-dominated SortingGenetic Algorithm
Ci	Impeller Clearance
CSBR	Continuously Stirred Bioreactor
CT	Computed Tomography
Di	Impeller Diameter
DES	Detached Eddy Simulation
DNA	Deoxyribonucleic Acid
DNS	Direct Numerical Simulation
DoE	Design of Experiments
E. coli	*Escherichia coli*
E-Factor	Environmental Factor
FEM	Finite Element Methods
Fr	Froude Number
FVM	Finite Volume Methods
Ga	Galilei Number
H	Liquid Height
HCl	Hydrochloric Acid
Kn	Knudsen Number
LB	Lattice Boltzmann
LBM	Lattice Boltzmann Methods
LCA	Life Cycle Assessment
LDA	Laser Doppler Anemometry
LDV	Laser Doppler Velocimetry
LES	Large Eddy Simulation
ML	Machine Learning
MMI	Mass Manufacturing Intensity
MRF	Multiple Reference Frames
MUSIG	Multiple Size Group
NaCl	Sodium Chloride
N-S	Navier-Stokes
Ne	Newton Number
OTR	Oxygen Take-up Rate
OUR	Oxygen Uptake

PBE	Population Balance Equation
PBM	Population Balance Model
PDEs	Partial Differential Equations
Pe	Peclet Number
PIV	Particle Image Velocimetry
PLIF	Planar Laser-Induced Fluorescence
PMI	Process Mass Intensity
Pr	Prandtl Number
QbD	Quality-by-Design
RANS	Reynolds-Averaged Navier–Stokes
rDNA	Recombinant Deoxyribonucleic Acid
Re	Reynolds Number
RNG	Re-Normalization Group
RPM	Revolutions Per Minute
RSM	Reynolds Stress Model
RTD	Residence Time Distribution
R&D	Research and Development
Sc	Schmidt Number
SIMPLE	Semi-Implicit Method for Pressure-Linked Equations
SM	Sliding Mesh
SPH	Smoothed Particle Hydrodynamics
SST	Shear Stress Transport
STBR	Stirred Tank Bioreactor
SUS	Single-Use Systems
T	Tank Diameter
TEA	Techno-Economic Analysis
UDF	User-Defined Function
UW	Upwind
VOF	Volume of Fluid
W	Impeller Blade Length
WARIEN	Water Related Impact of Energy
We	Weber Number
6BT	Six-Bent Blade Turbine
6ITD	Six-Inclined Blade Down-pumping Turbine
6ITU	Six-Inclined Blade Up-pumping Turbine

References

1. Buarque, F.S.; Lemes, A.C.; Coelho, M.A.Z. Advances in Industrial Biotechnology: Bioprocess and Bioseparation. *Processes* **2025**, *13*, 1101. [CrossRef]
2. Show, P.L. Special Issue on "Biotechnology for Sustainability and Social Well Being". *Processes* **2021**, *9*, 216. [CrossRef]
3. Szkodny, A.C.; Lee, K.H. Biopharmaceutical Manufacturing: Historical Perspectives and Future Directions. *Annu. Rev. Chem. Biomol. Eng.* **2022**, *13*, 141–165. [CrossRef]
4. Griffiths, E. Quality standards for biopharmaceuticals: The importance of good manufacturing practice. *GaBI J.* **2020**, *9*, 97–99. [CrossRef]
5. Martin, D.K.; Vicente, O.; Beccari, T.; Kellermayer, M.; Koller, M.; Lal, R.; Marks, R.S.; Marova, I.; Mechler, A.; Tapaloaga, D.; et al. A brief overview of global biotechnology. *Biotechnol. Biotechnol. Equip.* **2021**, *35*, S5–S14. [CrossRef]
6. Singh, V.K.; del Val, I.J.; Glassey, J.; Kavousi, F. Integration Approaches to Model Bioreactor Hydrodynamics and Cellular Kinetics for Advancing Bioprocess Optimisation. *Bioengineering* **2024**, *11*, 546. [CrossRef] [PubMed]
7. Nielsen, J.; Tillegreen, C.B.; Petranovic, D. Innovation trends in industrial biotechnology. *Trends Biotechnol.* **2022**, *40*, 1160–1172. [CrossRef]
8. Hu, X.; Dogan Ilgun, A.; Passalacqua, A.; Fox, R.O.; Bertola, F.; Milosevic, M.; Visscher, F. CFD simulations of stirred-tank reactors for gas-liquid and gas-liquid-solid systems using OpenFOAM®. *Int. J. Chem. React. Eng.* **2021**, *19*, 193–207. [CrossRef]
9. Gundinger, T.; Kittler, S.; Kubicek, S.; Kopp, J.; Spadiut, O. Recombinant Protein Production in *E. coli* Using the phoA Expression System. *Fermentation* **2022**, *8*, 181. [CrossRef]

10. Schmideder, A.; Weuster-Botz, D. High-performance recombinant protein production with *Escherichia coli* in continuously operated cascades of stirred-tank reactors. *Ind. Microbiol. Biotechnol.* **2017**, *44*, 1021–1029. [CrossRef]
11. Buffo, M.M.; Esperança, M.N.; Farinas, C.S.; Badino, A.C. Relation between pellet fragmentation kinetics and cellulolytic enzymes production by *Aspergillus niger* in conventional bioreactor with different impellers. *Enzym. Microb. Technol.* **2020**, *139*, 109587. [CrossRef] [PubMed]
12. Spadiut, O.; Capone, S.; Krainer, F.; Glieder, A.; Herwig, C. Microbials for the production of monoclonal antibodies and antibody fragments. *Trends Biotechnol.* **2014**, *32*, 54–60. [CrossRef]
13. Kopp, J.; Kittler, S.; Slouka, C.; Herwig, C.; Spadiut, O.; Wurm, D.J. Repetitive Fed-Batch: A Promising Process Mode for Biomanufacturing with *E. coli*. *Front. Bioeng. Biotechnol.* **2020**, *8*, 573607. [CrossRef]
14. Gu, Q.; Yang, S.; Mohsin, A.; Yu, J.; Zhuang, Y.; Li, C. Optimization of oxygen transfer and power consumption in aerobic bioprocess by designing disc turbine impeller based on CFD-Taguchi method. *Sci. Rep.* **2025**, *15*, 8102. [CrossRef]
15. Zhu, L.; Liao, Y.; Chang, X.; Su, M.; Ou, Y.; Wu, S.; Wu, Z.; Yang, H.; Li, J.; Huang, H. A Comparative Study of the Performance of Orbitally Shaken Bioreactors (OSRs) and Stirred Tank Bioreactors (STRs). *Processes* **2024**, *12*, 2849. [CrossRef]
16. Sarkis, M.; Fyfe, A.T.; Kontoravdi, C.; Papathanasiou, M.M. Towards a Net Zero, socially sustainable and eco-efficient biopharma industry: How far are we? *Curr. Opin. Chem. Eng.* **2024**, *44*, 101027. [CrossRef]
17. Sheldon, R.A. Metrics of Green Chemistry and Sustainability: Past, Present, and Future. *ACS Sustain. Chem. Eng.* **2018**, *6*, 32–48. [CrossRef]
18. Benison, C.H.; Payne, P.R. Manufacturing mass intensity: 15 Years of Process Mass Intensity and development of the metric into plant cleaning and beyond. *Curr. Res. Green Sustain. Chem.* **2022**, *5*, 100229. [CrossRef]
19. Jimenez-Gonzalez, C.; Lund, C. Green metrics in pharmaceutical development. *Curr. Opin. Green Sustain. Chem.* **2022**, *33*, 100564. [CrossRef]
20. Seidel, S.; Eibl-Schindler, R.; Eibl, D. Laboratory-independent exploration of stirred bioreactors and their fluid dynamics. *Educ. Chem. Eng.* **2023**, *42*, 80–87. [CrossRef]
21. Xu, C.; Liu, X.; Ding, C.; Zhou, X.; Xu, Y.; Gu, X. Power consumption and oxygen transfer optimization for C5 sugar acid production in a gas-liquid stirred tank bioreactor using CFD-Taguchi method. *Renew. Energy* **2023**, *212*, 430–442. [CrossRef]
22. Seidel, S.; Mozaffari, F.; Maschke, R.W.; Kraume, M.; Eibl-Schindler, R.; Eibl, D. Automated Shape and Process Parameter Optimization for Scaling Up Geometrically Non-Similar Bioreactors. *Processes* **2023**, *11*, 2703. [CrossRef]
23. Panunzi, A.; Moroni, M.; Mazzelli, A.; Bravi, M. Industrial Case-Study-Based Computational Fluid Dynamic (CFD) Modeling of Stirred and Aerated Bioreactors. *ACS Omega* **2022**, *7*, 25152–25163. [CrossRef]
24. Kersebaum, J.; Flaischlen, S.; Hofinger, J.; Wehinger, G.D. Simulating Stirred Tank Reactor Characteristics with a Lattice Boltzmann CFD Code. *Chem. Eng. Technol.* **2024**, *47*, 586–595. [CrossRef]
25. Sharma, C.; Malhotra, D.; Rathore, A.S. Review of Computational fluid dynamics applications in biotechnology processes. *Biotechnol. Prog.* **2011**, *27*, 1497–1510. [CrossRef] [PubMed]
26. Hoseini, S.S.; Najafi, G.; Ghobadian, B.; Akbarzadeh, A.H. Impeller shape-optimization of stirred-tank reactor: CFD and fluid structure interaction analyses. *Chem. Eng. J.* **2021**, *413*, 127497. [CrossRef]
27. Ramírez, L.A.; Pérez, E.L.; Díaz, C.G.; Luengas, D.A.C.; Ratkovich, N.; Reyes, L.H. CFD and Experimental Characterization of a Bioreactor: Analysis via Power Curve, Flow Patterns and k L a. *Processes* **2020**, *8*, 878. [CrossRef]
28. Mishra, S.; Kumar, V.; Sarkar, J.; Rathore, A.S. CFD based mass transfer modeling of a single use bioreactor for production of monoclonal antibody biotherapeutics. *Chem. Eng. J.* **2021**, *412*, 128592. [CrossRef]
29. Oblak, B.; Babnik, S.; Erklavec-Zajec, V.; Likozar, B.; Pohar, A. Digital Twinning Process for Stirred Tank Reactors/Separation Unit Operations through Tandem Experimental/Computational Fluid Dynamics (CFD) Simulations. *Processes* **2020**, *8*, 1511. [CrossRef]
30. Garcia-Ochoa, F.; Gomez, E.; Santos, V.E. Fluid dynamic conditions and oxygen availability effects on microbial cultures in STBR: An overview. *Biochem. Eng. J.* **2020**, *164*, 107803. [CrossRef]
31. Bach, C.; Yang, J.; Larsson, H.; Stocks, S.M.; Gernaey, K.V.; Albaek, M.O.; Krühne, U. Evaluation of mixing and mass transfer in a stirred pilot scale bioreactor utilizing CFD. *Chem. Eng. Sci.* **2017**, *171*, 19–26. [CrossRef]
32. Haddadi, B.; Jordan, C.; Harasek, M. Cost efficient CFD simulations: Proper selection of domain partitioning strategies. *Comput. Phys. Commun.* **2017**, *219*, 121–134. [CrossRef]
33. Wu, B. CFD Analysis of Mechanical Mixing in Anaerobic Digesters. *Trans. ASABE* **2009**, *52*, 1371–1382. [CrossRef]
34. Babi, D.K.; Griesbach, J.; Hunt, S.; Insaidoo, F.; Roush, D.; Todd, R.; Staby, A.; Welsh, J.; Wittkopp, F. Opportunities and challenges for model utilization in the biopharmaceutical industry: Current versus future state. *Curr. Opin. Chem. Eng.* **2022**, *36*, 100813. [CrossRef]
35. Rogers, L.; Jensen, K.F. Continuous manufacturing—The Green Chemistry promise? *Green Chem.* **2019**, *21*, 3481–3498. [CrossRef]
36. Baumann, M.; Moody, T.S.; Smyth, M.; Wharry, S. A Perspective on Continuous Flow Chemistry in the Pharmaceutical Industry. *Org. Process. Res. Dev.* **2020**, *24*, 1802–1813. [CrossRef]

37. Dallinger, D.; Kappe, C.O. Why flow means green—Evaluating the merits of continuous processing in the context of sustainability. *Curr. Opin. Green Sustain. Chem.* **2017**, *7*, 6–12. [CrossRef]
38. Lee, S.L.; O'Connor, T.F.; Yang, X.; Cruz, C.N.; Chatterjee, S.; Madurawe, R.D.; Moore, C.M.V.; Yu, L.X.; Woodcock, J. Modernizing Pharmaceutical Manufacturing: From Batch to Continuous Production. *J. Pharm. Innov.* **2015**, *10*, 191–199. [CrossRef]
39. Burange, A.S.; Osman, S.M.; Luque, R. Understanding flow chemistry for the production of active pharmaceutical ingredients. *iScience* **2022**, *25*, 103892. [CrossRef]
40. Partopour, B.; Pollard, D. Advancing biopharmaceutical manufacturing: Economic and sustainability assessment of end-to-end continuous production of monoclonal antibodies. *Trends Biotechnol.* **2025**, *43*, 462–475. [CrossRef]
41. Kopp, J.; Spadiut, O. A Guideline to Set Up Cascaded Continuous Cultivation with *E. coli* Bl21 (DE3). In *Bioreactors in Stem Cell Biology: Methods and Protocols*; Turksen, K., Ed.; Springer: New York, NY, USA, 2022; pp. 223–240. [CrossRef]
42. Domokos, A.; Nagy, B.; Szilágyi, B.; Marosi, G.; Nagy, Z.K. Integrated Continuous Pharmaceutical Technologies—A Review. *Org. Process. Res. Dev.* **2021**, *25*, 721–739. [CrossRef]
43. Jiménez-González, C.; Poechlauer, P.; Broxterman, Q.B.; Yang, B.; am Ende, D.; Baird, J.; Bertsch, C.; Hannah, R.E.; Dell'Orco, P.; Noorman, H.; et al. Key Green Engineering Research Areas for Sustainable Manufacturing: A Perspective from Pharmaceutical and Fine Chemicals Manufacturers. *Org. Process. Res. Dev.* **2011**, *15*, 900–911. [CrossRef]
44. Argoud, S.; Budzinski, K.; D'Aquila, D.; Madabhushi, S.R.; Smith, P. Green metrics for biologics. *Curr. Opin. Green Sustain. Chem.* **2022**, *35*, 100614. [CrossRef]
45. Cataldo, A.L.; Sissolak, B.; Metzger, K.; Budzinski, K.; Shirokizawa, O.; Luchner, M.; Jungbauer, A.; Satzer, P. Water related impact of energy: Cost and carbon footprint analysis of water for biopharmaceuticals from tap to waste. *Chem. Eng. Sci. X* **2020**, *8*, 100083. [CrossRef]
46. Yu, X.; Chen, K.; Zhou, C.; Wang, Q.; Chu, J.; Yao, Z.; Liu, Y.; Sun, Y. Bioreactor Design Optimization Using CFD for Cost-Effective ACPase Production in *Bacillus subtilis*. *Fermentation* **2025**, *11*, 386. [CrossRef]
47. Joshi, J.B.; Nere, N.K.; Rane, C.V.; Murthy, B.N.; Mathpati, C.; Patwardhan, A.W.; Ranade, V.V. CFD simulation of stirred tanks: Comparison of turbulence models. Part I: Radial flow impellers. *Can. J. Chem. Eng.* **2011**, *89*, 23–82. [CrossRef]
48. Ding, J.; Wang, X.; Zhou, X.-F.; Ren, N.-Q.; Guo, W.-Q. CFD optimization of continuous stirred-tank (CSTR) reactor for biohydrogen production. *Bioresour. Technol.* **2010**, *101*, 7005–7013. [CrossRef] [PubMed]
49. Cappello, V.; Plais, C.; Vial, C.; Augier, F. Scale-up of aerated bioreactors: CFD validation and application to the enzyme production by *Trichoderma reesei*. *Chem. Eng. Sci.* **2021**, *229*, 116033. [CrossRef]
50. Kamla, Y.; Ameur, H.; Karas, A.; Arab, M.I. Performance of new designed anchor impellers in stirred tanks. *Chem. Pap.* **2020**, *74*, 779–785. [CrossRef]
51. Coroneo, M.; Montante, G.; Paglianti, A.; Magelli, F. CFD prediction of fluid flow and mixing in stirred tanks: Numerical issues about the RANS simulations. *Comput. Chem. Eng.* **2011**, *35*, 1959–1968. [CrossRef]
52. Kálal, Z.; Jahoda, M.; Fořt, I. CFD Prediction of Gas-Liquid Flow in an Aerated Stirred Vessel Using the Population Balance Model. *Chem. Process. Eng.* **2014**, *35*, 55–73. [CrossRef]
53. Chen, Z.; Lian, J.Z.; Zhu, H.; Zhang, J.; Zhang, Y.; Xiang, X.; Huang, D.; Tjokro, K.; Barbarossa, V.; Cucurachi, S.; et al. Application of Life Cycle Assessment in the pharmaceutical industry: A critical review. *J. Clean. Prod.* **2024**, *459*, 142550. [CrossRef]
54. Fitzpatrick, J.J.; Gloanec, F.; Michel, E.; Blondy, J.; Lauzeral, A. Application of Mathematical Modelling to Reducing and Minimising Energy Requirement for Oxygen Transfer in Batch Stirred Tank Bioreactors. *Chemengineering* **2019**, *3*, 14. [CrossRef]
55. Humbird, D.; Davis, R.; Tao, L.; Kinchin, C.; Hsu, D.; Aden, A.; Schoen, P.; Lukas, J.; Olthof, B.; Worley, M.; et al. *Process Design and Economics for Biochemical Conversion of Lignocellulosic Biomass to Ethanol: Dilute-Acid Pretreatment and Enzymatic Hydrolysis of Corn Stover*; NREL/TP-5100-47764; National Renewable Energy Laboratory (NREL): Golden, CO, USA, 2011; p. 1013269. [CrossRef]
56. Ascanio, G.; Castro, B.; Galindo, E. Measurement of Power Consumption in Stirred Vessels—A Review. *Chem. Eng. Res. Des.* **2004**, *82*, 1282–1290. [CrossRef]
57. Fitzpatrick, J.J. Insights from Mathematical Modelling into Energy Requirement and Process Design of Continuous and Batch Stirred Tank Aerobic Bioreactors. *ChemEngineering* **2019**, *3*, 65. [CrossRef]
58. Lalor, F.; Fitzpatrick, J.; Sage, C.; Byrne, E. Sustainability in the biopharmaceutical industry: Seeking a holistic perspective. *Biotechnol. Adv.* **2019**, *37*, 698–707. [CrossRef]
59. Alves, S.S.; Vasconcelos, J.M.T. Optimisation of agitation and aeration in fermenters. *Bioprocess Biosyst. Eng.* **1996**, *14*, 119–123. [CrossRef]
60. Kaiser, S.C.; Werner, S.; Jossen, V.; Blaschczok, K.; Eibl, D. Power Input Measurements in Stirred Bioreactors at Laboratory Scale. *J. Vis. Exp.* **2018**, *135*, e56078. [CrossRef]
61. Davis, R.; Tao, L.; Tan, E.C.D.; Biddy, M.J.; Beckham, G.T.; Scarlata, C.; Jacobson, J.; Cafferty, K.; Ross, J.; Lukas, J.; et al. *Process Design and Economics for the Conversion of Lignocellulosic Biomass to Hydrocarbons: Dilute-Acid and Enzymatic Deconstruction of Biomass to Sugars and Biological Conversion of Sugars to Hydrocarbons*; NREL/TP-5100-60223; National Renewable Energy Laboratory (NREL): Golden, CO, USA, 2013. [CrossRef]

62. Jamshidian, R.; Scully, J.; Akker, H.E.V.D. A computational fluid dynamics study of mass transfer in a large-scale aerated stirred bioreactor. *Chem. Eng. J.* **2025**, *509*, 160723. [CrossRef]
63. Maluta, F.; Paglianti, A.; Montante, G. Towards a robust CFD modelling approach for reliable hydrodynamics and mass transfer predictions in aerobic stirred fermenters. *Biochem. Eng. J.* **2022**, *181*, 108405. [CrossRef]
64. Reid, A.; Rossi, R.; Cottini, C.; Benassi, A. CFD simulation of a Rushton turbine stirred-tank using open-source software with critical evaluation of MRF-based rotation modeling. *Meccanica* **2025**, *60*, 1613–1637. [CrossRef]
65. Nogueira, A.L. Transient CFD Simulation of Vortex Formation in a Stirred Multiphase Flow. In *Multiphase Flow Dynamics: A Perspective from the Brazilian Academy and Industry*; Ferreira Martins, M., Ramos, R., Belich, H., Eds.; Springer International Publishing: Cham, Switzerland, 2022; pp. 211–219. [CrossRef]
66. Becker, J.; Manske, C.; Randl, S. Green chemistry and sustainability metrics in the pharmaceutical manufacturing sector. *Curr. Opin. Green Sustain. Chem.* **2022**, *33*, 100562. [CrossRef]
67. Sheldon, R.A.; Bode, M.L.; Akakios, S.G. Metrics of green chemistry: Waste minimization. *Curr. Opin. Green Sustain. Chem.* **2022**, *33*, 100569. [CrossRef]
68. Nickel, N.; Fitschen, J.; Haase, I.; Kuschel, M.; Schulz, T.W.; Wucherpfennig, T.; Schlüter, M. Novel sparging strategies to enhance dissolved carbon dioxide stripping in industrial scale stirred tank reactors. *Front. Chem. Eng.* **2024**, *6*, 1470991. [CrossRef]
69. Hanspal, N.; DeVincentis, B.; Thomas, J.A. Modeling multiphase fluid flow, mass transfer, and chemical reactions in bioreactors using large-eddy simulation. *Eng. Life Sci.* **2022**, *23*, e2200020. [CrossRef] [PubMed]
70. Ottinger, M.; Wenk, I.; Pereira, J.C.; John, G.; Junne, S. Single-Use Technology in the Biopharmaceutical Industry and Sustainability: A Contradiction? *Chem. Ing. Tech.* **2022**, *94*, 1883–1891. [CrossRef]
71. Whitford, W.G.; Petrich, M.A.; Flanagan, W.P. Environmental impacts of single-use systems. In *Single-Use Technology in Biopharmaceutical Manufacture*; Eibl, R., Eibl, D., Eds.; Wiley: Hoboken, NJ, USA, 2019; pp. 169–179. [CrossRef]
72. Budzinski, K.; Constable, D.; D'aQuila, D.; Smith, P.; Madabhushi, S.R.; Whiting, A.; Costelloe, T.; Collins, M. Streamlined life cycle assessment of single use technologies in biopharmaceutical manufacture. *New Biotechnol.* **2022**, *68*, 28–36. [CrossRef]
73. Kreitmayer, D.; Gopireddy, S.R.; Matsuura, T.; Aki, Y.; Katayama, Y.; Sawada, T.; Kakihara, H.; Nonaka, K.; Profitlich, T.; Urbanetz, N.A.; et al. Numerical and Experimental Investigation of the Hydrodynamics in the Single-Use Bioreactor Mobius® CellReady 3 L. *Bioengineering* **2022**, *9*, 206. [CrossRef]
74. Scully, J.; Considine, L.B.; Smith, M.T.; McAlea, E.; Jones, N.; O'Connell, E.; Madsen, E.; Power, M.; Mellors, P.; Crowley, J.; et al. Beyond heuristics: CFD-based novel multiparameter scale-up for geometrically disparate bioreactors demonstrated at industrial 2kL–10kL scales. *Biotechnol. Bioeng.* **2020**, *117*, 1710–1723. [CrossRef]
75. Jamshidzadeh, M.; Griesz, A.U.; Jensen, J.W.; Krühne, U.; Woodley, J.M.; Gernaey, K.V.; Nikel, P.I.; Junicke, H. Cfd-Guided Scaling of *Pseudomonas putida* Fermentation. *Biochem. Eng. J.* **2025**, *213*, 109549. [CrossRef]
76. Yang, O.; Qadan, M.; Ierapetritou, M. Economic Analysis of Batch and Continuous Biopharmaceutical Antibody Production: A Review. *J. Pharm. Innov.* **2020**, *15*, 182–200. [CrossRef]
77. Posadas-Navarro, D.; Palacios, C.; Blancas-Cabrera, A.; Trujillo-Roldán, M.A.; Salinas-Vázquez, M.; Ascanio, G. Flow Patterns of Multiple Axial-Radial Impellers for Potential Use in Aerated Stirred Tanks. *Chem. Eng. Technol.* **2022**, *45*, 860–867. [CrossRef]
78. Zhang, P.; Chen, G.; Duan, J.; Wang, W. Mixing characteristics in a vessel equipped with cylindrical stirrer. *Results Phys.* **2018**, *10*, 699–705. [CrossRef]
79. Ebrahimi, M.; Tamer, M.; Villegas, R.M.; Chiappetta, A.; Ein-Mozaffari, F. Application of CFD to Analyze the Hydrodynamic Behaviour of a Bioreactor with a Double Impeller. *Processes* **2019**, *7*, 694. [CrossRef]
80. Heidari, A. CFD simulation of impeller shape effect on quality of mixing in two-phase gas–liquid agitated vessel. *Chin. J. Chem. Eng.* **2020**, *28*, 2733–2745. [CrossRef]
81. Stanbury, P.F.; Whitaker, A.; Hall, S.J. Chapter 9—Aeration and agitation. In *Principles of Fermentation Technology*, 3rd ed.; Stanbury, P.F., Whitaker, A., Hall, S.J., Eds.; Butterworth-Heinemann: Oxford, UK, 2017; pp. 537–618. [CrossRef]
82. Karimi, A.; Golbabaei, F.; Mehrnia, M.; Mohammad, K.; Neghab, M.; Nikpey, A.; Pourmand, M. Investigation of Gas Hold up and Power Consumption in a Stirred Tank Bioreactor Using Single and Dual Impeller Configurations. *J. Occup. Hyg.* **2013**, *5*, 109–116.
83. Kadic, E.; Heindel, T.J. Stirred-Tank Bioreactors. In *An Introduction to Bioreactor Hydrodynamics and Gas-Liquid Mass Transfer*; John Wiley & Sons, Ltd.: Hoboken, NJ, USA, 2014; pp. 69–123. [CrossRef]
84. Delafosse, A.; Collignon, M.; Calvo, S.; Delvigne, F.; Crine, M.; Thonart, P.; Toye, D. CFD-based compartment model for description of mixing in bioreactors. *Chem. Eng. Sci.* **2014**, *106*, 76–85. [CrossRef]
85. Debab, A.; Chergui, N.; Bekrentchir, K.; Bertrand, J. An Investigation of Heat Transfer in a Mechanically Agitated Vessel. *J. Appl. Fluid Mech.* **2011**, *4*, 43–50. [CrossRef]
86. Salho, A.K.; Hamzah, D.A. A Review of Stirred Tank Dynamics: Power Consumption, Mixing Time and Impeller Geometry. *Int. J. Heat Technol.* **2024**, *42*, 1081–1092. [CrossRef]
87. Antognoli, M.; Galletti, C.; Bacci di Capaci, R.; Pannocchia, G.; Scali, C. Numerical Investigation of the Mixing of Highly Viscous Liquids with Cowles Impellers. *Chem. Eng. Trans.* **2019**, *74*, 973–978. [CrossRef]

88. Werner, S.; Kaiser, S.; Kraume, M.; Eibl, D. Computational fluid dynamics as a modern tool for engineering characterization of bioreactors. *Pharm. Bioprocess.* **2014**, *2*, 85–99. [CrossRef]
89. Nadal-Rey, G.; McClur, D.D.; Kavanagh, J.M.; Cassells, B.; Cornelissen, S.; Fletcher, D.F.; Gernaey, K.V. Computational fluid dynamics modelling of hydrodynamics, mixing and oxygen transfer in industrial bioreactors with Newtonian broths. *Biochem. Eng. J.* **2022**, *177*, 108265. [CrossRef]
90. Kadic, E.; Heindel, T.J. Modeling Bioreactors. In *An Introduction to Bioreactor Hydrodynamics and Gas-Liquid Mass Transfer*; John Wiley & Sons, Ltd.: Hoboken, NJ, USA, 2014; pp. 58–68. [CrossRef]
91. Rathore, A.S.; Sharma, C.; Persad, A. Use of computational fluid dynamics as a tool for establishing process design space for mixing in a bioreactor. *Biotechnol. Prog.* **2012**, *28*, 382–391. [CrossRef]
92. Rushton, J.H. Power characteristics of mixing impellers Part 1. *Chem. Eng. Prog.* **1950**, *46*, 395–404.
93. Baehr, H.D.; Stephan, K. *Heat and Mass Transfer*; Springer: Berlin/Heidelberg, Germany, 2011. [CrossRef]
94. Reynolds, O. XXIX. An experimental investigation of the circumstances which determine whether the motion of water shall be direct or sinuous, and of the law of resistance in parallel channels. *Philos. Trans. R. Soc. Lond.* **1997**, *174*, 935–982. [CrossRef]
95. Nere, N.K.; Patwardhan, A.W.; Joshi, J.B. Liquid-Phase Mixing in Stirred Vessels: Turbulent Flow Regime. *Ind. Eng. Chem. Res.* **2003**, *42*, 2661–2698. [CrossRef]
96. Nienow, A.W.; Edwards, M.F.; Harnby, N. *Mixing in the Process Industries*, 2nd ed.; Butterworth-Heinemann: Oxford, UK, 1997.
97. Higbie, R. The Rate of Absorption of Pure Gas into a Still Liquid during Short Periods of Exposure. *Trans. Am. Inst. Chem. Engrs.* **1935**, *31*, 365–389.
98. Doran, P.M. Fluid Flow. In *Bioprocess Engineering Principles*; Elsevier: Amsterdam, The Netherlands, 2013; pp. 201–254. [CrossRef]
99. Knudsen, M. Molecular Effusion and Transpiration. *Nature* **1909**, *80*, 491–492. [CrossRef]
100. Hobbs, B.; Ord, A. (Eds.) Chapter 12—Fluid Flow. In *Structural Geology*; Elsevier: Amsterdam, The Netherlands, 2015; pp. 365–421. [CrossRef]
101. Schaepe, S.; Kuprijanov, A.; Sieblist, C.; Jenzsch, M.; Simutis, R.; Lübbert, A. k_La of stirred tank bioreactors revisited. *J. Biotechnol.* **2013**, *168*, 576–583. [CrossRef]
102. Hager, W.H.; Castro-Orgaz, O. William Froude and the Froude Number. *J. Hydraul. Eng.* **2017**, *143*, 02516005. [CrossRef]
103. Nienow, A.W. Stirring and Stirred-Tank Reactors. *Chem. Ing. Tech.* **2014**, *86*, 2063–2074. [CrossRef]
104. Hixson, A.W.; Luedeke, V.D. Wall Friction in Liquid Agitation Systems. *Ind. Eng. Chem.* **1937**, *29*, 927–933. [CrossRef]
105. Ruzicka, M. On dimensionless numbers. *Chem. Eng. Res. Des.* **2008**, *86*, 835–868. [CrossRef]
106. Moukalled, F.; Mangani, L.; Darwish, M. *The Finite Volume Method in Computational Fluid Dynamics: An Advanced Introduction with OpenFOAM and Matlab*; Springer International Publishing: Cham, Switzerland, 2016; Volume 113.
107. Courant, R.; Friedrichs, K.; Lewy, H. On the Partial Difference Equations of Mathematical Physics. *IBM J. Res. Dev.* **1967**, *11*, 215–234. [CrossRef]
108. Lomax, H.; Pulliam, T.H.; Zingg, D.W. *Fundamentals of Computational Fluid Dynamics*; Springer: Berlin/Heidelberg, Germany, 2001.
109. Newton, J.M.; Schofield, D.; Vlahopoulou, J.; Zhou, Y. Detecting cell lysis using viscosity monitoring in *E. coli* fermentation to prevent product loss. *Biotechnol. Prog.* **2016**, *32*, 1069–1076. [CrossRef] [PubMed]
110. Voulgaris, I.; Chatel, A.; Hoare, M.; Finka, G.; Uden, M. Evaluation of options for harvest of a recombinant *E. coli* fermentation producing a domain antibody using ultra scale-down techniques and pilot-scale verification. *Biotechnol. Prog.* **2016**, *32*, 382–392. [CrossRef]
111. Buckland, B.C.; Gbewonyo, K.; Jain, D.; Glazomitsky, K.; Hunt, G.; Drew, S.W. Oxygen transfer efficiency of hydrofoil impellers in both 800 L and 19,000 L fermentors. In Proceedings of the 2nd International Conference on Fluid Dynamics, London, UK, 11–13 May 1988; p. 16.
112. Sadino-Riquelme, M.C.; Rivas, J.; Jeison, D.; Donoso-Bravo, A.; Hayes, R.E. Investigating a Stirred Bioreactor: Impact of Evolving Fermentation Broth Pseudoplastic Rheology on Mixing Mechanisms. *Fermentation* **2022**, *8*, 102. [CrossRef]
113. Goudar, C.T.; Strevett, K.A.; Shah, S.N. Influence of microbial concentration on the rheology of non-Newtonian fermentation broths. *Appl. Microbiol. Biotechnol.* **1999**, *51*, 310–315. [CrossRef]
114. Nunez-Ramirez, D.M.; Medina-Torres, L.; Valencia-Lopez, J.J.; Calderas, F.; Lopez-Miranda, J.; Medrano-Roldan, H.; Solis-Soto, A. Study of the Rheological Properties of a Fermentation Broth of the Fungus *Beauveria bassiana* in a Bioreactor Under Different Hydrodynamic Conditions. *J. Microbiol. Biotechnol.* **2012**, *22*, 1494–1500. [CrossRef]
115. Kontogiannis, A.; Hodgkinson, R.; Reynolds, S.; Manchester, E.L. Learning rheological parameters of non-Newtonian fluids from velocimetry data. *J. Fluid Mech.* **2025**, *1011*, R3. [CrossRef]
116. Non-Newtonian Fluids in ANSYS Fluent. Available online: https://cfdland.com/non-newtonian-fluids-in-ansys-fluent/ (accessed on 5 September 2025).
117. Westermaier, S.; Kowalczyk, W. Implementation of Non-Newtonian Fluid Properties for Compressible Multiphase Flows in OpenFOAM. *Open J. Fluid Dyn.* **2020**, *10*, 135–150. [CrossRef]

118. Volger, R.; Puiman, L.; Haringa, C. Bubbles and Broth: A review on the impact of broth composition on bubble column bioreactor hydrodynamics. *Biochem. Eng. J.* **2024**, *201*, 109124. [CrossRef]
119. Mast, Y.; Ghaderi, A.; Takors, R. Real Case Study of 600 m^3 Bubble Column Fermentations: Spatially Resolved Simulations Unveil Optimization Potentials for l-Phenylalanine Production with *Escherichia coli*. *Biotechnol. Bioeng.* **2025**, *122*, 265–286. [CrossRef]
120. Haringa, C.; Tang, W.; Wang, G.; Deshmukh, A.T.; van Winden, W.A.; Chu, J.; van Gulik, W.M.; Heijnen, J.J.; Mudde, R.F.; Noorman, H.J. Computational fluid dynamics simulation of an industrial *P. chrysogenum* fermentation with a coupled 9-pool metabolic model: Towards rational scale-down and design optimization. *Chem. Eng. Sci.* **2018**, *175*, 12–24. [CrossRef]
121. Kaya, U.; Gopireddy, S.; Urbanetz, N.; Kreitmayer, D.; Gutheil, E.; Nopens, I.; Verwaeren, J. Quantifying the hydrodynamic stress for bioprocesses. *Biotechnol. Prog.* **2023**, *39*, e3367. [CrossRef]
122. Sharifi, F.; Behzadfar, E.; Ein-Mozaffari, F. Analyzing Local Shear Rate Distribution in a Dual Coaxial Mixing Bioreactor Handling Herschel–Bulkley Biopolymer Solutions through Computational Fluid Dynamics. *Processes* **2023**, *11*, 3387. [CrossRef]
123. Tu, J.; Yeoh, G.-H.; Liu, C. (Eds.) Chapter 3—Governing Equations for CFD—Fundamentals. In *Computational Fluid Dynamics*, 2nd ed.; Butterworth-Heinemann: Oxford, UK, 2013; pp. 61–121. [CrossRef]
124. Wechselberger, P.; Sagmeister, P.; Herwig, C. Real-time estimation of biomass and specific growth rate in physiologically variable recombinant fed-batch processes. *Bioprocess Biosyst. Eng.* **2012**, *36*, 1205–1218. [CrossRef]
125. Mahnert, C.; Oyarzún, D.A.; Berrios, J. Multiscale modelling of bioprocess dynamics and cellular growth. *Microb. Cell Factories* **2024**, *23*, 315. [CrossRef]
126. Hirsch, C. (Ed.) Chapter 1—The Basic Equations of Fluid Dynamics. In *Numerical Computation of Internal and External Flows*, 2nd ed.; Butterworth-Heinemann: Oxford, UK, 2007; pp. 27–64. [CrossRef]
127. Systèmes, D. 3DEXPERIENCE CATIA: Branchenführende Software für Produktdesign und Konstruktion. Dassault Systèmes. Available online: https://discover.3ds.com/de/3dexperience-catia-industry-leading-product-design-and-engineering-software (accessed on 1 September 2025).
128. FreeCAD: Your Own 3D Parametric Modeler. Available online: https://www.freecad.org/ (accessed on 1 September 2025).
129. Solidworks. The Solution for 3D CAD, Design and Product Development. Available online: https://www.solidworks.com/ (accessed on 1 September 2025).
130. OpenFOAM | Free CFD Software | The OpenFOAM Foundation. Available online: https://openfoam.org/ (accessed on 1 September 2025).
131. Ansys Fluent. Fluid Simulation Software. Available online: https://www.ansys.com/products/fluids/ansys-fluent (accessed on 1 September 2025).
132. Jia, Z.; Xu, L.; Duan, X.; Mao, Z.-S.; Zhang, Q.; Yang, C. CFD simulation of flow and mixing characteristics in a stirred tank agitated by improved disc turbines. *Chin. J. Chem. Eng.* **2022**, *50*, 95–107. [CrossRef]
133. Niño, L.; Gelves, R.; Ali, H.; Solsvik, J.; Jakobsen, H. Applicability of a modified breakage and coalescence model based on the complete turbulence spectrum concept for CFD simulation of gas-liquid mass transfer in a stirred tank reactor. *Chem. Eng. Sci.* **2020**, *211*, 115272. [CrossRef]
134. Zhang, C.; Yang, F. Gas–liquid mixing in the stirred tank equipped with semi-circular tube baffles. *Int. J. Chem. React. Eng.* **2023**, *21*, 299–312. [CrossRef]
135. Brannock, M.; Leslie, G.; Wang, Y.; Buetehorn, S. Optimising mixing and nutrient removal in membrane bioreactors: CFD modelling and experimental validation. *Desalination* **2009**, *250*, 815–818. [CrossRef]
136. Chen, S.; Ouyang, Y.; Vandewalle, L.A.; Heynderickx, G.J.; Van Geem, K.M. CFD analysis on hydrodynamics and residence time distribution in a gas-liquid vortex unit. *Chem. Eng. J.* **2022**, *446*, 136812. [CrossRef]
137. Tu, J.; Yeoh, G.-H.; Liu, C. (Eds.) Chapter 2—CFD Solution Procedure—A Beginning. In *Computational Fluid Dynamics*, 2nd ed.; Butterworth-Heinemann: Oxford, UK, 2013; pp. 31–60. [CrossRef]
138. Tu, J.; Yeoh, G.-H.; Liu, C. (Eds.) Chapter 4—CFD Techniques—The Basics. In *Computational Fluid Dynamics*, 2nd ed.; Butterworth-Heinemann: Oxford, UK, 2013; pp. 123–175. [CrossRef]
139. Liu, G.R.; Liu, M.B. Smoothed Particle Hydrodynamics. Available online: https://www.worldscientific.com/worldscibooks/10.1142/5340 (accessed on 3 September 2025).
140. Hafeez, M.B.; Krawczuk, M. A Review: Applications of the Spectral Finite Element Method. *Arch. Comput. Methods Eng.* **2023**, *30*, 3453–3465. [CrossRef]
141. Chen, S.; Doolen, G.D. Lattice Boltzmann Method for Fluid Flows. *Annu. Rev. Fluid Mech.* **1998**, *30*, 329–364. [CrossRef]
142. Haringa, C. An analysis of organism lifelines in an industrial bioreactor using Lattice-Boltzmann CFD. *Eng. Life Sci.* **2022**, *23*, e2100159. [CrossRef]
143. Aidun, C.K.; Clausen, J.R. Lattice-Boltzmann Method for Complex Flows. *Annu. Rev. Fluid Mech.* **2010**, *42*, 439–472. [CrossRef]
144. Nikolić, D.D.; Frawley, P.J. Application of the Lagrangian meshfree approach to modelling of batch crystallisation: Part I—Modelling of stirred tank hydrodynamics. *Chem. Eng. Sci.* **2016**, *145*, 317–328. [CrossRef]

145. Zadghaffari, R.; Moghaddas, J.; Revstedt, J. Large-eddy simulation of turbulent flow in a stirred tank driven by a Rushton turbine. *Comput. Fluids* **2010**, *39*, 1183–1190. [CrossRef]
146. Aubin, J.; Fletcher, D.; Xuereb, C. Modeling turbulent flow in stirred tanks with CFD: The influence of the modeling approach, turbulence model and numerical scheme. *Exp. Therm. Fluid Sci.* **2004**, *28*, 431–445. [CrossRef]
147. Rave, K.; Lehmenkühler, M.; Wirz, D.; Bart, H.-J.; Skoda, R. 3D flow simulation of a baffled stirred tank for an assessment of geometry simplifications and a scale-adaptive turbulence model. *Chem. Eng. Sci.* **2021**, *231*, 116262. [CrossRef]
148. Murthy, B.; Joshi, J. Assessment of standard k−ε, RSM and LES turbulence models in a baffled stirred vessel agitated by various impeller designs. *Chem. Eng. Sci.* **2008**, *63*, 5468–5495. [CrossRef]
149. Joshi, J.B.; Nere, N.K.; Rane, C.V.; Murthy, B.N.; Mathpati, C.; Patwardhan, A.W.; Ranade, V.V. CFD simulation of stirred tanks: Comparison of turbulence models (Part II: Axial flow impellers, multiple impellers and multiphase dispersions). *Can. J. Chem. Eng.* **2011**, *89*, 754–816. [CrossRef]
150. Sharma, K.V.; Straka, R.; Tavares, F.W. Lattice Boltzmann Methods for Industrial Applications. *Ind. Eng. Chem. Res.* **2019**, *58*, 16205–16234. [CrossRef]
151. Mast, Y.; Takors, R. Novel experimental data-driven bubble breakage model for universal application in Euler-Lagrange multiphase frameworks. *Chem. Eng. Sci.* **2024**, *284*, 119509. [CrossRef]
152. Wang, S.; Bu, Q.; Luan, D.; Zhang, Y.; Li, L.; Wang, Z.; Shi, W. Study on gas–liquid flow characteristics in stirred tank with dual-impeller based on CFD-PBM coupled model. *Chin. J. Chem. Eng.* **2021**, *38*, 63–75. [CrossRef]
153. Gu, D.; Wen, L.; Xu, H.; Ye, M. Study on hydrodynamics characteristics in a gas-liquid stirred tank with a self-similarity impeller based on CFD-PBM coupled model. *J. Taiwan Inst. Chem. Eng.* **2023**, *143*, 104688. [CrossRef]
154. Li, S.; Yang, R.; Wang, C.; Han, H.; Shen, S.; Wang, H. CFD–PBM Simulation on Bubble Size Distribution in a Gas–Liquid–Solid Flow Three-Phase Flow Stirred Tank. *ACS Omega* **2022**, *7*, 1934–1942. [CrossRef] [PubMed]
155. Krepper, E.; Lucas, D.; Frank, T.; Prasser, H.-M.; Zwart, P.J. The inhomogeneous MUSIG model for the simulation of polydispersed flows. *Nucl. Eng. Des.* **2008**, *238*, 1690–1702. [CrossRef]
156. Liao, Y.; Lucas, D.; Krepper, E.; Schmidtke, M. Development of a generalized coalescence and breakup closure for the inhomogeneous MUSIG model. *Nucl. Eng. Des.* **2011**, *241*, 1024–1033. [CrossRef]
157. Luzi, G.; McHardy, C. Modeling and Simulation of Photobioreactors with Computational Fluid Dynamics—A Comprehensive Review. *Energies* **2022**, *15*, 3966. [CrossRef]
158. Martins, R.C.; Fachada, N. Finite Element Procedures for Enzyme, Chemical Reaction and "In-Silico" Genome Scale Networks. *arXiv* **2015**, arXiv:1508.02506. [CrossRef]
159. Carfort, J.L.N.D.; Pinto, T.; Krühne, U. An Automatic Method for Generation of CFD-Based 3D Compartment Models: Towards Real-Time Mixing Simulations. *Bioengineering* **2024**, *11*, 169. [CrossRef]
160. Bisgaard, J.; Zahn, A.J.; Tajsoleiman, T.; Rasmussen, T.; Huusom, J.K.; Gernaey, K.V. Data-based dynamic compartment model: Modeling of *E. coli* fed-batch fermentation in a 600 m^3 bubble column. *J. Ind. Microbiol. Biotechnol.* **2022**, *49*, kuac021. [CrossRef]
161. Nadal-Rey, G.; McClure, D.D.; Kavanagh, J.M.; Cassells, B.; Cornelissen, S.; Fletcher, D.F.; Gernaey, K.V. Development of dynamic compartment models for industrial aerobic fed-batch fermentation processes. *Chem. Eng. J.* **2021**, *420*, 130402. [CrossRef]
162. Nauha, E.K.; Kálal, Z.; Ali, J.M.; Alopaeus, V. Compartmental modeling of large stirred tank bioreactors with high gas volume fractions. *Chem. Eng. J.* **2018**, *334*, 2319–2334. [CrossRef]
163. Tajsoleiman, T.; Spann, R.; Bach, C.; Gernaey, K.V.; Huusom, J.K.; Krühne, U. A CFD based automatic method for compartment model development. *Comput. Chem. Eng.* **2019**, *123*, 236–245. [CrossRef]
164. Deng, L.; Yin, J.; He, Q.; Cao, X.; Zhang, C.; Cui, J.; Li, B. An efficient three-dimensional mesh quality optimization method based on gradient-enhanced probabilistic model. *Comput. Phys. Commun.* **2025**, *312*, 109602. [CrossRef]
165. Zadghaffari, R.; Moghaddas, J.; Revstedt, J. A mixing study in a double-Rushton stirred tank. *Comput. Chem. Eng.* **2009**, *33*, 1240–1246. [CrossRef]
166. Ramonet, F.; Kovacevic, M.; Haddadi, B.; Jordan, C.; Harasek, M. Bioreactor Mixing: A Comparison of Computational Fluid Dynamics and Experimental Approaches in the Pursuit of Sustainable Bioprocessing for the Bioeconomy. *Chem. Eng. Trans.* **2023**, *105*, 265–270. [CrossRef]
167. Sadino-Riquelme, M.C.; Rivas, J.; Jeison, D.; Donoso-Bravo, A.; Hayes, R.E. Computational modelling of mixing tanks for bioprocesses: Developing a comprehensive workflow. *Can. J. Chem. Eng.* **2022**, *100*, 3210–3226. [CrossRef]
168. Seidel, S.; Schirmer, C.; Maschke, R.W.; Rossi, L.; Eibl, R.; Eibl, D. Computational Fluid Dynamics for Advanced Characterisation of Bioreactors Used in the Biopharmaceutical Industry—Part I: Literature Review. In *Computational Fluid Dynamics—Recent Advances, New Perspectives and Applications*; IntechOpen: London, UK, 2023. [CrossRef]
169. Huang, W.; Li, K. CFD Simulation of Flows in Stirred Tank Reactors Through Prediction of Momentum Source. In *Nuclear Reactor Thermal Hydraulics and other Applications*; IntechOpen: London, UK, 2013. [CrossRef]
170. Dubey, H.; Das, S.K.; Panda, T. Numerical simulation of a fully baffled biological reactor: The differential circumferential averaging mixing plane approach. *Biotechnol. Bioeng.* **2006**, *95*, 754–766. [CrossRef]

171. Foukrach, M.; Bouzit, M.; Ameur, H.; Kamla, Y. Effect of Agitator's Types on the Hydrodynamic Flow in an Agitated Tank. *Chin. J. Mech. Eng.* **2020**, *33*, 37. [CrossRef]
172. Concli, F.; Gorla, C. Analysis of the power losses in geared transmissions—Measurements and CFD calculations based on open source codes. In *International Gear Conference 2014, Lyon, France, 26–28 August 2014*; Velex, P., Ed.; Chandos Publishing: Oxford, UK, 2014; pp. 1131–1140. [CrossRef]
173. Yang, C.; Mao, Z.-S. (Eds.) Chapter 3—Multiphase stirred reactors. In *Numerical Simulation of Multiphase Reactors with Continuous Liquid Phase*; Academic Press: Oxford, UK, 2014; pp. 75–151. [CrossRef]
174. De-La-Concha-Gómez, A.; Metropolitana, U.A.; Ramírez-Muñoz, J.; Márquez-Baños, V.; Haro, C.; Alonso-Gómez, A. Effect of The Rotating Reference Frame Size for Simulating A Mixing Straight-Blade Impeller in a Baffled Stirred Tank. *Rev. Mex. Ing. Quimica* **2019**, *18*, 1143–1160. [CrossRef]
175. Kresta, S.M.; Etchels, A.W., III; Dickey, D.S.; Atiemo-Oteng, V.A. *Advances in Industrial Mixing: A Companion to the Handbook of Industrial Mixing*; John Wiley and Sons: Hoboken, NJ, USA, 2016; Available online: https://technology.matthey.com/content/journals/10.1595/205651317X696225 (accessed on 6 September 2025).
176. Crowe, C.T.; Schwarzkopf, J.D.; Sommerfeld, M.; Tsuji, Y. Turbulence. In *Multiphase Flows with Droplets and Particles*, 2nd ed.; CRC Press: Boca Raton, FL, USA, 2011.
177. Mathieu, J.; Scott, J. An Introduction to Turbulent Flow. Cambridge Aspire Website. Available online: https://www.cambridge.org/highereducation/books/an-introduction-to-turbulent-flow/1544AA34040E22C492D357EDCB06810A/space-and-time-scales-of-turbulence/89523F1124CADBCA05F6E97D77CFAD18 (accessed on 2 September 2025).
178. Chen, G.; Xiong, Q.; Morris, P.J.; Paterson, E.G.; Sergeev, A.; Wang, Y.-C. OpenFOAM for Computational Fluid Dynamics. *Not. Am. Math. Soc.* **2014**, *61*, 354. [CrossRef]
179. Kolmogorov, A.N.; Levin, V.; Hunt, J.C.R.; Phillips, O.M.; Williams, D. Dissipation of energy in the locally isotropic turbulence. *Proc. R. Soc. Lond. Ser. A Math. Phys. Sci.* **1997**, *434*, 15–17. [CrossRef]
180. Coleman, G.N.; Sandberg, R.D. *A Primer on Direct Numerical Simulation of Turbulence—Methods, Procedures and Guidelines*; AFM-09/01a; University of Southampton: Southampton, UK, 2010.
181. Wagner, C.; Shishkin, A.; Shishkina, O. The use of Direct Numerical Simulations for solving industrial flow problems. In *Direct and Large-Eddy Simulation VIII*; Kuerten, H., Geurts, B., Armenio, V., Fröhlich, J., Eds.; Springer: Dordrecht, The Netherlands, 2011; pp. 397–404. [CrossRef]
182. Yeoh, S.; Papadakis, G.; Yianneskis, M. Numerical Simulation of Turbulent Flow Characteristics in a Stirred Vessel Using the LES and RANS Approaches with the Sliding/Deforming Mesh Methodology. *Chem. Eng. Res. Des.* **2004**, *82*, 834–848. [CrossRef]
183. Launder, B.E.; Spalding, D.B. The numerical computation of turbulent flows. *Comput. Methods Appl. Mech. Eng.* **1974**, *3*, 269–289. [CrossRef]
184. Launder, B.E.; Reece, G.J.; Rodi, W. Progress in the development of a Reynolds-stress turbulence closure. *J. Fluid Mech.* **1975**, *68*, 537–566. [CrossRef]
185. Van den Akker, H.E. The Details of Turbulent Mixing Process and their Simulation. In *Computational Fluid Dynamics*; Marin, G.B., Ed.; Academic Press: Cambridge, MA, USA, 2006; Volume 31, pp. 151–229. [CrossRef]
186. Revstedt, J.; Fuchs, L.; Trägårdh, C. Large eddy simulations of the turbulent flow in a stirred reactor. *Chem. Eng. Sci.* **1998**, *53*, 4041–4053. [CrossRef]
187. Jia, Z.; Zhang, S.; Fang, K.; Kong, B.; Xie, M.; Zhang, Q.; Yang, C. Assessment of stress-blended eddy simulation on prediction of flow characteristics in a Rushton impeller stirred tank. *Chem. Eng. Sci.* **2024**, *284*, 119442. [CrossRef]
188. Agarwal, A.; Singh, G.; Prakash, A. Numerical investigation of flow behavior in double-rushton turbine stirred tank bioreactor. *Mater. Today Proc.* **2021**, *43*, 51–57. [CrossRef]
189. Elmisaoui, S.; Boukharfane, R.; Khamar, L.; Ghidaglia, J.-M. Assessment of subgrid-scale models for large-eddy simulation of a gas-liquid stirred reactor. In *Computer Aided Chemical Engineering*; Kokossis, A.C., Georgiadis, M.C., Pistikopoulos, E., Eds.; Elsevier: Amsterdam, The Netherlands, 2023; Volume 52, pp. 175–181. [CrossRef]
190. Tamburini, A.; Brucato, A.; Ciofalo, M.; Gagliano, G.; Micale, G.; Scargiali, F. CFD simulations of early- to fully-turbulent conditions in unbaffled and baffled vessels stirred by a Rushton turbine. *Chem. Eng. Res. Des.* **2021**, *171*, 36–47. [CrossRef]
191. Pohar, A.; Babnik, S.; Erklavec-Zajec, V.; Oblak, B.; Likozar, B. A Review of Computational Fluid Dynamics (CFD) Simulations of Mixing in the Pharmaceutical Industry. *Biomed. J. Sci. Tech. Res.* **2020**, *27*, 20732–20736. [CrossRef]
192. Jamshidian, R.; Scully, J.; Van den Akker, H.E. Two-fluid simulations of an aerated lab-scale bioreactor. *Chem. Eng. Res. Des.* **2023**, *196*, 254–275. [CrossRef]
193. Gu, D.; Song, Y.; Xu, H.; Wen, L.; Ye, M. CFD simulation and experimental analysis of solid-liquid mixing characteristics in a stirred tank with a self-similarity impeller. *J. Taiwan Inst. Chem. Eng.* **2023**, *146*, 104878. [CrossRef]
194. Zhang, J.; Gao, Z.; Cai, Y.; Cao, H.; Cai, Z.; Bao, Y. Power consumption and mass transfer in a gas-liquid-solid stirred tank reactor with various triple-impeller combinations. *Chem. Eng. Sci.* **2017**, *170*, 464–475. [CrossRef]

195. Zheng, C.; Guo, J.; Wang, C.; Chen, Y.; Zheng, H.; Yan, Z.; Chen, Q. Experimental study and simulation of a three-phase flow stirred bioreactor. *Chin. J. Chem. Eng.* **2019**, *27*, 649–659. [CrossRef]
196. Hirt, C.W.; Nichols, B.D. Volume of fluid (VOF) method for the dynamics of free boundaries. *J. Comput. Phys.* **1981**, *39*, 201–225. [CrossRef]
197. Katopodes, N.D. (Ed.) Chapter 12—Volume of Fluid Method. In *Free-Surface Flow*; Butterworth-Heinemann: Oxford, UK, 2019; pp. 766–802. [CrossRef]
198. Seidel, S.; Eibl, D. Influence of Interfacial Force Models and Population Balance Models on the k_La Value in Stirred Bioreactors. *Processes* **2021**, *9*, 1185. [CrossRef]
199. Drew, D.A.; Passman, S.L. *Theory of Multicomponent Fluids*; Springer Science & Business Media: Berlin/Heidelberg, Germany, 2006.
200. Ishii, M. Thermo-fluid dynamic theory of two-phase flow. *NASA STI/Recon Tech. Rep. A* **1975**, *75*, 29657.
201. Krýsa, P.; Šoóš, M. Modelling of Bubble Breakage and Coalescence in Stirred and Sparged Bioreactor Using the Euler-Lagrange Approach. *Int. J. Heat Mass Transf.* **2022**, *199*, 123466. [CrossRef]
202. Weber, A.; Bart, H.-J. Flow Simulation in a 2D Bubble Column with the Euler-Lagrange and Euler-Euler Method. *Open Chem. Eng. J.* **2017**, *12*, 1–13. [CrossRef]
203. Maluta, F.; Paglianti, A.; Montante, G. Towards a CFD-PBE simulation of aerated stirred tanks at high gas hold ups and different flow regimes. *Chem. Eng. Res. Des.* **2022**, *180*, 425–436. [CrossRef]
204. Montante, G.; Horn, D.; Paglianti, A. Gas–liquid flow and bubble size distribution in stirred tanks. *Chem. Eng. Sci.* **2008**, *63*, 2107–2118. [CrossRef]
205. Chernyshev, A.; Schmidt, A.; Chernysheva, V. An Impact of the Discrete Representation of the Bubble Size Distribution Function on the Flow Structure in a Bubble Column Reactor. *Water* **2023**, *15*, 778. [CrossRef]
206. Ranganathan, P.; Sivaraman, S. Investigations on hydrodynamics and mass transfer in gas–liquid stirred reactor using computational fluid dynamics. *Chem. Eng. Sci.* **2011**, *66*, 3108–3124. [CrossRef]
207. Nienow, A.W. Reactor Engineering in Large Scale Animal Cell Culture. *Cytotechnology* **2006**, *50*, 9–33. [CrossRef]
208. Amer, M.; Feng, Y.; Ramsey, J.D. Using CFD simulations and statistical analysis to correlate oxygen mass transfer coefficient to both geometrical parameters and operating conditions in a stirred-tank bioreactor. *Biotechnol. Prog.* **2019**, *35*, e2785. [CrossRef] [PubMed]
209. Lapin, A.; Schmid, J.; Reuss, M. Modeling the dynamics of *E. coli* populations in the three-dimensional turbulent field of a stirred-tank bioreactor—A structured–segregated approach. *Chem. Eng. Sci.* **2006**, *61*, 4783–4797. [CrossRef]
210. Ahmed, S.U.; Ranganathan, P.; Pandey, A.; Sivaraman, S. Computational fluid dynamics modeling of gas dispersion in multi impeller bioreactor. *J. Biosci. Bioeng.* **2010**, *109*, 588–597. [CrossRef]
211. Delafosse, A.; Calvo, S.; Collignon, M.-L.; Delvigne, F.; Crine, M.; Toye, D. Euler–Lagrange approach to model heterogeneities in stirred tank bioreactors—Comparison to experimental flow characterization and particle tracking. *Chem. Eng. Sci.* **2015**, *134*, 457–466. [CrossRef]
212. Sarkar, J.; Shekhawat, L.K.; Loomba, V.; Rathore, A.S. CFD of mixing of multi-phase flow in a bioreactor using population balance model. *Biotechnol. Prog.* **2016**, *32*, 613–628. [CrossRef] [PubMed]
213. Shu, L.; Yang, M.; Zhao, H.; Li, T.; Yang, L.; Zou, X.; Li, Y. Process optimization in a stirred tank bioreactor based on CFD-Taguchi method: A case study. *J. Clean. Prod.* **2019**, *230*, 1074–1084. [CrossRef]
214. Wright, M.R.; Bach, C.; Gernaey, K.V.; Krühne, U. Investigation of the effect of uncertain growth kinetics on a CFD based model for the growth of *S. cerevisiae* in an industrial bioreactor. *Chem. Eng. Res. Des.* **2018**, *140*, 12–22. [CrossRef]
215. Mittal, G.; Kikugawa, R.I. Computational fluid dynamics simulation of a stirred tank reactor. *Mater. Today Proc.* **2021**, *46*, 11015–11019. [CrossRef]
216. Nadal-Rey, G.; Kavanagh, J.M.; Cassells, B.; Cornelissen, S.; Fletcher, D.F.; Gernaey, K.V.; McClure, D.D. Modelling of industrial-scale bioreactors using the particle lifeline approach. *Biochem. Eng. J.* **2023**, *198*, 108989. [CrossRef]
217. Mayer, F.; Cserjan-Pusch, M.; Haslinger, B.; Shpylovyi, A.; Sam, C.; Soos, M.; Hahn, R.; Striedner, G. Computational fluid dynamics simulation improves the design and characterization of a plug-flow-type scale-down reactor for microbial cultivation processes. *Biotechnol. J.* **2023**, *18*, e2200152. [CrossRef] [PubMed]
218. Ganguly, S.K.; Majumder, C.B.; Ray, A. The Effect of Impeller–Sparger Geometry on the Gas Holdup in an Oxygen–Water System Using an Agitated and Sparged Tank Contactor. *Ind. Eng. Chem. Res.* **2021**, *60*, 10445–10453. [CrossRef]
219. Prado, E.; Dyrness, A. Using CFD Multiphase Modeling to Predict Bioreactor Performance | Pharmaceutical Engineering. Available online: https://ispe.org/pharmaceutical-engineering/september-october-2020/using-cfd-multiphase-modeling-predict-bioreactor (accessed on 6 September 2025).
220. Maluta, F.; Alberini, F.; Paglianti, A.; Montante, G. Hydrodynamics, power consumption and bubble size distribution in gas-liquid stirred tanks. *Chem. Eng. Res. Des.* **2023**, *194*, 582–596. [CrossRef]

221. Ali, H.; Zhu, S.; Solsvik, J. Effects of geometric parameters on volumetric mass transfer coefficient of non-Newtonian fluids in stirred tanks. *Int. J. Chem. React. Eng.* **2022**, *20*, 697–711. [CrossRef]
222. Sadino-Riquelme, M.; Donoso-Bravo, A.; Zorrilla, F.; Valdebenito-Rolack, E.; Gómez, D.; Hansen, F. Computational fluid dynamics (CFD) modeling applied to biological wastewater treatment systems: An overview of strategies for the kinetics integration. *Chem. Eng. J.* **2023**, *466*, 143180. [CrossRef]
223. Cantarero-Rivera, F.J.; Yang, R.; Li, H.; Qi, H.; Chen, J. An artificial neural network-based machine learning approach to correct coarse-mesh-induced error in computational fluid dynamics modeling of cell culture bioreactor. *Food Bioprod. Process.* **2024**, *143*, 128–142. [CrossRef]
224. Chen, F.; Xiao, Z.; Luo, Z.; Jiang, P.; Chen, J.; Ji, Y.; Zhu, J.; Lu, X.; Mu, L. Prediction of mass transfer performance in gas-liquid stirred bioreactor using machine learning. *Chin. J. Chem. Eng.* **2025**, *84*, 211–226. [CrossRef]
225. Chen, M.; Xia, J. Chapter 3—Optimization parameters for efficient scale-up of fermentation process. In *Scale-Up and Chemical Process for Microbial Production of Plant-Derived Bioactive Compounds*; Wei, Y., Ji, X.-J., Cao, M., Eds.; Academic Press: Cambridge, MA, USA, 2024; pp. 29–42. [CrossRef]
226. Helleckes, L.M.; Hemmerich, J.; Wiechert, W.; von Lieres, E.; Grünberger, A. Machine learning in bioprocess development: From promise to practice. *Trends Biotechnol.* **2023**, *41*, 817–835. [CrossRef]
227. Jiang, Z.; Chen, J.; Xie, S.; Li, X.; Liu, H.; Wang, L.; Hong, C.; Li, G.; Chen, K. Establishment of CFD-ANN-NSGA-II model for stirred reactor design. *Chem. Eng. Sci.* **2025**, *311*, 121614. [CrossRef]
228. Zhao, X.; Fan, H.; Lin, G.; Fang, Z.; Yang, W.; Li, M.; Wang, J.; Lu, X.; Li, B.; Wu, K.; et al. Multi-objective optimization of radially stirred tank based on CFD and machine learning. *AIChE J.* **2024**, *70*, e18324. [CrossRef]
229. Rahimzadeh, A.; Ranjbarrad, S.; Ein-Mozaffari, F.; Lohi, A. Application of Machine Learning Models in Coaxial Bioreactors: Classification and Torque Prediction. *ChemEngineering* **2024**, *8*, 42. [CrossRef]
230. Alavijeh, M.K.; Lee, Y.Y.; Gras, S.L. A perspective-driven and technical evaluation of machine learning in bioreactor scale-up: A case-study for potential model developments. *Eng. Life Sci.* **2024**, *24*, e2400023. [CrossRef]
231. Savage, T.; Basha, N.; McDonough, J.; Krassowski, J.; Matar, O.; del Rio Chanona, E.A. Machine learning-assisted discovery of flow reactor designs. *Nat. Chem. Eng.* **2024**, *1*, 522–531. [CrossRef]
232. Fyfe, C.; Barrington, H.; Gordon, C.M.; Reid, M. A Computer Vision Approach toward Verifying CFD Models of Stirred Tank Reactors. *Org. Process. Res. Dev.* **2024**, *28*, 3661–3673. [CrossRef]
233. McConkey, R.; Yee, E.; Lien, F.-S. A curated dataset for data-driven turbulence modelling. *Sci. Data* **2021**, *8*, 255. [CrossRef]
234. Luo, Y.; Chen, Y.; Zhang, Z. CFDBench: A Large-Scale Benchmark for Machine Learning Methods in Fluid Dynamics. *arXiv* **2023**, arXiv:2310.05963.
235. Isoko, K.; Cordiner, J.L.; Kis, Z.; Moghadam, P.Z. Bioprocessing 4.0: A pragmatic review and future perspectives. *Digit. Discov.* **2024**, *3*, 1662–1681. [CrossRef]
236. Duraisamy, K.; Iaccarino, G.; Xiao, H. Turbulence Modeling in the Age of Data. *Annu. Rev. Fluid Mech.* **2019**, *51*, 357–377. [CrossRef]
237. Seidel, S.; Maschke, R.W.; Werner, S.; Jossen, V.; Eibl, D. Oxygen Mass Transfer in Biopharmaceutical Processes: Numerical and Experimental Approaches. *Chem. Ing. Tech.* **2021**, *93*, 42–61. [CrossRef]
238. Shi, P.; Rzehak, R. Bubbly flow in stirred tanks: Euler-Euler/RANS modeling. *Chem. Eng. Sci.* **2018**, *190*, 419–435. [CrossRef]
239. Luan, D.; Zhang, S.; Wei, X.; Chen, Y. Study on mathematical model to predict aerated power consumption in a gas-liquid stirred tank. *Results Phys.* **2017**, *7*, 4085–4088. [CrossRef]
240. Karimi, A.; Golbabaei, F.; Mehrnia, M.; Neghab, M.; Nikpey, A.; Pourmand, M. Oxygen mass transfer in a stirred tank bioreactor using different impeller configurations for environmental purposes. *J. Environ. Health Sci. Eng.* **2013**, *10*, 6. [CrossRef]
241. Miana, M.; Santamaría, A.M.; Carbajo, J.B.; Bengoechea, C.; García, G.; Izquierdo, S. A Practical Approach for Biochemical Modeling in the CFD Evaluation of Novel Anaerobic Digester Concepts for Biogas Production. *Processes* **2023**, *11*, 2851. [CrossRef]
242. Hutmacher, D.W.; Singh, H. Computational fluid dynamics for improved bioreactor design and 3D culture. *Trends Biotechnol.* **2008**, *26*, 166–172. [CrossRef]
243. Rotondi, M.; Grace, N.; Betts, J.; Bargh, N.; Costariol, E.; Zoro, B.; Hewitt, C.J.; Nienow, A.W.; Rafiq, Q.A. Design and development of a new ambr250® bioreactor vessel for improved cell and gene therapy applications. *Biotechnol. Lett.* **2021**, *43*, 1103–1116. [CrossRef] [PubMed]
244. Huang, W.; Wu, C.; Xiao, B.; Xia, W. Computational Fluid Dynamic Approach for Biological System Modeling. *arXiv* **2005**, arXiv:q-bio/0508006. [CrossRef]
245. Eibl, P.; Rustige, S.; Witz, C.; Khinast, J. Chapter Four—LBM for two-phase (bio-)reactors. In *Advances in Chemical Engineering*; Van den Akker, H.E.A., Ed.; Academic Press: Cambridge, MA, USA, 2020; Volume 55, pp. 219–285. [CrossRef]
246. Delvigne, F.; Goffin, P. Microbial heterogeneity affects bioprocess robustness: Dynamic single-cell analysis contributes to understanding of microbial populations. *Biotechnol. J.* **2014**, *9*, 61–72. [CrossRef]

247. Wang, G.; Haringa, C.; Tang, W.; Noorman, H.; Chu, J.; Zhuang, Y.; Zhang, S. Coupled metabolic-hydrodynamic modeling enabling rational scale-up of industrial bioprocesses. *Biotechnol. Bioeng.* **2020**, *117*, 844–867. [CrossRef]
248. Nadal-Rey, G.; McClure, D.D.; Kavanagh, J.M.; Cornelissen, S.; Fletcher, D.F.; Gernaey, K.V. Understanding gradients in industrial bioreactors. *Biotechnol. Adv.* **2021**, *46*, 107660. [CrossRef]
249. Sadrehaghighi, I. *Mesh Sensitivity & Mesh Independence Study*; CFD Open Series: Annapolis, MD, USA, 2021. [CrossRef]
250. Ali, B.A.; Kumar, B.; Madana, V.S.T. Experimental and computational investigation of solid suspension and gas dispersion in a stirred vessel. *Phys. Fluids* **2022**, *34*, 113318. [CrossRef]
251. Fan, Y.; Sun, J.; Jin, J.; Zhang, H.; Chen, W. The effect of baffle on flow structures and dynamics stirred by pitch blade turbine. *Chem. Eng. Res. Des.* **2021**, *168*, 227–238. [CrossRef]
252. Mendoza, F.; Bañales, A.L.; Cid, E.; Xuereb, C.; Poux, M.; Fletcher, D.F.; Aubin, J. Hydrodynamics in a stirred tank in the transitional flow regime. *Chem. Eng. Res. Des.* **2018**, *132*, 865–880. [CrossRef]
253. de Lamotte, A.; Delafosse, A.; Calvo, S.; Delvigne, F.; Toye, D. Investigating the effects of hydrodynamics and mixing on mass transfer through the free-surface in stirred tank bioreactors. *Chem. Eng. Sci.* **2017**, *172*, 125–142. [CrossRef]
254. Taghavi, M.; Moghaddas, J. Using PLIF/PIV techniques to investigate the reactive mixing in stirred tank reactors with Rushton and pitched blade turbines. *Chem. Eng. Res. Des.* **2019**, *151*, 190–206. [CrossRef]
255. Bisgaard, J.; Muldbak, M.; Tajsoleiman, T.; Rydal, T.; Rasmussen, T.; Huusom, J.K.; Gernaey, K.V. Characterization of mixing performance in bioreactors using flow-following sensor devices. *Chem. Eng. Res. Des.* **2021**, *174*, 471–485. [CrossRef]
256. Ochieng, A.; Onyango, M. CFD simulation of the hydrodynamics and mixing time in a stirred tank. *Chem. Ind. Chem. Eng. Q.* **2010**, *16*, 379–386. [CrossRef]
257. Mavros, P. Flow Visualization in Stirred Vessels: A Review of Experimental Techniques. *Chem. Eng. Res. Des.* **2001**, *79*, 113–127. [CrossRef]
258. Luty, P.A.; Prończuk, M.R.; Bizon, K.D. Optical shadowgraphy analysis of gas bubble equivalent diameters: Factors influencing measurement accuracy in bubble flows. *Green Sci.* **2024**, *26*, 72–80. [CrossRef]
259. Povolny, A.; Batsaikhan, M.; Ihara, T.; Takahashi, H.; Kikura, H. Bubble Size Measurement by the Ultrasonic Pulse Echo with Tracking Technique. *J. Flow Control Meas. Vis.* **2018**, *7*, 11–27. [CrossRef]
260. Lucas, D. Qualification of CFD-models for multiphase flows. *Kerntechnik* **2016**, *81*, 167–169. [CrossRef]
261. Rzehak, R.; Krepper, E. Euler-Euler simulation of mass-transfer in bubbly flows. *Chem. Eng. Sci.* **2016**, *155*, 459–468. [CrossRef]
262. Khan, I.; Wang, M.; Zhang, Y.; Tian, W.; Su, G.; Qiu, S. Two-phase bubbly flow simulation using CFD method: A review of models for interfacial forces. *Prog. Nucl. Energy* **2020**, *125*, 103360. [CrossRef]
263. Moser, A.; Appl, C.; Pörtner, R.; Baganz, F.; Hass, V.C. A New Concept for the Rapid Development of Digital Twin Core Models for Bioprocesses in Various Reactor Designs. *Fermentation* **2024**, *10*, 463. [CrossRef]
264. Xing, Z.; Duane, G.; Chelius, C.; Smith, L.; Borys, M.C.; Khetan, A. Validation of a CFD model for cell culture bioreactors at large scale and its application in scale-up. *J. Biotechnol.* **2024**, *387*, 79–88. [CrossRef] [PubMed]
265. Oliveira, C.L.; Pace, Z.; Thomas, J.A.; DeVincentis, B.; Sirasitthich, C.; Egan, S.; Lee, J. CFD-based bioreactor model with proportional-integral-derivative controller functionality for dissolved oxygen and pH. *Biotechnol. Bioeng.* **2024**, *121*, 655–669. [CrossRef]
266. Chu, M. Uncertainty Quantification in Computational Fluid Dynamics: Physics and Machine Learning Based Approaches. *arXiv* **2024**, arXiv:2312.14684v2.
267. Jahanian, A.; Ramirez, J.; O'HAra, I. Advancing precision fermentation: Minimizing power demand of industrial scale bioreactors through mechanistic modelling. *Comput. Chem. Eng.* **2024**, *188*, 108755. [CrossRef]
268. Piscaglia, F.; Ghioldi, F. GPU Acceleration of CFD Simulations in OpenFOAM. *Aerospace* **2023**, *10*, 792. [CrossRef]
269. de León, H.M.; Straathof, A.; Haringa, C. Dynamic compartment models: Towards a rapid modeling approach for fed-batch fermentations. *Chem. Eng. Sci.* **2025**, *308*, 121396. [CrossRef]
270. Madabhushi, S.R.; Gavin, J.; Xu, S.; Cutler, C.; Chmielowski, R.; Rayfield, W.; Tugcu, N.; Chzen, H. Quantitative assessment of environmental impact of biologics manufacturing using process mass intensity analysis. *Biotechnol. Prog.* **2018**, *34*, 1566–1573. [CrossRef]
271. NEA. *Best Practice Guidelines for the Use of CFD in Nuclear Reactor Safety Applications—2024 Update*; OECD Publishing: Paris, France, 2025.
272. Cudak, M.; Rakoczy, R. Hydrodynamics of gas-liquid and biophase-gas-liquid systems in stirred tanks of different scales. *Korean J. Chem. Eng.* **2022**, *39*, 2959–2971. [CrossRef]

273. Li, X.; Scott, K.; Kelly, W.J.; Huang, Z. Development of a Computational Fluid Dynamics Model for Scaling-up Ambr Bioreactors. *Biotechnol. Bioprocess Eng.* **2018**, *23*, 710–725. [CrossRef]
274. Pathak, M.; Devi, T.T. CFD Investigation of Impact of Vessel configuration and Different Impeller Types in Stirred Tank. *IOP Conf. Ser. Mater. Sci. Eng.* **2020**, *1004*, 012006. [CrossRef]